Advancements in 2D MXene-Based Supercapacitor Electrodes: Synthesis, Mechanisms, Electronic Structure Engineering, Flexible Wearable Energy Storage for Real-World Applications, and Future Prospects

Journal:	*Journal of Materials Chemistry A*
Manuscript ID	TA-REV-01-2024-000328.R1
Article Type:	Review Article
Date Submitted by the Author:	13-May-2024
Complete List of Authors:	Kadam, Sujit; National Dong Hwa University, Physics; Jackson State University, Department of Chemistry Physics and Atmospheric Sciences Kadam, Komal; National Dong Hwa University, Chemistry Pradhan, Nihar; Jackson State University, Department of Chemistry Physics and Atmospheric Sciences

Advancements in 2D MXene-Based Supercapacitor Electrodes: Synthesis, Mechanisms, Electronic Structure Engineering, Flexible Wearable Energy Storage for Real-World Applications, and Future Prospects

Sujit Anil Kadam [a,b*], Komal Prakash Kadam[c], Nihar R. Pradhan[b*]

[a] Department of Physics, National Dong Hwa University, Hualien 97401, Taiwan
[b] Department of Chemistry Physics and Atmospheric Sciences, Jackson State University, Jackson, MS, 39217, United States
[c] Department of Chemistry, National Dong Hwa University, Hualien 97401, Taiwan

***Corresponding author: Email-id: ksujit17@gmail.com, nihar.r.pradhan@jsums.edu**

Abstract

Supercapacitors are widely recognized as a favorable option for energy storage due to their higher power density compared to batteries, despite their lower energy density. However, to meet the growing demand for increased energy capacity, it is crucial to explore innovative materials that can enhance energy storage efficiency. Recent research has focused on investigating various electrode materials for use in supercapacitors, with particular attention given to MXenes. MXenes exhibit immense potential for energy storage due to their unique characteristics, including a 2D van der Waals layered structure, small band gaps, hydrophilic surface, excellent electrical conductivity, high specific surface area, and active redox sites on the surface facilitated by transition metals. These attributes collectively contribute to their promising stability, energy and power density, and overall lifespan. This comprehensive review explores a diverse array of topics pertaining to the latest 2D MXene-based supercapacitor electrodes. It encompasses discussions on different synthesis methods, electrode structures, the underlying working mechanisms, and the impact of electrolytes on supercapacitor performance. Additionally, a concise overview of various types of MXene materials is presented, ranging from titanium-based MXenes to niobium-based MXenes, vanadium-based MXenes, molybdenum-based MXenes, and tantalum-based MXenes.

Furthermore, this review focuses on electronic structure engineering strategies such as heterostructures based on MXene, heteroatom-doping based on MXene, Polymer based MXene, and ternary composites based on MXene, all of which contribute to improving the electrochemical performance of supercapacitors. The review thoroughly examines the advantages and disadvantages of MXene-based supercapacitor electrodes, offering a comprehensive understanding of their strengths and limitations. Additionally, it discusses the structural stability of MXene-based electrodes after electrochemical testing, as well as their applications in daily human life, particularly focusing on the uses of MXene-based flexible wearable energy storage for real-world applications. In the end, the challenges and prospects of MXene in supercapacitors are discussed.

Keywords: MXenes; Synthesis and design; Supercapacitor; Electronic structure engineering

1. Introduction

The rapid technological advancements have fueled the global demand for portable and wearable electronic devices such as mobile phones, healthcare devices, and implantable medical devices [1-3]. As these devices continue to evolve, there is a growing need for high-performance energy storage solutions due to the escalating power consumption [4,5]. Among the electrochemical energy storage systems, supercapacitors, fuel cells, batteries, and conventional capacitors stand out as promising candidates for future energy storage devices [6,7]. In the energy storage system, supercapacitors outperform batteries, fuel cells and conventional capacitors with their higher power density, faster charge-discharge rate, and longer cycling life, making them superior to other energy storage systems [8-10]. Supercapacitors function on the principle of electrostatic energy storage, utilizing the electrostatic attraction of opposite charges at the interface between high-surface-area electrodes and an electrolyte [11,12]. When charged, ions from the electrolyte accumulate on the electrode surfaces, forming a double layer of charge. This process allows for the rapid storage and release of electrical energy [13]. Supercapacitors utilize three charge storage mechanisms, one of which is the electric double layer supercapacitor (EDLC), which stores charge electrostatically at the surface of the electrode or electrolyte [9,14]. The second is pseudocapacitive, which employs a quick and reversible electrochemical process at the surface of the electrode to store charge [9,14]. Pseudocapacitive materials store charge in two ways: (i) through surface redox reactions [15] and (ii) by electrolyte ion intercalation into the electrode [9,15,16]. The third mechanism utilized by supercapacitors is the combination of EDLC and pseudocapacitance, often referred to as a battery-type supercapacitor [9,14,16]. These devices incorporate both the electrostatic charge storage of EDLCs and the rapid and reversible electrochemical processes of pseudocapacitance.

Numerous materials have been investigated for use as electrode materials in supercapacitors, including carbon-based materials [17,18], transition metal oxides [19,20], transition metal nitrides [9,21], transition metal dichalcogenides [22,23], transition metal phosphates [24,25], and polymers [26,27]. But even though these materials have their own benefits, they face challenges and restrictions that prevent them from reaching their maximum potential. For instance, pure carbon materials are restricted to a specific capacitance of 250 F/g and have limited energy density in practical applications [28]. On the other hand, while transition metal oxides (TMOs), transition metal dichalcogenides (TMDs), transition metal nitrides (TMNs), transition metal phosphates (TMPs) and polymers have shown improved energy density, they struggle to maintain long-term cycling stability [29-31]. These limitations significantly hinder the practical use of these materials as electrodes in supercapacitors [29]. Therefore, it is crucial to investigate new electrode materials for supercapacitors that are affordable, have a high capacity for storing power and energy, and can maintain stable performance over many charge-discharge cycles. This is important in order to fulfill the increasing energy demands of electronic devices and promote the development of innovative energy storage technologies. Researchers have turned their focus to MXene as a promising avenue to address the aforementioned limitations [32-34]. Compared to other candidates, MXenes possess unique superiorities, pros of MXenes, and cons of other materials, as demonstrated in **Figure 1**. As a member of the 2D materials family, MXene belongs to the category of layered transition metal carbides or nitrides [35-37]. Unlike graphene's, which consists of single-atom thick sheet of sp^2-hybridized carbon atoms, MXene exhibits a unique layered structure similar to transition metal dichalcogenides [38,39]. It features a "sandwich" structure with a carbon or nitrogen layer sandwiched between two transition metal layers (such as Ti, Mo, or W), which is a distinguishing characteristic of MXene material [40,41]. In general, MXene is obtained through the etching process of hexagonal layered ternary transition metal carbides and nitrides, known as MAX phase materials, as depicted in **Figure 2(a)** [42,43]. The MAX phase consists of three main elements: M, which represents an early transition metal (e.g., Ti, V, Ta); A, which is an element from group 12 or 14 (e.g., Al, Zn, Si); and X, which represents either carbon (C) or nitrogen (N) [44,45], as illustrated in **Figure 2(b)**. During the etching process, the "A" elements are selectively removed, resulting in the formation of MXene materials [46,47]. The etching process of MXene commonly employs HF (hydrofluoric acid) or fluoric salt is commonly employed [48]. This etching procedure leads to the decoration of functional groups, referred to as "T_x," on the surface of MXene. This surface functional groups such as -OH, -F, -O, and others [49,50]. These fascinating surface groups inherently offer a significant number of active sites, enabling efficient surface modification and effective loading of active materials [51,52]. Consequently, the formula to describe the resulting MXene material includes these functional groups, and it is represented as $M_{n+1}X_nT_x$, where n can be 1, 2, or 3 [53,54].

MXenes demonstrate remarkable physical and chemical properties that set them apart, including their atomically thin nanosheet structure, better environmental sustainability [55], high electrical conductivity (6500 S/cm) [56], tunable surface chemistry [57], excellent thermal stability [58], remarkable solubility in water and a plentiful number of terminal groups, enabling rapid movement of charge carriers from the bulk to the surface and ensuring efficient charge transport within the material [59], as depicted in **Figure 2(c)**. Moreover, MXene nanosheets possess an abundance of hydrophilic surface functional groups that facilitate strong chemical bonding with semiconductor, leading to enhanced interfacial charge transfer and stable interactions with electrolytes and water molecules [60-64]. Additionally, MXenes, with their typical composition of atomic layers of transition metals as the top and bottom layers, possess transition metals that exhibit strong redox activities [65-67]. This characteristic allows them to modify the oxidation states of the transition metal within MXene materials, resulting in high electrochemical activity, makes them the ideal choice for electrode materials in supercapacitor devices [68-70]. **Figure 2(d)** depicts a trend in the number of publications on MXene-based supercapacitor electrodes each year. The growing number of research paper indicates that researcher maintain a significant interest in MXene-based supercapacitor electrodes as an outstanding and active area of research.

The exceptional electrochemical properties of MXenes, stemming from their inherent conductivity, charge transfer capability attributed the variable oxidation number transition metal M, and special stacking structure, have sparked significant interest in their potential for supercapacitor applications [71-73]. Notably, $Ti_3C_2T_x$ has emerged as a representative MXene, demonstrating an impressive volumetric capacitance of around 1500 F/cm^3 (380 F/g) in an H_2SO_4 electrolyte, even at a thickness of 90 nm [74]. Furthermore, MXene electrode films exhibit remarkable performance with thickness of up to 200 micrometers, showcasing both high transparency and conductivity [75]. This characteristic makes them suitable for the development of transparent solid-state supercapacitors [76]. These findings underscore the promising potential of MXenes in advancing the field of supercapacitor technology. Conversely, there has been considerable research focus on utilizing MXenes in flexible wearable supercapacitors, aiming to boost their efficiency and performance for wearable electronics [77]. In designing flexible electronics, particularly for wearable energy storage devices, the presence of free-standing electrodes with outstanding electrical conductivity and appropriate deformability/durability is paramount [78-80]. MXenes, with their chemical stability, electrochemical advantages, layered structures, high metallic conductivity, and hydrophilicity, have been instrumental in developing top-tier batteries and supercapacitors [81,82].

Despite numerous reviews discussing MXenes in relation to electrochemical energy storage, there remains a dearth of comprehensive reviews specifically focusing on $Ti_3C_2T_x$ and Nb_2CT_x-based MXenes for supercapacitor electrodes. To date, no reviews have been reported that encompass various MXene-based electrodes for supercapacitors. Given the rapid growth and promising applications of MXenes in flexible and wearable devices, there is a pressin required for a comprehensive review that encompasses supercapacitor electrodes based on all other MXenes. In this review, we present a comprehensive and systematic analysis of recent advancements in MXene-based electrode materials for supercapacitors. We briefly examine titanium-based MXenes ($Ti_3C_2T_x$, Ti_2CT_x, $Ti_4N_3T_x$, Ti_3CNT_x MXenes), niobium-based MXenes (Nb_2CT_x and $Nb_4C_3T_x$ MXenes), vanadium-based MXenes (V_4C_3, V_2C, V_2CT_x, and V_2NT_x MXenes), molybdenum-based MXenes (M_2CT_x, $M_3C_2T_x$, $M_4C_3T_x$, $Mo_{1.33}CT_x$ and $Mo_{1.33}C$ i-MXenes), and tantalum-based MXenes ($Ta_4C_3T_x$ MXene). This overview highlights their significant contributions to excellent electrochemical performance as well as elucidates the underlying principles and mechanisms. Firstly, we briefly discuss the correlation between the structure of MXenes and their charge storage capabilities, exploring how the specific structural characteristics of MXenes influence their electrochemical properties. Secondly, we delve into the energy storage mechanisms employed by MXene-based electrodes, examining the fundamental processes that occur during charge and discharge cycles and how MXenes facilitate efficient energy storage. Thirdly, we address the impact of electrolyte properties on MXenes for supercapacitor applications, investigating how different electrolytes affect the overall efficiency as well as cyclic stability of MXene-based supercapacitors. Fourthly, we summarize and discuss the various synthesis strategies employed for MXenes and their effects on supercapacitor performance. We explore different methods used to fabricate MXenes and how these methods influence their electrochemical properties. Fifthly, we review the modification strategies utilized to engineer the electronic structure of MXenes for enhancing supercapacitor performance, examining how modifications to the MXene structure can optimize their energy storage capabilities. Sixthly, we provide a detailed analysis of the structural stability of MXene-based electrodes during electrochemical examination. Lastly, we provide details on the practical applications of MXene-based electrodes for improving human life, particularly focusing on the uses of MXene-based flexible wearable energy storage for real-world applications. We investigate the effects of cycling and aging on the structural integrity of MXenes and their long-term performance as supercapacitor electrodes. This review extensively examines the present obstacles and future potential of MXene-based materials in the field of supercapacitor applications. It provides a comprehensive analysis of various topics, including various synthesis method, supercapacitor performance, structure of electrodes, affecting variables, chemical and physical properties and the benefits and drawbacks of MXene supercapacitor electrodes. This thorough analysis purposes to offer fundamental comprehension and crucial recommendations for the advancement, production, and utilization of innovative supercapacitors.

2. Fundamental of supercapacitors

2.1 Fundamental Components Influencing Supercapacitor Performance

In its fundamental form, a supercapacitor comprises two electrodes, an electrolyte, and a separator, mirroring the basic structure of a conventional capacitor [9,83]. The performance of supercapacitors is influenced by several key components:

2.1.1 Electrode Material: Electrodes stand as pivotal components and the foremost element in supercapacitors [84]. The electrochemical efficacy of supercapacitors relies heavily on the attributes of electrode materials utilized in their creation. Numerous researchers are dedicated to devising cost-effective, high-performance electrode materials featuring exceptional stability, extensive specific surface area, and superior electronic conductivity [9]. Carbon-based materials are notably prominent among the favored choices for supercapacitor electrodes, closely followed by conducting polymers and metal oxides, among others.

2.2.2 Electrolyte: The electrolyte in a supercapacitor is a compound dissolved in a solvent, separating into ions. These ions facilitate ionic conductivity between the electrodes, enabling electric charge transport [85,86]. The choice of electrolyte significantly impacts supercapacitor performance, lifespan, and safety. Electrolytes are typically categorized into three types: aqueous, organic, and ionic liquid. Each class has unique characteristics concerning voltage range and ionic resistance [9].

2.2.3 Separator: The separator in a supercapacitor serves a critical role in its overall functionality and safety. Essentially, it acts as a physical barrier between the positive and negative electrodes, preventing electrical short circuits that could occur through direct contact between them. This function is pivotal in ensuring the stable and reliable operation of the supercapacitor [86,87]. The choice of separator material is of utmost importance. It must possess certain characteristics to fulfill its role effectively. Firstly, the separator material should be inert, meaning it should not react with the electrolyte or other components of the supercapacitor, thereby maintaining its stability over time. Additionally, the separator needs to be permeable to electrolyte ions to facilitate their movement between the electrodes during charging and discharging processes. Several materials are commonly utilized in the fabrication of supercapacitor separators [87]. Polypropylene, a widely used polymer, offers excellent chemical stability and mechanical strength, making it a popular choice. Polyvinylidene difluoride (PVDF) is another commonly employed material due to its high chemical resistance and good electrolyte wettability. Polyvinyl alcohol (PVA) is valued for its ability to retain electrolyte within its pores while allowing the passage of ions [87,88].

2.2.4 Operating Voltage: The operating voltage is a critical parameter for supercapacitors due to its direct impact on the device's performance, safety, and lifespan. Supercapacitors have a maximum voltage limit beyond which they can be damaged or even fail catastrophically, determined by the materials used in their construction [89]. Exceeding this limit can cause irreversible damage, reducing performance or leading to complete failure. Moreover, the operating voltage directly affects both the energy and power densities of supercapacitors. Higher voltages allow for higher energy densities, crucial for compact energy storage in applications like portable electronics or electric vehicles. Similarly, higher voltages enable higher power densities, advantageous for rapid energy delivery or absorption in systems like regenerative braking in electric vehicles [9,89]. Additionally, maintaining voltage stability within the specified range is essential for consistent performance during charging and discharging cycles. Beyond safety concerns, exceeding the voltage limit can lead to internal short circuits or thermal runaway, risking fire or explosion. Adhering to the recommended voltage range ensures both safety and long-term reliability of supercapacitors and the systems they power [89,90].

2.2 Key Parameters for Evaluating Supercapacitor Performance-

Several key parameters are essential for evaluating the performance of supercapacitors: capacitance, internal resistance, energy density, power density, and cycle life [9,83,91].

2.2.1 Capacitance: Capacitance is a fundamental parameter that measures the ability of a supercapacitor to store electrical charge [9]. It determines the amount of energy that can be stored in the device and is typically measured in farads (F) or its submultiples such as microfarads (μF) or picofarads (pF).

2.2.2 Energy Density: Energy density quantifies the amount of energy that a supercapacitor can store per unit volume or mass [83]. It is a crucial metric for assessing the efficiency of energy storage systems and is often expressed in watt-hours per liter (Wh/L) or watt-hours per kilogram (Wh/kg).

2.2.3 Power Density: Power density measures the rate at which a supercapacitor can deliver or absorb energy. It reflects the device's ability to respond quickly to changes in demand and is essential for high-power applications such as electric vehicles and industrial equipment [89]. Power density is typically measured in watts per liter (W/L) or watts per kilogram (W/kg).

2.2.4 Voltage Range: The operating voltage range specifies the maximum and minimum voltages within which a supercapacitor can safely operate. Operating within this range ensures device reliability and prevents damage due to overvoltage or undervoltage conditions [89].

2.2.5 Cycle Life: Cycle life refers to the number of charge-discharge cycles that a supercapacitor can undergo before its performance deteriorates beyond acceptable levels. It is a crucial parameter for assessing the long-term reliability and durability of the device, especially in applications requiring frequent cycling [83].

*2.2.6 Internal Resistance***:** Internal resistance, also known as equivalent series resistance (ESR), quantifies the resistance encountered by the flow of electrical current within the supercapacitor. Lower internal resistance results in higher efficiency and faster charge-discharge rates, making it a critical parameter for high-performance applications [83].

*2.2.7 Self-Discharge Rate***:** The self-discharge rate indicates the rate at which a supercapacitor loses its stored charge over time, in the absence of any external load. A lower self-discharge rate signifies better retention of stored energy and longer shelf life for the device.

3. Energy storage mechanisum of MXenes based electrodes

The capacity characteristics of double-layer capacitors depend directly on the electrodes surface areas [92]. EDLCs often employ materials like mesoporous carbon and graphene, which have notable specific surface areas, due to their ability to provide high capacitance performances. The presence of layeres and porous structures facilitates the adsorption and diffusion of ions, leading to significantly higher power density compared to batteries. Nonetheless, the lower energy densities of these materials become a drawback due to the strong correlation between specific surface area and capacitance performance [29-31]. On the other hand, the electrode materials of pseudocapacitive such as conducting polymers, RuO_2, and MnO_2 is heavily influenced by the presence of redox centers on their surfaces [93]. These redox centers play significant roles in the process of energy storage. The chemical reactions occurring enhance the energy density of pseudocapacitive materials by their surface. However, these reactions can negatively impact the rate performance, causing it to deteriorate [93,94]. Addressing these challenges, MXenes, a family of two-dimensional (2D) transition metal carbides, nitrides, and carbonitrides, have emerged as promising candidates for energy storage applications [93,95]. MXenes' distinctive 2D structure, consisting of transition metal layers separated by intercalated species, provides abundant ion-accessible sites, facilitating efficient ion diffusion and rapid charge storage. Moreover, MXenes can be functionalized with hydroxyl (-OH) or carboxyl (-COOH) groups, introducing additional redox-active centers that enhance pseudocapacitive behavior [54,96]. These functional groups enhance the pseudocapacitive behavior of MXenes, allowing for both non-faradaic double-layer capacitance and faradaic charge storage mechanisms [97]. This combination of double-layer and pseudocapacitive charge storage contributes to superior energy density of MXene-based electrodes. In contrast, energy storage mechanisms, particularly involving ion intercalation in MXene materials, are integral to the development of hybrid supercapacitors, particularly concerning anodic energy storage [98]. MXenes, 2D transition metal carbides, nitrides, and carbonitrides, possess a unique layered structure conducive to ion intercalation [99]. During charging, ions from the electrolyte migrate towards the surface of MXene electrodes, facilitated by their high surface area and active sites. Ion intercalation then occurs, with ions inserting between MXene layers, leading to reversible electrochemical reactions at the electrode-electrolyte interface [100-102]. This process enhances capacitance and contributes significantly to energy storage [102]. MXene materials offer advantages such as high surface area, good electrical conductivity, and chemical stability, making them promising candidates for anodic energy storage [100]. Leveraging these properties, researchers aim to develop high-performance hybrid supercapacitors with improved energy density, power density, and cycling stability for various applications in various fields including portable electronics, electric vehicles, and grid energy storage systems [98].

The remarkable rate performance of MXenes stems from their unique electronic conductivity, which is inherent to these materials owing to the inclusion of transition metal atoms in their structure. This feature facilitates swift electron transport during charge and discharge processes [103,104]. This high conductivity allows for efficient utilization of active sites and fast redox reactions, resulting in enhanced power capability and superior rate performance. On the basis, Gogotsi et al. [74] successfully achievement of 310 F/g capacitance by fabricating a 13-µm-thick mesoporous $Ti_3C_2T_x$ film. This capacitance was measured at scan rate of 10 mV/s using a 3 M H_2SO_4 electrolyte. The strongly ion-accessible porous electrode design allows for extraordinarily fast energy storage and delivery, obtaining a capacitance of 210 F/g when evaluated at a scan rate of 10 V/s. In comparison to graphene supercapacitors with a capacitance of 78 F/g as well as common commercial supercapacitors that typically exhibit a capacitance of around 80 to 200 F/g using carbon electrodes [105]. MXenes have demonstrated capacitances that surpass the performance of the best-known carbon supercapacitors. The high capacitance observed in MXene materials is predominantly influenced by the process of intercalation and deintercalation of electrolyte cations across the MXene layers over the charge as well as discharge cycles

[106,107]. This ion intercalation mechanism plays a important role in the enhanced MXenes capacitance performance. According to Lukatskaya et al. [108], when $Ti_3C_2T_x$ is immersed in different salt solutions, intercalation occurs in the majority of cases. This intercalation process leads to changes in the c-lattice parameter, which can be observed as a downward shift in the X-ray diffraction (XRD) patterns. These observed changes in the XRD patterns provide evidence of ion intercalation into the MXene layers, supporting the intercalation mechanism in MXene-based systems as shown in **Figure 3(a)**. When evaluating the behavior of MXenes with various solutions of salt, it has been observed that the form of cation possesses a substantial influence upon the capacitor's performance. This finding confirms that cations are indeed intercalating into the MXene layers [108]. The choice of cation in the electrolyte plays a critical role in the intercalation process, affecting the capacitance and overall performance of MXene-based capacitors. By delaminating the multilayer $Ti_3C_2T_x$ to form MXene few-layer, excellent capacitance of 340 F/cm^3 was achieved specifically for KOH electrolytes [108]. This improvement in performance can be attributed to the enhanced ability of ion intercalation facilitated by the unique structure of the few-layer MXene paper.

The variation arises due to the contrasting mechanisms involved in the intercalation of these two types. In order to comprehend the paradox presented in MXene materials, an analysis was conducted on mechanical distortion of MXene electrodes over the charging process. This analysis utilized electrochemical quartz-crystal admittance in conjunction about electrochemical experiments [109]. The findings revealed that cationic intercalation occurred at a similar rate to ion adsorption at the interfaces of the electrode and electrolyte. Additionally, water molecules are existing within the layers of MXene also influenced the deformation of MXene particles. The rate of cationic intercalation was observed to be comparable to that of ion adsorption at the interfaces of the electrode and electrolyte. Furthermore, the presence of water molecules between the layers of MXene was found to impact the deformation of MXene particles. The performance of MXene supercapacitors is greatly influenced by the surface chemistry as well [29,110]. In their study, Dall'Agnese et al. [111] discovered that MXenes treated with potassium hydroxide, wherein fluorine was substituted with oxygen-containing terminals, exhibited a three-fold increase in capacitance. This performance disparity resulting from the alteration of surface chemistry could potentially serve as a key indication of the involvement of pseudocapacitance. In addition to surface chemistry and ion intercalation, the electrolyte solvent selection is critical to the process of storing energy [73,100]. On the basis Shpigel et al. [112] reported incorporation of various types of cations across the layers of MXene can effectively regulate the presence of water ions within the restricted area. Understanding the atomic-level interaction between proton intercalation and solvent molecules is of great significance in comprehending the MXene's pseudocapacitance in acidic electrolytes. This is because the pseudocapacitive behavior of MXene in such electrolytes is primarily governed by protonation reactions. Tests of proton movement within different layers of restricted water, as depicted in **Figure 3(b)**, unveiled that the redox and transport of protons were closely linked to thickness of water in the restricted space [113]. Highly confined monolayer waters exhibit greater surface redox reactivity compared to less confined environments.

The coefficient of diffusion of protons raises with the number of water layers until it reaches the value observed in bulk water [113]. Structured water can be generated among the layers within a confined area, leading to the establishment of a rapid network for proton transfer through a Grotthuss process [113-115]. The restricted voltage windows of aqueous electrolytes pose a challenge to advancement of MXene supercapacitors. Despite the importance of developing MXene supercapacitors with higher voltage windows using organic systems, there have been relatively few studies investigating the pseudocapacitive mechanism of MXene in organic electrolytes. In their research, Wang et al. [116] discovered that the energy storage process of $Ti_3C_2T_x$ in Lithium bis(trifluoromethanesulfonyl) imide (LiTFSI) electrolytes is influenced by the choice of organic solvents. By choosing LiTFSI in propylene carbonate (PC) as the organic electrolyte, desolvated lithium ions are effectively inserted into the $Ti_3C_2T_x$ interlayer. This process results in pseudocapacitive charge storage, showcasing the significance of the selected electrolyte in enhancing energy storage capabilities. This finding highlights the significance of the electrolyte composition in influencing the energy storage mechanism of $Ti_3C_2T_x$. If the solvent had been transformed into acetonitrile (ACN) or dimethyl sulfoxide (DMSO), a reduction in capacitance was observed. This decrease can be attributed to the coinsertion of solvent molecules, which impacts the charge storage process in $Ti_3C_2T_x$.

4. Electrolyte Impact on the Performance of MXene Supercapacitor Electrodes

MXenes, a family of 2D materials, exhibit promising potential as electrolytes in supercapacitor application. Central to their functionality is the intricate interplay between ions in the electrolyte solution and the MXene surface [117]. When immersed in the electrolyte, MXenes attract ions through electrostatic forces, initiating a desolvation process crucial for effective ion interaction [118,119]. As ions approach the MXene surface, solvent molecules surrounding them are shed, facilitating desolvation. This process primes ions for efficient charge transport [120,121]. Moreover, the resulting solvation sheath, enveloping desolvated ions, plays a pivotal role. Its structure, shaped by various factors including ion nature and solvent properties, influences ion mobility and diffusivity near the MXene surface [122]. Consequently, understanding the desolvation process and solvation sheath structure is paramount for tailoring MXene-based electrolytes with enhanced ion transport characteristics, thereby advancing the performance of energy storage devices [35,123,124].

The choice of electrolyte can significantly impact the performance and behavior of MXene electrodes [125-127]. The electrolyte plays a crucial role in facilitating ion transport and charge storage within the electrode material [126,128]. Different electrolytes have varying properties such as ion concentration, pH, and specific ion interactions, which can affect the electrochemical behavior of MXene electrodes [129]. In this section discuss the influence of different electrolytes, including aqueous electrolytes, ionic liquids, as well as organic electrolytes on MXene electrodes.

4.1 Aqueous Electrolyte

Sulfuric acid electrolyte is commonly used as an aqueous electrolyte in various energy storage devices. In this electrolyte, the cation present is the small-sized hydrogen ion (H+), which can easily permeate through the nanosheet layers of MXene [130]. This characteristic leads to high ionic conductivity within the material. When MXene is immersed in a sulfuric acid electrolyte, the dominant mechanism for energy storage involves reversible redox reactions taking place at the surface of the MXene material, which include the adsorption and desorption of ions [128,130]. On the basis, Wang et al. [128] reported intercalation of hydrogen ions in the sulfuric acid electrolyte causes the protonation of the oxygen functional groups present on the $Ti_3C_2T_x$ MXene surface. This protonation process results in growth of hydroxyl groups on the surface [128,131]. In H_2SO_4 electrolyte, the number of SO_4^{2-} and HSO_4^- ions can increase or decrease depending on the applied potentials on the negative electrode. This phenomenon is attributed to ion exchange processes that occur during the discharging of the electrode. During discharging, the exchange of ions takes place between the electrolyte and the MXene electrode, leading to changes in the concentration of SO_4^{2-}

and HSO_4^- ions. On the other hand, in electrolytes such as $(NH_4)_2SO_4$ or $MgSO_4$, a different behavior is observed. In these electrolytes, counter ion adsorption occurs, as indicated in **Figure 4(a)** [128]. This is evidenced by the consistent number of anions, indicating that the concentration of ions remains relatively constant during the electrochemical processes. In this case, the ions do not undergo significant exchange with the MXene electrode. The favorable mobility of ions between the layers of MXene contributes to the occurrence of ion exchange processes. When ions can move easily within the MXene structure, ion exchange becomes more favorable, leading to significant changes in ion concentrations. The excellent capacitance of $Ti_3C_2T_x$ film electrodes in H_2SO_4 electrolyte can also be understood from a kinetic perspective. The charge storage and ion transport kinetics are enhanced in H_2SO_4 electrolyte, leading to improved capacitive performance [132]. The specific properties of H_2SO_4, such as its high ionic conductivity and favorable ion mobility, facilitate efficient ion transport and increase the all electrochemical kinetics of MXene electrode. Additionally, according to Dall'Agnese et al. [111] reported the oxidation state of titanium (Ti) undergoes reversible changes in the presence of H_2SO_4 electrolyte. The Ti atoms transition between the +3 and +4 oxidation states, which correspond to the bonding as well as bond breaking of the oxygen functional groups [111]. This reversible alteration in the oxidation state of Ti facilitates the storage and release of charge during the electrochemical processes. The above electrochemical reaction described by equation (2) and (3);

$$Ti_3C_2O_x + \delta e^- + \delta H^+ = Ti_3C_2O_{x-\delta}\,(OH)_\delta \qquad (2)$$

$$Ti_3C_2O_x\,(OH)_yF_z + \delta e^- + \delta k^+ = K_\delta Ti_3C_2O_x\,(OH)_yF_z \qquad (3)$$

Equations (2) and (3) show that the ion conductivity and specific capacitance of supercapacitors are significantly impacted by the concentration of sulfuric acid in the electrolyte.

Equation (2) suggests that increasing the concentration of sulfuric acid results in improved ion conductivity within the electrolyte. This enhanced ion conductivity, in turn, contributes to an increase in the specific capacitance of the supercapacitors. Therefore, the concentration of sulfuric acid is crucial role in optimizing the supercapacitors performance.

Comparable to acid electrolytes, alkaline electrolytes, such as potassium hydroxide (KOH), facilitate ion intercalation without involving reactions with surface functional groups, as shown in Equation (3). This means that in alkaline electrolytes, the electrochemical process primarily involves the intercalation of ions into the interlayer spaces of the $Ti_3C_2T_x$ MXene material. The absence of surface functional group reactions simplifies the electrochemical mechanism in alkaline electrolytes [133,134]. **Figure 4(b)** displays the cyclic voltammetry (CV) curves of $Ti_3C_2T_x$ MXene in an alkaline electrolyte (KOH), illustrating the electrochemical behavior of the material in this specific environment [133]. Li^+ ions, being metal cations with a small radius, are commonly utilized as neutral electrolyte ions in systems including Li_2SO_4 aqueous solutions. The redox reaction occurs during the cycling process when Li+ ions intercalate and deintercalate reversibly. Using water-based electrolytes has advantage of improving safety of supercapacitors. However, one limitation of using aqueous electrolytes is the oxidation of $Ti_3C_2T_x$ when the potential applied to the material becomes high (e.g., anodic oxidation occurring at potentials exceeding 0.6 V) [135]. This oxidation process restricts the expansion of the voltage window available for aqueous electrolytes and consequently limits the achievable energy density of the supercapacitors [136].

4.2 Ionic liquid electrolytes

Ionic liquid electrolytes consist of organic salts that are in a liquid state at or near room temperature, distinguishing them from traditional electrolytes dissolved in solvents [137]. The combination of ionic liquid electrolytes and MXenes holds great promise for advancing energy storage systems. Ionic liquid electrolytes, with their unique properties of low volatility and high ionic conductivity, provide a stable and efficient medium for ion transport. MXenes [138], on the other hand, offer exceptional electrical conductivity and a large surface area, which can facilitate rapid charge and discharge processes in supercapacitors devices [139]. By incorporating MXenes into ionic liquid electrolytes, the overall conductivity can be significantly enhanced, leading to lower internal resistance and improved performance of supercapacitors. This combination opens up exciting opportunities for developing high-performance energy storage systems that are not only efficient but also durable and stable. With ongoing research and development, the synergistic integration of MXenes with ionic liquid electrolytes has the potential to revolutionize the field of energy storage and drive advancements in renewable energy technologies [140]. On the basis, Presser et al. [141] investigated that volume variation behavior of $Ti_3C_2T_x$ MXene in the presence of ionic liquids using an electrochemical tracing technique. The findings showed that the volume increase in $Ti_3C_2T_x$ MXene in ionic liquids is irreversible. This irreversible expansion is attributed to rapid ion intercalation that occurs after the MXene electrodes come into interaction with the ionic liquid electrolytes. During electrochemical cycling, the volume of $Ti_3C_2T_x$ MXene expands at negative potentials. This expansion is driven by a negative charge present upon the $Ti_3C_2T_x$ surface, which enhances the intercalation of cations in order to preserve electrostatic balance. On the other hand, at positive potentials, ion delamination and volume shrinkage occur due to the electrostatic desorption of adsorbed ions from the MXene surface. Furthermore, humidity of the environment performs an important role in the behavior of $Ti_3C_2T_x$ MXene in ionic liquid electrolytes. Elevated humidity levels lead to the replacement of ions on the surface of $Ti_3C_2T_x$ by water molecules, which in turn increases the fluidity in the ionic liquid [142]. Therefore, when using ionic liquid electrolytes, it becomes crucial to control the humidity of the environment to maintain stable electrochemical performance. On the other hand, non-aqueous electrolyte solutions often face challenges related to poor conductivity [143]. This issue arises from the larger size of the ions present in these electrolytes, which hinders their efficient intercalation into the $Ti_3C_2T_x$ MXene material. The reduced intercalation effect results in lower capacitance and can limit the overall performance of supercapacitors or energy storage devices utilizing non-aqueous electrolyte solutions.

4.3 Organic Electrolyte

Combining MXenes with organic electrolytes presents a promising avenue for advancing energy storage [144]. Organic electrolytes, composed of organic solvents and salts, offer benefits like wide electrochemical stability and high conductivity. MXenes, known for their exceptional electrical conductivity and unique structure, show great potential in enhancing energy storage device performance [145]. The integration of MXenes into organic electrolytes improves conductivity, reducing internal resistance and enhancing charge/discharge rates [144,146]. Additionally, MXenes contribute to mechanical stability, preventing electrode degradation. This collaboration holds promise for high-performance supercapacitors with improved energy density and overall efficiency [147]. On the basis, Gogotsi et al. [116] investigated the intercalation behavior of lithium ions from lithium hexafluorophosphate ($LiPF_6$) electrolyte in various solvents was investigated to understand the impact of the electrolyte solvent on the capacitance of $Ti_3C_2T_x$ MXene. This experiment revealed that the desolvation process of lithium intercalation, where the solvent molecules are removed, is beneficial in extending the voltage range of 2.4 V as well as improving $Ti_3C_2T_x$ MXene capacitance performance. It was observed that when organic solvents intercalate with lithium ions, the efficiency of lithium ion intercalation is reduced **(Figure 4c,d)** [116]. The presence of the organic solvent molecules hinders the intercalation process, resulting in decreased intercalation efficiency. Additionally, the solvent's ion conductivity has an impact on how easily ions penetrate the MXene material. For instance, in the case of DMSO solvent, the oxygen atoms in the DMSO molecules cannot be desolvated and interact with lithium ions, keeping $Ti_3C_2T_x$ MXene's hydrophobic methyl groups apart from of its surface. This interaction weakens the electrostatic interaction between the MXene layers, potentially affecting the overall capacitance performance.

The choice of electrolyte profoundly influences the performance and behavior of MXene electrodes. Aqueous electrolytes, such as sulfuric acid, offer high ionic conductivity and facilitate reversible redox reactions, leading to efficient energy storage. However, limitations include oxidation of MXene at high potentials, restricting the achievable energy density. Alkaline electrolytes, like potassium hydroxide, simplify the electrochemical mechanism by primarily involving ion intercalation without surface reactions, yet they face challenges in expanding the voltage window. Ionic liquid electrolytes, with their low volatility and high conductivity, show promise in enhancing MXene performance, although irreversible expansion of MXene in these electrolytes presents a challenge. Control of humidity is crucial in maintaining stable performance. Organic electrolytes provide wide electrochemical stability and high conductivity, but the efficiency of ion intercalation can be hindered by solvent molecules, affecting overall capacitance performance. Understanding the interplay between MXene and different electrolytes is essential for optimizing energy storage device performance and driving advancements in renewable energy technologies.

5. Synthesis strategies of MXene electrodes

Until now, substantial efforts have been dedicated to the development of innovative synthetic techniques for both newly discovered MXenes and those that have been previously studied. These constructed approaches are broadly divided in two main categories: top-down techniques, which involve the transformation of MAX phase precursors into MXenes, and bottom-up techniques that involve the assembly of components to produce MXene thin films, as depicted in **Figure 5(a)**. It is worth noting that the synthesis conditions employed during MXene production possess a profound effects upon the resulting structure, performance, surface group termination, as well as general characteristics of the MXene materials [148]. Factors such as etchant concentration, reaction temperature, duration, and post-treatment procedures influence the final MXene structure and properties [149,150]. Optimizing these synthetic parameters is crucial for obtaining MXenes with desired attributes, such as specific surface terminations, controlled layer thickness, and enhanced supercapacitors performance [77].

5.1. Top-down approach

The top-down synthesis process aims to weaken the binding forces between the A sheet and MX sheet (metallic bond) in the MAX phase [118,151]. This helps create separate, very thin MXene nanosheets, either as single layers or just a few layers. The process involves using etching exfoliation to separate the layers and then employing methods like ultrasonic or other mechanical techniques to further separate them [151]. In these methods, the chemical structure of the MAX precursor, the composition of the etchant, and the type of intercalating agent are all very important [152]. They perform important functions in deciding the quality of the final products and overall yield of the process. Choosing the right combination of these factors is essential to obtain high-quality MXene nanosheets in significant quantities [152]. Functional groups such as -OH, -F, and -O are generated on the surface of MXene during the synthesis process. In contrast, the top-down strategy involves several synthetic procedures, including the HF etching method, Molten salt etching In Situ HF Etching (Fluoride Salt), fluoride-free etching, and the ball milling method, which will be discussed below.

5.1.1. HF etching method

The synthesis of MXenes by the HF etching method involves a sequence of steps to selectively remove the A element from the MAX phase precursor [153]. Initially, a bulk MAX phase material is prepared, which typically consists of closely packed atom layers. The MAX phase is then immersed in an etching solution, commonly hydrofluoric acid (HF) or a mixture of HF and other solvents. HF acts as the etchant, severing the A and M elements' strong chemical bonds [153,154]. The etching process selectively removes the A element, leading to the delamination of the MAX phase layers [153]. As a result, MXene layers are formed, which have a two-dimensional structure with a high surface area. After etching, the MXene layers are thoroughly washed to remove any residual etchant or by-products. The following equations illustrates the most typical procedure for selective etching and functionalizing the MAX phase using hydrofluoric acid (HF) [155]:

$$M_{n+1}AX_n + 3HF \rightleftharpoons AF_3 + 3/2H_2 + M_{n+1}X_n \qquad (4)$$

$$M_{n+1}X_n + 2H_2O \rightleftharpoons M_{n+1}+X_n\,(OH)_2 + H_2 \qquad (5)$$

$$M_{n+1}X_n + 2HF \rightleftharpoons M_{n+1}+X_n\,F_2 + H_2 \qquad (6)$$

Therefore, equation (4) illustrates the process of removing the 'A' elements from the MAX phase to produce the $M_{n+1}X_n$ phase. The functionalization processes of the $M_{n+1}X_n$ phase with OH and F elements, respectively, to produce $M_{n+1}X_n T_x$ (T = F or OH), are described in equation (5) and (6). The 'T_x' denotes as the surface terminations, including O, OH, F, and/or Cl elements, that are bound to the outer 'M' layers [156]. The MXenes can then be collected and further processed in different applications, including catalysis, energy storage devices, as well as electronic devices. The HF etching technique allows for the synthesis of MXenes by selectively removing the A element, allowing for the exploration of their unique properties and supercapacitor applications [73]. In the study conducted by Naguib et al. [157], Ti_3AlC_2 powders were subjected to a treatment process involving immersion in a 50% concentrated hydrofluoric acid (HF) solution for a duration of 2 hours. As a result of this treatment, $Ti_3C_2T_x$ MXene was formed, indicating the successful exfoliation and etching of the Al layers from the Ti_3AlC_2 structure. Furthermore, Syamsai and colleagues synthesized vanadium carbide MXene through the process of HF etching for supercapacitor applications [158]. The MXenes electrode demonstrated a specific capacitance of 330 F/g when tested at a scan rate of 5 mV/s in an electrolyte solution of 1 M H_2SO_4 electrolyte.

HF etching, a widely employed method, has several advantages and disadvantages. One of its primary advantages is its efficiency in exfoliating the A-layer from the MAX phase, leading to the formation of MXenes with a layered structure and a large surface area. This controlled synthesis allows for precise tuning of MXene properties such as surface chemistry and layer thickness, crucial for tailoring them to specific applications in electrochemical energy storage. Additionally, MXenes synthesized via HF etching exhibit high electrical conductivity, which is essential for efficient charge transport in devices like batteries and supercapacitors. Moreover, HF etching can be scaled up for large-scale production, facilitating industrial applications. However, the use of HF poses significant safety concerns due to its corrosive and toxic nature, requiring strict safety protocols. Furthermore, HF etching generates hazardous waste, necessitating careful disposal to mitigate environmental impact. Achieving high selectivity and purity in MXene synthesis via HF etching can be challenging, and the stability of MXene materials against oxidation and hydrolysis needs improvement for long-term performance.

5.1.2. Molten salt etching

Molten salt etching is indeed a technique proposed for the synthesis of novel MAX and MXene compounds by replacing the A element in traditional MAX phases [48,159]. The process involves using Lewis acids in the molten state as strong electron acceptors to selectively etch or remove the A elements from MAX phases [160]. The Lewis acid reacts with the A element, leading to the insertion of cations or anions within to the A element's original position. These inserted species then form bonds that have the unaltered transition metal atoms palced upon each side, resulting in a substitution of A element. Using this molten salt etching technique, Huang et al. [159] successfully prepared new MAX compounds such as Ti_3ZnC_2, Ti_2ZnC, Ti_2ZnN, and V_2ZnC. The Al atom layers in Ti_3AlC_2, Ti_2AlC, Ti_2AlN, and V_2AlC were replaced by molten $ZnCl_2$ as the etchant, leading to the formation of the new compounds.

$$Ti_3AlC_2 + 1.5ZnCl_2 = Ti_3ZnC_2 + 0.5Zn + AlC_3 \quad (7)$$

$$Ti_3AlC_2 + 1.5ZnCl_2 = Ti_3C_2 + 1.5Zn + AlC_3 \quad (8)$$

The reactions represented by equations (7) and (8) illustrate the replacement of aluminum (Al) in Ti_3AlC_2 with zinc (Zn) through the use of zinc chloride ($ZnCl_2$) as the etchant.

$$Ti_3C_2 + Zn = Ti_3ZnC_2 \quad (9)$$

The (9) equation indicates the formation of Ti_3ZnC_2 by combining Ti_3C_2 with Zn. It suggests the synthesis of a new MAX phase compound, Ti_3ZnC_2, by incorporating Zn into the structure of Ti_3C_2. Furthermore, the Zn-MAX compounds, such as Ti_3ZnC_2, can be further etched with $ZnCl_2$, leading to the formation of MXene with chlorine functional groups. This represents the first successful synthesis of MXene with chlorine functional groups, which is an alternative to the conventional fluorine- based manufacturing methods. This novel etching technique using $ZnCl_2$ is considered less harmful to the environment compared to the fluorine-based methods, as it avoids the use of fluorine-containing etchants. Additionally, it enables the production of MXenes with single functional groups, which can be advantageous for supercapcitor applications. On the basis, Bai et al. [161] synthesized Ti_3C_2 MXene-Cu/Co hybrids using molten salt etching for symmetric supercapacitor device. The preparartion process of Ti_3C_2 MXene-Cu/Co hybrids, as depicted in **Figure 5(b)**. The symmetric supercapacitor device showed a remarkable specific capacitance of 290.5 mF/cm^2 at a current density of 1 mA/cm^2. Additionally, the device demonstrated excellent capacitance retention, with 89% retention over 10,000 cycles. Khan et al. [48] synthesized $Ti_3C_2Cl_2$, $Ti_3C_2I_2$, and $Ti_3C_2Br_2$ MXene electrodes for use in supercapacitor. This MXene electrodes demonstrated exceptional specific capacities of 92 C/g, 63 C/g, and 29 C/g, respectively. Additionally, they exhibited excellent cyclic stability, indicating their ability to maintain consistent performance over multiple charge-discharge cycle.

The molten salt etching method offering several advantages along with certain drawbacks. One significant advantage is its enhanced safety profile, as molten salt etchants are generally less corrosive and toxic compared to HF, reducing the risk of accidents and exposure to harmful chemicals. Additionally, molten salt etching generates fewer hazardous byproducts, making it more environmentally friendly and simplifying waste disposal processes. This method also allows for selective etching, leading to higher purity MXene materials with improved electrochemical performance. However, molten salt etching typically requires higher processing temperatures and may pose challenges in scalability, process optimization, and material compatibility. Despite these challenges, the versatility and potential sustainability of molten salt etching make it a promising avenue for the synthesis of high-quality MXene electrodes, provided that optimization efforts address its limitations for practical application and large-scale production.

5.1.3. In Situ HF Etching (Fluoride Salt)

MXene materials are synthesized via the In Situ HF etching method, involving the use of fluoride salts. This approach includes use of a mixture containing a fluoride salt and an acid to produces in situ hydrofluoric acid (HF) for etching the MAX phase and obtaining MXene [162]. The process typically begins with a MAX phase material, such as Ti_3AlC_2, which consists of layers of transition metal nitride or carbide sandwiched between aluminum layers [163]. To transform the MAX phase into MXene, a fluoride salt (such as LiF, KF, NaF, CsF, CaF_2, or tetrabutylammonium fluoride) is combined with an acid (such as HCl or H_2SO_4) [163]. This mixture generates HF in situ, which is a strong etchant capable of selectively removing the aluminum layers from the MAX phase. By controlling the composition and ratio of the fluoride salt and acid, the etching process can be fine-tuned to obtain desired MXene properties [164]. The optimal conditions depend on the specific requirements of the MXene material being synthesized. In situ HF etching using fluoride salts offers several advantages over direct HF etching. It provides a safer and more controllable approach by using less aggressive acids instead of concentrated HF [165]. Additionally, it eliminates the need for additional intercalation and delamination steps, simplifying the MXene synthesis process [166]. In addition to LiF, other fluoride salts such as

NH_4HF_2 and NH_4F were employed to generate in situ HF, which facilitated of the MAX phase into MXene [167]. This expanded the options for MXene synthesis using different fluoride salt combinations. The use of fluoride salts in the etching process enables the control of MXene features including interlayer spacing, surface area as well as surface chemistry. These properties play a crucial role in improving the stability, conductivity as well as specific capacitance of MXene electrodes. On the basis, Ghidiu et al. [163] synthesized $Ti_3C_2T_x$ using the HF Etching (Fluoride Salt) process for supercapacitors application. Synthesis process of $Ti_3C_2T_x$ as depicted in **Figure 5(c)**. The morphology of $Ti_3C_2T_x$ shows layers flakes with superior flexibility, as depicted in **Figure 5(d)**. The $Ti_3C_2T_x$ electrode demonstrated exceptional volumetric capacitance, reaching 900 F/cm^3 when tested at a scan rate of 2 mV/s in a 1M H_2SO_4 electrolyte.

In situ HF etching using fluoride salts has both advantages and disadvantages. By utilizing fluoride salts instead of concentrated HF solutions, the process reduces the risk of accidents and exposure to toxic substances, enhancing operational safety. Additionally, the controlled release of HF ions from fluoride salts enables precise etching of the MAX phase, resulting in high-quality MXene materials with improved structural integrity and electrochemical properties. Moreover, the use of fluoride salts reduces the environmental impact associated with traditional HF etching methods, simplifying waste management and disposal. However, this method may involve more complex synthesis procedures, potential for side reactions, and considerations regarding cost-effectiveness and scalability. Despite these challenges, in situ HF etching with fluoride salts holds significant promise for advancing MXene synthesis towards safer, more controlled, and environmentally sustainable processes.

5.1.4. Fluoride-free etching

Fluoride-based etching approaches, although effective in preparing MXene materials, can have detrimental effects on the environment and pose risks to biological tissues [168]. These limitations hinder the practical applications of MXene in various fields. Additionally, the use of fluoridated etchants can negatively impact the specific capacitance of supercapacitors when MXene is used as the electrode material [169]. To overcome these challenges, researchers have developed fluoride-free synthesis strategies for MXene. The high-temperature alkali solution etching and electrochemical etching represent two frequently employed methods. The technique of concentrated alkali etching draws inspiration from the Bayer process employed in the refined bauxite industry. This process utilizes an alkali to selectively extract the aluminum (Al) layer from the MAX parent phase, such as Ti_3AlC_2. The amphoteric nature of aluminum, which has a strong binding ability with hydroxide ions (OH-), allows it to react with the alkali during etching. When alkali is used at low temperatures, insoluble aluminum hydroxides are produced. These insoluble hydroxides form protective layers on the surface of Ti_3AlC_2, impeding the etching reaction and preventing the formation of $Ti_3C_2T_x$ MXene. However, at high temperatures, soluble aluminum hydroxides can be generated. These soluble hydroxides can effectively remove the aluminum layers, leading to the creation of $Ti_3C_2T_x$ MXene. The removal of aluminum layers exposes the desired MXene structure with layers of transition metal carbides. By controlling the temperature during the etching process, it is possible to achieve the selective removal of aluminum layers and the production of $Ti_3C_2T_x$ MXene. High temperatures promote the formation of soluble aluminum hydroxides, enabling efficient etching and MXene synthesis. On the basis, Zhang et al. [170] successfully prepared a high-purity $Ti_3C_2T_x$ (T = -OH, -O) MXene through treatment with a sodium hydroxide (NaOH) solution. They observed that lower temperatures ranging from 100 to 200 °C were not favorable for $Ti_3C_2T_x$ MXene formation because of the growth of insoluble aluminum hydroxides, such as $Al(OH)_3$ and AlO(OH). Conversely, higher temperatures exceeding 250 °C resulted in the generation of dissolvable aluminum hydroxides ($Al(OH)_4^-$), facilitating the formation of $Ti_3C_2T_x$ MXene. Furthermore, Ghidiu et al. [163] successfully synthesized $Ti_3C_2T_x$ MXene using a fluoride-free etching method for supercapacitor applications. The $Ti_3C_2T_x$ MXene electrode displayed an impressive gravimetric capacitance, reaching 314 F/g when measured at a scan rate of 2 mV/s in a 1 M sulphuric acid (H_2SO_4) electrolyte. Furthermore, electrochemical etching is an effective approach for producing MXene materials with excellent capacitive performance. This method can be carried out in electrolytes that are free of fluorides, resulting in the production of ($Ti_3C_2T_x$) MXene without any fluorine terminations. In contrast, constant potential is used to selectively etch aluminum (Al) layers in this process. Chloride ions (Cl^-) play a crucial role in this etching process as they possess a strong binding capability with Al, causing the Ti-Al bonds to break. Particularly, when the Ti_3AlC_2 electrode is positively charged, the attack of chloride ions results in a growth of $AlCl_3$, causing the Ti atoms at the edges to terminate with chlorine. This, in turn, opens up grain boundaries, allowing for additional penetration of Cl^- ions and other intercalated species from the electrolyte. Based on this, Yang et al. [171] findings outstanding fluoride-free etching technique to convert bulk Ti_3AlC_2 into $Ti_3C_2T_x$ MXene, specifically for solid-state supercapacitor applications. Tetramethylammonium hydroxide (TMAOH) as well as ammonium chloride were combined in a mixed aqueous electrolyte to facilitate the electrochemical etching process, as depicted in in **Figure 5(e)**. The $Ti_3C_2T_x$ MXene electrode demonstrated high area-specific capacitances of 220 mF/cm^2 at a scan rate of 10 mV/s.

Fluoride-free etching methods for synthesizing MXene electrodes offer both advantages and disadvantages. One of the primary advantages is the elimination of fluoride-related safety concerns, as these methods do not involve the use of corrosive and toxic fluoride-containing compounds such as HF or fluoride salts. This enhances operational safety and simplifies handling procedures, reducing the risk of accidents and minimizing potential exposure to hazardous chemicals for researchers and operators. Additionally, fluoride-free etching methods typically result in MXene materials with reduced risk of fluoride contamination, which can be advantageous for applications where fluoride impurities may be undesirable, such as in biomedical, energy storage and environmental applications. However, fluoride-free etching methods may also present challenges in terms of achieving efficient exfoliation and selective removal of the A-layer from the MAX phase. Optimization of etching conditions and development of alternative etchants are necessary to overcome these challenges and ensure the synthesis of high-quality MXene materials with desirable properties. Furthermore, fluoride-free etching methods may require additional steps or alternative approaches compared to fluoride-based methods, potentially complicating the synthesis process and impacting scalability and cost-effectiveness. Despite these challenges, ongoing research efforts are focused on refining fluoride-free etching methods to address these limitations and expand the applicability of MXene materials in various fields.

5.1.5. Ball milling method

Ball milling is commonly employed as a top-down method to reduce dimensions of nanoparticles, proving to be highly effective in generating diverse MXenes [172]. The properties of materials, both physical and morphological, are influenced by several factors in this process. These factors include the type of milling (wet as well as dry), grinding rapidity, the ratio of balls to powder, and the duration of milling [172,173]. By manipulating these parameters, researchers can precisely customize the resulting materials, allowing for a detailed exploration of the intricate relationship between synthesis conditions and material properties. This comprehensive approach emphasizes the interconnected nature of the various parameters in ball milling, underscoring the importance of a holistic understanding for optimal outcomes in nanoparticle synthesis and material design [174]. On the basis, Xue and colleagues introduced a method for synthesizing fluorine-free Ti_3C_2 MXene using a chemical ball-milling process [174]. **Figure 5(f)** presents a schematic illustration of the synthesis process of Ti_3C_2 MXene. The resultant MXene had a hierarchical porous morphology, characterized by a significantly maximum surface area (38.93 m^2/g) then conventional Ti_3C_2 MXenes produced through HF treatment (4.87 m^2/g). Compared to other etching methods, the ball milling technique utilizing TMAOH as well as a LiCl solvent, in combination with Ti_3AlC_2 powder, offers a simpler and more environmentally friendly approach. Similarly, Su et al. [175] synthesized Ti_3C_2 MXene using ball milling method and HF etchinng. Synthesized Ti_3C_2 MXene exhibited excellent specific capacitances of 61.5 F/g at 0.2 A/g current density.

The ball milling method for synthesizing MXene electrodes offers several advantages along with certain disadvantages. One of its primary advantages is its versatility and simplicity, as ball milling provides a straightforward and scalable approach to produce MXene materials from bulk MAX phase precursors. This method involves the mechanical exfoliation of the MAX phase through high-energy ball collisions, leading to the formation of MXene nanosheets with a high surface area. Additionally, ball milling can be easily tailored to tune the size, morphology, and composition of the synthesized MXene materials by adjusting milling parameters such as milling time, ball-to-powder ratio, and milling speed. Moreover, ball milling does not require the use of hazardous chemicals or specialized equipment, making it a cost-effective and environmentally friendly method for MXene synthesis. However, ball milling also has certain disadvantages, including the potential for structural defects and contamination introduced during the milling process, which can affect the quality and electrochemical performance of the synthesized MXene materials. Furthermore, prolonged milling times or high-energy milling conditions may lead to excessive heating and phase transformations, requiring careful optimization to prevent degradation of MXene properties. Despite these disadvantages, ball milling remains a widely used method for MXene synthesis due to its simplicity, scalability, and versatility, with ongoing research focused on addressing its drawbacks and optimizing synthesis conditions for various applications in electrochemical energy storage and beyond.

5.2. Bottom-up approach

The bottom-up approach involves using molecules as potential precursors to construct MXene structures from the ground up. This approach offers more control over the atomic arrangement and allows for the design of MXenes with specific properties [100]. Using functional precursors can improve surface termination as well as enhance the desired characteristics [176]. Moreover, the bottom-up method is appropriate for low-toxic components, secure reaction conditions to prevent contamination, and straightforward and extremely effective precursors [152].

5.2.1. Magnetron sputtering

Magnetron sputtering deposition is indeed a widely used technique in the realm of physical vapor deposition (PVD), especially for the growth of thin films, including those made of 2D materials [177]. While synthesizing MXene using magnetron sputtering can be challenging, this technique has been successfully employed to fabricate MAX phase precursors with desirable thickness [178-180]. The synthesis process of Ti_3AlC_2 MAX thin film involves the sputtering of titanium (Ti), aluminum (Al), and carbon (C) onto a sapphire substrate, as depicted in the provided **Figure 6(a)** [181]. The sputtering process entails the deposition of these materials onto the substrate using high-energy ions. By controlling the deposition parameters such as sputtering power, pressure, and deposition time, a Ti_3AlC_2 MAX thin film is formed on the sapphire substrate. This thin film structure exhibits a layered arrangement of Ti, Al, and C atoms, resulting in the formation of the desired Ti_3AlC_2 MAX phase. In a study conducted by Joseph et al. [178] reported Nb, Al, and C elements were utilized to grow a thin film of the MAX phase. The deposition process involved DC magnetron sputtering under an inert condition of 99.9% Ar. Prior to deposition, the Al_2O_3 substrate was thoroughly cleaned using acetone and isopropanol in an ultrasonicator and dried with nitrogen gas. The substrate was then preheated at 950 °C in the DC magnetron sputtering system to facilitate the growth of a 15 nm thick Nb_2AlC thin film. Another study by Li et al. [182] employed magnetron sputtering to grow a few layers of 2D Nb_2C nanolayers for the generation of square wave laser pulses. In this case, a substrate material of K-9 class was used. The Nb_2C MXene layer thickness was controlled at 10–15 nm, exhibiting broadband absorption properties ranging from 400 nm to 2000 nm, making it suitable for ultrafast photonic applications. Magnetron sputtering deposition offers promising prospects for the fabrication of MAX phase precursors and MXene nanolayers with controlled thicknesses. Despite the challenges associated with synthesizing 2D MXene using this technique, it offers promising prospects for the fabrication of MXene thin films with tailored properties for supercapacitors application. Chen et al. reported the synthesis of scandium-based MXene (Sc_2CO_x) utilizing magnetron sputtering. The experimental conditions involved using silicon and sapphire substrates and maintaining a 6×10^{-4} m Torr pressure. The deposition rates for carbon (C) and scandium (Sc) were set at 30 nm/h and 60 nm/h, respectively, under an argon flow at room temperature.

The magnetron sputtering method for synthesizing MXene electrodes offers several advantages along with certain drawbacks. One of its primary advantages is its ability to deposit thin films of MXene materials with precise control over composition, thickness, and morphology.

This technique involves bombarding a target material (typically a MAX phase) with high-energy ions in a vacuum chamber, causing atoms to be ejected and deposited onto a substrate to form a thin MXene film. This precise control enables the production of MXene films with tailored properties suitable for various applications in electronics, sensors, and energy storage devices. Additionally, magnetron sputtering allows for the deposition of MXene films onto diverse substrates, including flexible or irregularly shaped surfaces, expanding the potential range of applications. Moreover, the process is relatively simple and can be easily scaled up for industrial production, making it suitable for large-scale manufacturing. However, magnetron sputtering also has certain limitations, such as limited deposition rates and substrate heating during the process, which may affect film quality and adhesion. Furthermore, the equipment required for magnetron sputtering can be expensive and complex, requiring skilled operators and maintenance. Despite these drawbacks, magnetron sputtering remains a valuable method for synthesizing high-quality MXene films with precise control over properties, with ongoing research aimed at optimizing deposition parameters and overcoming limitations for broader applications in various fields~~.~~

5.2.2. Chemical vapor deposition (CVD)

The CVD technique is commonly used to produce very thin films, often consisting of multiple layers (at least six layers) [151]. Numerous literature reports have described the synthesis of MXene using CVD [183,184]. In the first MXene synthesis using CVD, high-quality ultrathin Mo_2C (molybdenum carbide) films were created. The process involved utilizing methane gas (CH_4) as the carbon source and a Cu/Mo (copper/molybdenum) foil as the substrate. The synthesis was carried out at temperatures exceeding 1085 °C [185]. By optimizing the growth temperature and time, a range of films with lateral sizes ranging from 10 to 100 μm were obtained. The synthesized Mo_2C films were found to be defect-free and exhibited high crystallinity, suggesting the absence of surface functional groups. Furthermore, Cu/Mo bilayer substrates were used by Xu et al. [186] for fabricating 2D Mo_2C MXene superconducting crystals. The layer-by-layer fromation process involved the deposition of Mo_2C MXene onto the substrate. Methane was used as the precursor gas for the synthesis. The resulting MXene crystals achieved an approximate thickness of 100 μm and exhibited superconducting properties.

CVD is a highly versatile method for synthesizing MXene electrodes, offering several distinct advantages along with some limitations. One of its primary advantages is its ability to produce high-quality MXene films with precise control over thickness, composition, and morphology. CVD involves the decomposition of gaseous precursor molecules on a substrate surface, resulting in the deposition of MXene layers in a controlled manner. This precise control enables the synthesis of uniform and defect-free MXene films with tailored properties, making CVD particularly well-suited for energy storage and energy conversation applications. Additionally, CVD can be employed to deposit MXene films onto a variety of substrates, including flexible or temperature-sensitive materials, allowing for the integration of MXene-based devices into diverse platforms. Furthermore, CVD offers scalability and reproducibility, making it suitable for industrial-scale production. However, CVD also has certain limitations, such as the requirement for high vacuum conditions and specialized equipment, which can increase the complexity and cost of the process. Additionally, the deposition rates in CVD may be relatively slow compared to other methods, and the need for precise control over process parameters can make optimization challenging. Despite these limitations, ongoing research efforts are focused on refining CVD techniques and overcoming obstacles to unlock the full potential of MXene materials in various technological application.

5.3 Other methods

5.3.1. MXene Synthesis from non-MAX Phase Precursors:

Metals in the transition group, like Zr and Hf, have a higher tendency to create layered compounds with the formula $(MC)_n\ [Al\text{-}\ (A)]_m\ C_{m-1}$ compared to $M_{n+1}AlC_n$ phases that contain aluminum. The values of n, m, and A for these compounds are typically n=2-4, m= 3 or 4, and A represents Ge and/or Si, respectively [187]. It is possible to utilize these non-MAX phase precursors for producing MXenes such as $Zr_3C_2T_x$ and $Hf_3C_2T_x$. Using hydrofluoric acid (HF), the Al-C units in the $Zr_3Al_3C_5$ precursor and the $[Al(Si)]_4C_4$ units in $Hf_3[Al(Si)]_4C_6$ can be etched to produce $Zr_3C_2T_x$ and $Hf_3C_2T_x$ MXenes, respectively [188,189]. In addition, Mo_2Ga_2C, which is a layered carbide consisting of Mo_2C layers separated by two stacked Ga layers, has also been utilized for the large-scale production of Mo_2C MXenes. This is achieved through the use of HF and LiF/HCl etchants, as illustrated in **Figure 6(b)**. In contrast, Mei et al. [190] reported Mo_2C MXene can be synthesized without the use of fluoride, by etching multiple layers of Ga in Mo_2Ga_2C. This process involves using a mild phosphoric acid solution and exposing the sample to ultraviolet (UV) light irradiation for several hours, as depicted in **Figure 6(c)**. Wang et al. have recently introduced another fluoride-free etching method for the synthesis of Mo_2CT_x MXene from the Mo_2Ga_2C MAX phase precursor. This method is called the HCl-assisted hydrothermal method [191].

The top-down approach to synthesizing MXenes involves several methods, each offering unique advantages and facing specific challenges. The HF etching method efficiently exfoliates the A-layer from the MAX phase, resulting in MXenes with a layered structure and large surface area. However, the use of HF raises significant safety concerns due to its corrosive and toxic nature, necessitating careful handling and waste disposal. Molten salt etching offers enhanced safety and reduced environmental impact compared to HF etching but may require higher processing temperatures and pose challenges in scalability. In Situ HF Etching using fluoride salts provides a safer alternative to direct HF etching, yet it involves more complex synthesis procedures and considerations regarding cost-effectiveness. Fluoride-free etching methods address environmental and safety concerns but may face challenges in achieving efficient exfoliation and selective removal of the A-layer. The ball milling method offers simplicity, scalability, and versatility but may introduce structural defects and contamination. Conversely, the bottom-up approach, including magnetron sputtering and CVD, offers precise control over MXene properties but may involve complex synthesis procedures and require specialized equipment. Each method underscores the need for continued research and optimization to fully harness the potential of MXene materials for supercapacitor applications.

6. MXene electrodes for Supercapcitors

2D materials like activated carbon, carbon nanotubes (CNTs), and graphene exhibit enhanced capacitive storage capacity in supercapacitors as a result of their significantly large effective surface area. This increased capacity is attributed to the strong correlation between capacitance and the ion-accessible surface area of the electrode materials. Nevertheless, their application in compact and portable capacitive storage devices has faced limitations due to their low volumetric capacitance. This is primarily attributed to their low density (usually below 1.0 g/cm^3) and high gravimetric capacitance (typically less than 300 F/g) [192]. Pseudocapacitive materials, such as TMOs like WO_3, MoO_3, and MnO_2, as well as conducting polymers like polyaniline (PANI) and polypyrrole (PPy), exhibit higher capacitance values ranging from 300 to 2000 F/g [193,194]. Nevertheless, electrodes made of TMOs or conducting polymers often suffer from inadequate electrochemical stability, leading to low electrical conductivity (for instance,

MnO_2 typically exhibits conductivity ranging from 10^{-5} to 10^{-6} S/cm) [195-197]. 2D MXenes are employed as active electrode materials for supercapacitors devices due to its layered structures, low cost, superior conductivity, excellent reversibility, superior pseudocapacitance performance, excellent energy as well as power density [198-201]. Numerous studies have highlighted the suitability of MXenes-based materials in supercapacitors. This includes various types of MXenes, such as titanium-based MXenes (e.g., $Ti_3C_2T_x$, Ti_2CT_x, $Ti_4N_3T_x$, Ti_3CNT_x MXenes) [202],[203] niobium-based MXenes (Nb_2CT_x and $Nb_4C_3T_x$ MXenes) [204,205], vanadium-based MXenes (V_2CT_x, and V_2NT_x MXenes) [206], molybdenum-based MXenes (M_2CT_x, $M_3C_2T_x$, $M_4C_3T_x$, $Mo_{1.33}CT_x$ and $Mo_{1.33}C$ i-MXenes) [207,208], and tantalum-based MXenes ($Ta_4C_3T_x$ MXene) [209,210].

The initial utilization of MXenes in supercapacitors dates back to 2013, when researchers explored 2D Titanium Carbide as a potential substitute for dichalcogenide electrodes [211]. Since this initial investigation, MXenes have risen in prominence and become a major area of research in area of supercapacitors. Scientists have shown significant attention in various MXenes, including $Ti_3C_2T_x$ [202], Nb_2CT_x [212], V_2NT_x [213], Mo_2CT_x [214], and $Ta_4C_3T_x$ [215]. **Table 1** provides a summary of MXenes electrodes in three electrode configurations. In this section, we concentrated on the primary advancements in MXenes designed for supercapacitor devices, meticulously incorporating both geometric and electrical characteristics.

6.1. Titanium -based MXene

Titanium-based MXenes specifically refer to MXenes derived from titanium-containing MAX phases. These MXenes include variants such as $Ti_3C_2T_x$ [202], Ti_2CT_x [203], $Ti_4N_3T_x$ [216], and Ti_3CNT_x [217], all of which hold significance for supercapacitor applications. The "x" in their formulas denoting the degree of surface functionalization. Notably, $Ti_3C_2T_x$ has been one of the most investigated MXene family members for supercapacitors because to its unique flake morphology, significant volumetric capacitances at high current densities and spontaneous intercalation for a number of cations [163,211,218]. The electrolyte, surface functional groups, electrode structure and physical and chemical properties all have a significant impact on the supercapacitors performance of $Ti_3C_2T_x$ MXene electrode [219]. In contrast, the electrolyte has a major impact on the voltage window and ionic transport efficiency; surface terminations and electrochemically active sites have a major impact on $Ti_3C_2T_x$ electrochemical behavior. This section summarizes the $Ti_3C_2T_x$ materials and composites for supercapacitor applications.

The energy-storage capacitive behavior of the $Ti_3C_2T_x$ electrode in an electrolyte can be described by the reaction that follows [74,169,220]:

$$T_3C_2O_x\,(OH)_y\,F_z + \delta e^- +\ \delta H^+ \rightarrow T_3C_2O_{x-\delta}\ (OH)_{y+\delta} + F_Z \qquad (5)$$

Numerous studies have demonstrated that larger capacitances are a result of the presence of a higher number of -O functional groups as well as a reduced number of -F functional groups, particularly in acid electrolytes where protons may interact with the terminal O on the $Ti_3C_2T_x$ surface [221-224]. Based on the basis, Wang et al. [224] demonstrated the importance of controlling and quantity of functional groups for obtaining best electrochemical behavior of $Ti_3C_2T_x$ electrode. The capacitance of $Ti_3C_2T_x$ layers demonstrated a notable increase when subjected to a lower HF concentration of 6 mol/L, reaching 400 F/g at a scan rate of 2 mV/s. In contrast, under a higher HF concentration of 15 mol/L, the capacitance was comparatively lower at 208 F/g (at 2 mV/s). This augmented capacitance can be attributed to the higher concentration of -O surface terminations and the presence of high mobility H_2O molecules within the interlayers of $Ti_3C_2T_x$. The phenomenon suggests that manipulating the HF concentration plays a crucial role in optimizing the electrochemical performance of $Ti_3C_2T_x$ layers. Moreover, Pan et al. [225] conducted a synthesis of Ti_3C_2 MXene by selectively removing aluminum (Al) from Ti_3AlC_2 using hydrofluoric acid (HF) in order to explore its potential for supercapacitor applications. The resulting Ti_3C_2 MXene electrode displayed a specific capacity of 28.5 C/g when tested at a density of 1 A/g. Furthermore, many researchers modify the surface terminal groups of $Ti_3C_2T_x$ to improve electrochemical behavior, such as by eliminating -F species and enhancing the proportion of terminal -O groups [111,226]. Li et al. [219] revealed that $Ti_3C_2T_x$ MXenes electrode synthesized by KOH post-treatment for supercapacitors application. The gravimetric capacitance of $Ti_3C_2T_x$ electrode after KOH post-treatment was 517 F/g at 1 A/g in H_2SO_4 electrolyte, whereas the pure $Ti_3C_2T_x$ electrode without KOH post-treatment exhibited a smaller capacitance of 244 F/g. Furthermore, KOH post-treatment electrode exhibited 99% retention after 10,000 charge–discharge cycles. The elimination of terminal (-OH/-F) groups by K^+ ions intercalation to $Ti_3C_2T_x$ interlayers by KOH treatment was primarily responsible for the much improved supercapacitive performance. Chen et al. [227] demonstrated that $Ti_3C_2T_x$ that employing *n*-butyllithium as an organic reagent to treat $Ti_3C_2T_x$ MXene may successfully avoid oxidation during the annealing process and prevent the development of $Ti_3C_2T_x$ nanoribbons, which is commonly observed after alkaline aqueous treatment. The electrochemical study showed that *n*-butyllithium treated $Ti_3C_2T_x$ performs significantly better than its LiOH-treated. A high capacitance of 523 F/g at 2 mV/s could be produced for the $Ti_3C_2T_x$ MXenes treated with n-butyllithium, and 96% capacity could be maintained even after 10,000 cycles. In contrast, the LiOH-treated $Ti_3C_2T_x$ MXene exhibited a low capacitance of 259 F/g at a scan rate of 2 mV/s. Lower –F terminal group content and increased -O terminal group content in n-butyllithium treated $Ti_3C_2T_x$ MXenes resulted in enhanced pseudocapacitor performance. In addition, Huang et al. [228] reported a symmetric on-chip microstructure with $Ti_3C_2T_x$ MXene blended ink for all-in-one Si-based electronics. The MXene-SiO_2 electrode was produced using a technique involving drop-coating and natural sedimentation, as depicted in **Figure 7 (a)**. Cross-sectional SEM analysis (**Figure 7(b))** reveals that the MXene film with a water and acetone (W/A) blend has a thickness of 1.13 μm and an open structure. This emphasizes the role of acetone in preventing restacking of 2D $Ti_3C_2T_x$ MXene flakes during film fabrication. In contrast, the MXene film fabricated without acetone is only 0.42 μm thick and exhibits a closely packed structure. The fabrication process of $Ti_3C_2T_x$ MXene-based micro-supercapacitors on a Si/SiO_2 wafer involves a series of steps, including controlled ink dispersion through acetone, drop-coating, laser-etched interdigital patterning, and deposition of PVA/H_2SO_4 gel electrolyte. The characteristic cyclic voltammetry profiles of micro-supercapacitors -W/A at varying scan rates are presented in **Figure 7(c)**. $Ti_3C_2T_x$ MXene micro-supercapacitors with the W/A configuration exhibit remarkable volumetric capacitances, reaching 350.1 F/cm^3. This significantly surpasses the capacitance of micro-supercapacitors-Water (276.0 F/cm^3). These high volumetric capacitance values are maintained even under demanding conditions, such as a high scan rate of 1 V/s, where the capacitances remain at 106.2 and 65.4 F/cm^3, respectively. For high voltage and energy practical applications, on-chip micro-supercapacitor devices can be integrated using MXene due to its excellent wettability and conductivity, serving as both an active material and collector as illustrated in **Figure 7(d)**. This enables the realization of all-in-one Si-based electronics via laser-etching. The CV curves demonstrate uniform micro-supercapacitor shapes (single, series, parallel), with the series configuration widening the voltage window to 2.4 V and the parallel configuration doubling the capacity as depicted in **Figure 7(e).** $Ti_3C_2T_x$ MXene's conductivity enables integrated circuits, as evidenced by the integration of three micro-supercapacitors, chip-LEDs, and an inching switch, as shown in **Figure 7(f)**. The remarkable performance of MXene-based micro-supercapacitors arises from various factors, including the optimized interaction of MXene ink with the SiO_2/Si wafer, prevention of restacking via acetone and sedimentation, enhanced ion accessibility, widened voltage window due to MXene-SiO_2 hydrogen bonding, and the overall high compatibility of the all-MXene design. Furthermore, Simon et al. [111] investigated the impact of intercalation and delamination on the surface chemistry for electrochemical capacitance of $Ti_3C_2T_x$. After chemical intercalation of potassium salts, terminal fluorine was effectively substituted with oxygenic functional groups. This modification in surface chemistry produced in a high- capacitance of 520 F/cm^3 at 2 mV/s in 1M H_2SO_4 electrolyte, with no significant loss after 10000 cycles. Furthermore. Yang et al. [171] developed fluoride-free etching technique for converting bulk Ti_3AlC_2 into $Ti_3C_2T_x$ for solid-state supercapacitor. The all-solid-state supercapacitor fabricated using two $Ti_3C_2T_x$ MXene electrodes and PVA/H_2SO_4 electrolyte. The all-solid-state supercapacitor device exhibited areal capacitance of 220 mF cm^{-2} at 10 mV/s and capacitance retention of 94.2 over 10000 cycles. excellent stability. Rakhi and co-workers prepared 2D Ti_2CT_x nanosheets by HF etching and investigated the effect of annealing environment on its structure and electrochemical performance [223]. MXene retained its layered structure after heat treatment under Ar, N_2, and N_2/H_2 atmospheres. However, annealing in air resulted in the conversion of MXene to TiO_2 nanoparticles and graphitic carbon. In a symmetrical two-electrode system, the N_2/H_2-treated MXene exhibited a maximum capacitance of 51 F/g at scan rate of 1 A/g. The outstanding capacitance performance due to the stable layered structure, low fluorine content, and high carbon content on the surface of the N_2/H_2-treated MXene. Wang et al. [229] developed Fiber-Based $Ti_3C_2T_x$ MXene on silver-plated nylon fibers for solid-state flexible symmetric supercapacitor devices. These solid-state supercapacitors comprise two $Ti_3C_2T_x$@silver-plated nylon fiber electrodes and a PVA-H_2SO_4 hydrogel electrolyte. The device exhibits a maximum areal capacitance of 328 mF/cm^2 at 2 mV/s, with an excellent capacitance retention of 100% over 10,000 cycles. Additionally, the device achieves energy and power densities of 7.3 µWh/cm^2 and 132 µW/cm^2. The superior supercapacitor device performance due to the unique structure formed by depositing $Ti_3C_2T_x$ flakes onto the fibrous support also contributes to an increased effective surface area for charge accumulation.

The limited electrochemical stability of $Ti_3C_2T_x$ MXene is a notable drawback, as it could restrict the operational voltage range of the material, potentially hindering its ability to withstand higher voltages. Such higher voltages are essential for achieving greater energy densities in supercapacitor applications.

6.2. Niobium-based MXenes

Niobium-carbide MXene, particularly Nb_2CT_x and $Nb_4C_3T_x$, has gained significant attention in the MXene family [204,205]. Nb_2CT_x, discovered in 2013, has demonstrated excellent performance in handling high cycling rates (10 C) and possesses a good ion intake capacity, making it a superior candidate for energy storage devices [230,231]. Nb_2CT_x and $Nb_4C_3T_x$ are commonly synthesized by acid etching of their MAX phases Nb_2AlC and Nb_4AlC_3, respectively [230,232,233]. Nb_2CT_x exhibits outstanding conductivity with a band gap near zero or even smaller, making it a metallic material with flexible functional group combinations [234]. These metallic MXene phases act as conductive layers, facilitating faster charge transfer between catalyst surfaces and electrodes. This characteristic proves advantageous for various electrochemical applications. On the basis, Sofer et al. [212] reported capacitance behavior of Nb_2CT_x MXene by intercalating different cations [Na^+, K^+, Li^+]. Among the tested cations, Li^+ showed better electrochemical performance and capacitance behavior compared to Na^+ and K^+. Specifically, when Nb_2CT_x electrodes were used in 1M Li_2SO_4 electrolyte, they had a higher specific capacitance of 153.9 F/g at 5 mV/s compared to 1M K_2SO_4 electrolyte (90.1 F/g at 5 mV/s) and 1M Na_2SO_4 electrolyte (55.69 F/g at 5 mV/s) as depicted in **Figure 8(a)-(b)**. This improved capacitance was attributed to the fast transport and easy intercalation of the small-sized Li^+ ions between the layers of Nb_2CT_x MXene as depicted in **Figure 8(c).** Similarly, Xiao and colleagues conducted the synthesis of Nb_2CT_x MXene through the etching process of Nb_2AlC for supercapacitors application [235]. The resulting Nb_2CT_x MXene electrode demonstrated a specific capacitance of 186 F/g when tested at a scan rate of 2 mV/s in a 1M H_2SO_4 electrolyte.

The most commonly used niobium MXenes, Nb_2CT_x and $Nb_4C_3T_x$, are derived from the acid etching of their corresponding MAX phases, Nb_2AlC and Nb_4AlC_3, respectively. During the exfoliation process, the metallic M-Al bonds are lost, resulting in increased resistivity compared to their MAX phases. However, $Nb_4C_3T_x$ MXene demonstrates lower resistivity compared to Nb_2CT_x, attributed to the higher n value and the presence of additional NbC layers, which retain more MAX phase characteristics [232]. It has been observed that $Nb_4C_3T_x$ exhibits nearly 100 times higher electrical conductivity than Nb_2CT_x [232]. In fact, individual single-layer flakes of $Nb_4C_3T_x$ show an electrical conductivity of 1,024 ± 165 S/cm, which is twice as high as that of bulk $Nb_4C_3T_x$ assemblies. Based on these findings, Zhao et al. [236] reported the volumetric capacitance of a free-standing film of $Nb_4C_3T_x$ MXene with large interlayer spacing has been investigated in different electrolytes. **Figure 8(d)** presents an SEM image, illustrating that the $Nb_4C_3T_x$ sample consists of both a limited number of layers and individual layers, with the flake's dimensions spanning approximately 5 µm. The electrodes exhibited high volumetric capacitance values of 506 F/cm^3 in 1 M $MgSO_4$, 687 F/cm^3 in 1M KOH, and 1075 F/cm^3 in 1M H_2SO_4 when measured at 5 mV/s scan rate, as depicted in **Figure 8(e)**. Among the tested electrolytes, the

MXene film in 1 M $MgSO_4$ demonstrated the highest series resistance, which is represented by the intercept of the semicircle on the real impedance axis. Conversely, the electrode in 1 M H_2SO_4 exhibited the lowest charge transfer resistance, as indicated by the smallest semicircle on the Nyquist plot in the low-frequency range (**Figure 8(f)).** Additionally, the H_2SO_4 electrolyte facilitated the fastest diffusion of ions, as denoted by the steepest slope of the Nyquist plot. The mobility of potassium ions fell between that of protons and magnesium ions, possibly due to the smaller radius of H^+ ions, enabling them to migrate more easily within the interlayer space of the MXene material. Consequently, the performance of the H_2SO_4 electrolyte was enhanced, resulting in higher volumetric capacitance values. Furthermore, Zhao and colleagues reported the capacitance performance of $Nb_4C_3T_x$ in an acidic electrolyte comprising Li_2SO_4 and Na_2SO_4 [237]. The $Nb_4C_3T_x$ electrode displayed a maximum specific capacitance of 177 F/g in a 1 M Li_2SO_4 electrolyte when tested at a scan rate of 5 mV/s. Similarly, in a 1 M Na_2SO_4 electrolyte at the same scan rate, the electrode exhibited a maximum specific capacitance of 111 F/g. Notably, the electrode demonstrated excellent stability of 90% after 10,000 cycles. The higher capacitance observed in the Li_2SO_4 electrolyte compared to the Na_2SO_4 electrolyte can be attributed to the increased interlayer spacing resulting from the intercalation and deintercalation of Li-ions.

One of the primary drawbacks associated with niobium-based MXene electrodes in the realm of supercapacitor devices is their inherent limitation in achieving high energy density. While these materials have exhibited promising properties for various applications, including supercapacitors, their ability to store and deliver energy efficiently is hampered by their relatively low energy density. This deficiency can be attributed to several factors, such as a limited surface area available for charge accumulation, potential faradaic reactions that introduce sluggish chemical transformations, and a constrained electrochemical potential window. Furthermore, the presence of interlayer water content, which is characteristic of many MXenes, contributes to the overall mass without substantially contributing to charge storage. Consequently, these factors collectively result in reduced energy storage capacity and overall performance in supercapacitor devices utilizing niobium-based MXene electrodes.

6.3. Vanadium-based MXenes

Extensive research has been conducted on Vanadium based MXenes as electrode materials for supercapacitors. These MXenes exhibit remarkable characteristics, making them highly intriguing for study. Notably, they possess a lightweight nature, display pseudocapacitive behavior, demonstrate a high capacity for Li-ion intercalation, and exhibit excellent conductivity [238,239]. Furthermore, Vanadium MXenes offer an additional advantage over Ti- and Mo-based MXenes by possessing a larger interlayer spacing [240]. This increased spacing proves beneficial for the storage, intercalation, and deintercalation of energy. Another notable aspect lies in the various valence states of +2, +3, and +4 exhibited by the Vanadium MXenes [241]. These diverse valence states have proven advantageous for improving the supercapacitor performance. On the basis, Zhu et al. [240] synthesized V_4C_3 MXene by etching aluminum (Al) from V_4AlC_3 for supercapacitor applications. The V_4C_3 MXene electrode demonstrated impressive performance, exhibiting a maximum specific capacitance of 209 F/g at a scan rate of 2 mV/s in a 1M H_2SO_4 electrolyte. Remarkably, the electrode also displayed excellent capacitance retention, retaining 97.23% over 10,000 cycles. The excellent supercapacitors performance of V_4C_3 MXene can be attributed to several factors. Firstly, its wide interlayer spacing allows for efficient ion transport and storage, enhancing its energy storage capabilities. Additionally, the MXene possesses a large surface area, there are lots of active sites available for electrochemical reactions. Moreover, the material exhibits favorable pore volumes, facilitating electrolyte penetration and enhancing ion accessibility. Lastly, V_4C_3 MXene demonstrates excellent hydrophilicity, promoting effective interaction between the electrode and electrolyte, thereby further improving its electrochemical performance. Moreover, Shan et al. [238] reported the electrochemical behavior of V_2C MXene in three different aqueous electrolytes: $MgSO_4$, H_2SO_4, and KOH. Among these electrolytes, the highest specific capacitance for the V_2C MXene electrode was observed in a 1M H_2SO_4 electrolyte, reaching a value of 487 F/g at a scan rate of 2 mV/s with excellent stability of 99% after 10000 cycles at 10A/g. On the other hand, in 1M $MgSO_4$ and 1M KOH electrolytes, the specific capacitance values achieved were 225 F/g and 184 F/g, respectively, also at a scan rate of 2 mV/s. The higher specific capacitance of V_2C MXene in 1M H_2SO_4 compared to 1M $MgSO_4$ and 1M KOH is likely attributed to favorable chemical interactions, enhanced ion mobility, and the specific redox chemistry of sulfuric acid, which collectively contribute to improved capacitive performance. In addition, Syamsai et al. [158] investigated the supercapacitor performance of Vanadium carbide (V_4C_3) MXenes prepared through HF etching. The V_4C_3 MXenes electrode demonstrated an impressive high specific capacitance of 330 F/g at a scan rate of 5 mV/s in 1M H_2SO_4 electrolyte. Furthermore, the electrode exhibited excellent capacitance retention, maintaining 90% over 3000 cycles. Furthermore, Zhou et al. [206] conducted the synthesis of V_2CT_x MXenes specifically for application as supercapacitor electrodes in a seawater electrolyte. The V_2CT_x MXenes electrode demonstrated a noteworthy volumetric specific capacitance of 317.8 F/cm^3 when tested at 0.2 A/g in the seawater electrolyte. Additionally, the electrode exhibited excellent capacitance retention, maintaining 89.1% of its initial capacitance over 5000 cycles. These remarkable results can be attributed to the favorable interfacial contact between the V_2CT_x MXenes electrode and the electrolyte, which enables fast ion transport channels within the stimulating seawater electrolyte. Ming et al. [242] synthesized V_2CT_x MXenes electrodes for potassium ion capacitors. V_2C MXene was obtained by removing aluminum (Al) from V_2AlC MAX through a combination of LiF and HCl. The resulting V_2C MXene powders were then subjected to further processing with a 2 M KOH solution to obtain K-V_2C MXene, as illustrated in **Figure 9(a)**. Upon treatment, the morphology of K-V_2C MXene revealed an increased presence of pores and cracks compared to pristine V_2C MXene, as depicted in **Figure 9(b)-(c)**. Notably, K-V_2C MXene exhibited a significant enhancement in its ability to store K^+ ions in non-aqueous electrolytes compared to the original V_2C MXene. The K-V_2C MXenes device electrode demonstrated a maximum energy and power densities of 145 Wh/kg and 112.6 W/kg, as shown in **Figure 9(d)**. Guan et al. [243] synthesized V_2C MXene by etching V_2AlC powders using a mixture of LiF and HCl. The V_2C MXene electrode exhibited a specific capacitance of 164 F/g at 2 mV/s in 1M Na_2SO_4 electrolyte. The electrode demonstrated excellent capacitance retention of 90% after 10,000 cycles. Venkateshalu et al. [213] produced V_2NT_x MXene by removing "Al" from V_2AlN through V_2AlN powders in a LiF−HCl mixture. The V_2NT_x MXene material demonstrated a specific capacitance of 112.8 F/g at a current density of 1.85 mA/cm^2, and it retained 96% of its capacitance after 10,000 cycles in a 3.5 KOH electrolyte. The electrodes made from V_2NT_x MXene exhibited an energy and power densities of 15.66 W h/kg and 3748.4 W/kg. Furthermore, the aqueous asymmetric supercapacitor devices fabricated using V_2NT_x MXene as the negative electrode and Mn_3O_4 as the positive electrode. The specific capacitance of the device electrode was measured to be 23.5 F/g at a current density of 1.85 mA/cm^2. In their research, Chen et al [244]. employed a selective etching process to synthesize V_2CT_x MXene, which involved utilizing NaF and HCl to remove the aluminum (Al) layer from V_2AlC (MAX phase). SEM images of layered V_2CT_x MXene are depicted in **Figure 9(e)**. The resulting V_2CT_x MXene electrode displayed a specific capacitance of 481 F/g at 1 A/g. Remarkably, it exhibited a capacitance retention of 84% even over undergoing 60,000 charge-discharge cycles in a 2 M $ZnSO_4$ electrolyte. To further explore its potential, the researchers fabricated an aqueous asymmetric supercapacitor device utilizing V_2CT_x as anode as well as active carbon as cathode in a $ZnSO_4$ electrolyte, as demonstrated in **Figure 9(f)**. The CV curves of the assembled V_2CT_x//AC device maintain a distinct rectangle-like shape without noticeable distortion, demonstrating favorable rate performance (**Figure 9(g)**). Notably, the device's electrode exhibited a specific capacitance of 76 F/g at 1 A/g, while maintaining a capacitance retention of 79% after 100,000 cycles at 10 A/g, as depicted in **Figure 9(h)**. Additionally, the device electrode possessed notable energy density, power and energy densities values of 13.4 kW/kg as well as 17 Wh/kg. The exceptional specific capacitance observed in the V_2CT_x MXene electrode can be attributed to the intercalation and deintercalation of H^+ and Zn^{2+} ions between the layers of V_2CT_x MXene. This charge storage mechanism is visually illustrated in **Figure 9(i)**, providing a clear representation of the intercalation process.

Vanadium-based MXenes exhibit several inherent disadvantages that pose challenges to their effective utilization in supercapacitor applications. Notably, these materials demonstrate poor cyclic stability, experiencing gradual degradation in electrochemical performance over repeated charge and discharge cycles. Additionally, the complexity of their synthesis process contributes to difficulties in achieving scalability for large-scale production. While possessing high surface area and excellent conductivity, vanadium-based MXenes still exhibit relatively weak electrochemical performance in terms of specific capacitance and energy density, potentially limiting their competitiveness against alternative supercapacitor materials. Another drawback is their lower potential window, constraining the voltage range within which they can operate efficiently.

Despite these limitations, ongoing research is focused on optimizing the electrochemical performance of vanadium-based MXenes, involving refinement of synthesis methods, structural modifications, and integration strategies. This concerted effort aims to unlock their full potential and address the challenges associated with their practical implementation in supercapacitor technologies.

6.4. Molybdenum based MXene

Molybdenum-based MXenes, such as M_2CT_x, $M_3C_2T_x$, $M_4C_3T_x$, and $Mo_{1.33}C$ i-MXene, are attracting interest as potential electrode materials for electrochemical energy storage applications due to their exceptional electrical and mechanical properties [207,208]. These MXenes are derived from parent MAX phases by selectively etching away the A-group elements (such as aluminum (Al) and scandium (Sc)) to obtain the desired MXene structure [245-247]. $Mo_{1.33}C$ i-MXene, obtained by eliminating both Sc and Al from the $Mo_{2/3}Sc_{1/3}AlC$ i-MAX phase, has demonstrated an impressive volumetric capacitance of 1150 F/cm^3 [248-250]. This notable improvement in capacitance can be attributed to the presence of ordered vacancies within the MXene structure. These vacancies provide additional active sites for ion adsorption, leading to higher capacitance and improved energy storage performance [251]. Another important aspect contributing to the possibilities of molybdenum-based MXenes in energy storage devices is the ability of molybdenum to exist in multiple oxidation states [214,252]. Molybdenum ions can undergo reversible redox reactions, allowing for a wide range of electrochemical processes to occur within the MXene material. During charge and discharge cycles in an electrochemical energy storage device, ions can intercalate and deintercalate within the MXene structure, facilitated by these redox reactions [214,252]. This dynamic mechanism of Molybdenum ion intercalation facilitates efficient energy storage and retrieval, leading to improved device performance and higher energy densities. On the basis, He et al. [214] reported the impact of different electrolytes on the performance of Mo_2CT_x MXene. The Mo_2CT_x MXene electrode exhibited the maximum specific capacitance of 79.14 F/g at 0.3 A/g in H_2SO_4 electrolyte. In comparison, the specific capacitance was lower in 1 M KOH (11.27 F/g) and $MgSO_4$ (18.97 F/g) electrolytes, both at 0.3 A/g. The Mo_2CT_x MXene electrode demonstrated superior capacitance retention in the H_2SO_4 electrolyte, with 98% retention over 5000 cycles, whereas KOH showed 89.9% retention and $MgSO_4$ showed 96% retention. The higher performance observed in the H_2SO_4 electrolyte can be attributed to hydrogen (H) having the highest adsorption energy and the maximum number of atoms adsorbed. H atoms diffuse on the surface of Mo_2CO_2 MXene and directly attach to its surface, leading to enhanced performance. Furthermore, the researchers fabricated a solid-state symmetric supercapacitor device using two electrodes of Mo_2CT_x MXene with PVA/H_2SO_4 electrolyte. The device's Mo_2CT_x MXene electrode exhibited a specific capacitance of 64.74 F/g at scan rate of 0.2 A/g as well as demonstrated superior cyclic stability of 89.2% after 10,000 cycles. The device electrode achieved a maximum energy density of 16.0 Wh/L and a power density of 1449.1 W/L. Furthermore, Ghazaly et al. [70] synthesized $Mo_{1.33}C$ MXene for asymmetric supercapacitor devices utilizing LiCl electrolyte. The side view of the $Mo_{1.33}C$ MXene exhibited free-standing layered films with an average thickness of 5 μm, as depicted in **Figure 10(a)**. The $Mo_{1.33}C$ MXene electrode demonstrated a specific capacitance of 217 F/g at a scan rate of 2 mV/s and retained 85% of its capacitance after 7000 charging/discharging cycles in a 5 M LiCl electrolyte. For the fabrication of symmetric supercapacitor devices, $Mo_{1.33}C$ MXene served as the anode electrode, while Mn_xO_n was utilized as the cathode electrode, as shown in **Figure 10(b)**. The asymmetric supercapacitor devices exhibited a maximum gravimetric capacitance of 38 F/g at a scan rate of 2 mV/s, with a capacitance retention of 92% after 10,000 charging/discharging cycles, as depicted in **Figures 10(c)-10(f)**. The galvanostatic charge-discharge curves displayed a symmetric triangular shape without any noticeable IR drop, indicating the high reversibility of redox reactions at the $Mo_{1.33}C$ electrode/electrolyte interface. The device electrode achieved a maximum energy density of 19 Wh/kg and a power density of 1.08 W/kg. The presence of atomic vacancies within the $Mo_{1.33}C$ MXene structure significantly enhanced the diffusion as well as adsorption of Li-ions on the MXene surface. These atomic vacancies provided additional active sites for ion adsorption, leading to higher capacitance and improved overall performance of the supercapacitor device. Moreover, Etman et al. [199] reported the use of $Mo_{1.33}CT_z$ MXene in a symmetric supercapacitor device.. Cross-sectional scanning electron microscope (SEM) images revealed a morphology characterized by stacked flakes, as depicted in **Figure 10(g)**. The $Mo_{1.33}CT_z$ MXene exhibited excellent flexibility, as shown in **Figure 10(h).** The density of the $Mo_{1.33}CT_z$ MXene material was measured to be 3.5 g/cm^2. The $Mo_{1.33}CT_z$ MXene electrode demonstrated an impressive maximum volumetric capacitance of 681.5 F/cm^3 at 2 mV/s. To fabricate the symmetric supercapacitor device, two electrodes composed of $Mo_{1.33}CT_z$ MXene were employed, along with a LiCl electrolyte with a concentration of 19.5 M. The resulting $Mo_{1.33}CT_z$ MXene device exhibited a volumetric capacitance of 140 F/cm^3 at a scan rate of 2 mV/s, demonstrating a superior capacitance retention of 84.8% over 20,000 cycles. Furthermore, the device electrode displayed an energy density of 41.3 mWh/cm^3 and a power density of 165.2 mW/cm^3 as depicted in **Figure 10(i)**. Additionally, El-Ghazaly et al. [253] investigated the $Mo_{1.33}CT_z$ MXene in different electrolytes for supercapacitor application. They investigated the electrochemical behavior of $Mo_{1.33}CT_z$ electrodes in six different aqueous sulfate electrolytes, namely K_2SO_4, Na_2SO_4, Li_2SO_4, $ZnSO_4$, $MnSO_4$, and $MgSO_4$. Among these electrolytes, 1M $MnSO_4$ showed the highest specific capacitance of 185 F/g at a scan rate of 2 mV/s. Furthermore, the researchers fabricated symmetric and asymmetric supercapacitor devices using a 0.5 M K_2SO_4 electrolyte. The symmetric supercapacitor exhibited a capacitance of 24 F/g at 2 mV/s, with a cyclic stability of 82% after 5000 cycles. On the other hand, the asymmetric supercapacitor device exhibited a capacitance of 22 F/g at 2 mV/s, with a cyclic stability of 97% after 5000 cycles. The higher capacitance observed in the presence of Mn^{2+} in the $Mo_{1.33}CT_z$ electrodes can be attributed to several factors. Firstly, Mn^{2+} ions carry a double positive charge, making them more charge dense than Li^+, Na^+ and K^+ ions. This higher charge density allows for stronger electrostatic interactions between the Mn^{2+} ions and the negatively charged MXene surface. The stronger electrostatic interactions promote greater ion adsorption and thus increased capacitance. Secondly, Mn^{2+} ions have a larger atomic radius compared to other ions. The larger size of Mn^{2+} ions may facilitate their intercalation into the interlayer spaces of the MXene structure. The intercalation of Mn^{2+} ions provides more active sites for charge storage, leading to an increase in the overall capacitance of the electrode. Additionally, the specific intercalation mechanism of the $Mo_{1.33}CT_z$ MXene material may favor the intercalation of Mn^{2+} ions more effectively than Li^+ ions. The MXene structure and surface chemistry can influence the intercalation behavior of different cations. It is possible that the $Mo_{1.33}CT_z$ structure provides more favorable sites or channels for the accommodation of Mn^{2+} ions, resulting in a higher capacitance compared to other ions.

Building flexible hybrid supercapacitors using Molybdenum-based MXene electrodes presents several challenges. Firstly, achieving a robust interface between the flexible substrate and MXene electrode while maintaining mechanical integrity is complex. Secondly, optimizing the energy density and power density balance without sacrificing flexibility is demanding due to material limitations. Thirdly, ensuring long-term cycling stability and charge-discharge efficiency remains a hurdle due to potential MXene degradation. Moreover, integrating complementary components like current collectors and electrolytes seamlessly into the flexible design requires intricate engineering. Lastly, upscaling production while maintaining consistent performance raises manufacturing complexities. Overcoming these challenges is crucial for realizing efficient and durable flexible hybrid SCs based on Molybdenum-based MXene electrodes.

6.5. Tantalum based Mxene

Tantalum-based MXene, specifically Ta_4C_3 MXene, has garnered significant interest in the field of supercapacitors [254]. Researchers have been captivated by the potential of tantalum-based MXene owing to its range of desirable properties, which include flexible conductivity, superior thermal and chemical properties, extraordinary mechanical features, outstanding wear resistance, and superior heat resistance [209,210]. On the basis, Syamsai and colleagues synthesized Ta_4C_3 MXene by eliminating an intermediate Al from the initial Ta_4AlC_3 MAX phase using HF acid [254]. The resulting Ta_4C_3 MXene electrode displayed a specific capacitance of 481 F/g at 5 mV/s in a 0.1 M H_2SO_4 electrolyte. Notably, it exhibited cyclic stability of 89% over 2000 cycles. The synthesis process facilitated the efficient penetration of electrolytic ions into the Ta_4C_3 MXene electrode, creating a pathway for ion movement and enhancing the electrochemical activity. By providing a favorable pathway for ion movement, the synthesized electrode allowed for enhanced electrochemical activity. Furthermore, Rafieerad et al. [255] synthesized fluorine-free tantalum carbide MXene for supercapacitors applications. They achieved this by modifying the Ta_4AlC_3 MAX phase through selective etching of the aluminum (Al) atoms present on the edge and outer surface of the material using a KOH solution. This process resulted in the formation of oxidized

$Ta_4C_3T_x$ MXene nanosheets. The $Ta_4C_3T_x$ MXene electrode demonstrated a specific capacitance of 95 F/g at a scan rate of 1 mV/s in PVA/H_3PO_4 gel electrolyte.

Tantalum-based MXenes exhibit certain drawbacks that need to be carefully considered in their potential application for supercapacitors. One notable concern is the relative rarity and expense of tantalum as an element. This inherent scarcity could potentially hinder the widespread adoption of tantalum-based MXenes in supercapacitor applications, as the elevated cost associated with tantalum procurement might raise significant economic concerns. Furthermore, another limitation of tantalum-based MXenes pertains to their low cyclic stability. Over successive charge-discharge cycles, these materials can experience degradation, leading to a reduced lifespan and overall performance of supercapacitor devices.

Table 1 clearly indicate that Titanium-based MXene as well as Vanadium-based MXenes exhibit better energy density, specific capacitance, capacitance retention, surface area as well as power density in comparison to other MXene-based materials, including those based on Niobium, Molybdenum, and Tantalum. This superiority can be attributed to their distinct electronic and structural characteristics. The inherent properties of Titanium and Vanadium-based MXenes enable them to achieve higher energy storage capabilities. Their 2D layered structure provides a massive surface area, promoting efficient ion adsorption and enhanced charge storage capacity. Moreover, the unique combination of transition metal atoms in these MXenes facilitates enhanced electron mobility, which translates to higher power density during charge-discharge cycles. The electronic conductivity of both Titanium and Vanadium based MXenes is substantially higher compared to other MXenes, leading to reduced internal resistance and improved charge transport kinetics. This, in turn, results in lower energy losses during operation, contributing to the observed higher energy density. Additionally, the chemical stability of these MXenes, particularly Titanium-based ones, ensures prolonged cycling stability, making them ideal candidates for long-lasting supercapacitor applications. Furthermore, Niobium-based MXenes, Molybdenum-based MXenes, and Tantalum-based MXenes exhibit certain pros and cons. Niobium-based MXenes and Molybdenum-based MXenes have relatively low capacitances and energy densities compared to Titanium-based MXene as well as Vanadium-based MXenes because of their small surface and electric conductivity. Under certain conditions, tantalum-based MXenes have limited cycling stability and stability problems.

MXene-based materials offer several pros in the realm of energy storage technology. Firstly, their hydrophilic surface ensures high capacitance, making them efficient for storing and releasing electrical energy. Moreover, their superior conductivity facilitates swift charge transfer, thereby enhancing the performance of supercapacitor devices. Additionally, certain variants exhibit a wide voltage window, enabling the storage of higher energy densities compared to conventional electrode materials. Furthermore, the pseudocapacitive behavior of MXenes contributes to their electrochemical performance, further bolstering their appeal in energy storage applications. Another benefit lies in their larger interlayer spacing, which enhances ion transport and accessibility, ultimately improving overall capacitance. However, the utility of MXene-based materials is not without its challenges. One notable con is the intricate and potentially hazardous synthesis process involved. The use of hazardous chemicals poses scalability issues and hurdles in large-scale production. Furthermore, certain MXene variants, such as Niobium-based, Molybdenum-based, and Tantalum-based MXenes, suffer from limited cycle stability. Over repeated charge and discharge cycles, these materials may experience gradual degradation in their electrochemical performance, reducing their longevity and reliability. Despite these cons, ongoing research and development efforts aim to address these challenges and further unlock the potential of MXene-based materials for supercapacitor applications.

MXene-based materials show promising advantages when compared to other popular electrode materials in supercapacitors. In comparison to activated carbon, MXenes boast higher conductivity and potentially greater capacitance, although challenges remain in achieving equivalent energy density and cycle life [73,150]. When juxtaposed with carbon nanotubes and graphene, MXenes demonstrate comparable or even superior capacitance and conductivity [215]. Moreover, MXenes offer scalability advantages and can be tailored for specific electrochemical performances due to their versatile surface chemistry [256]. In contrast to pseudocapacitive materials such as TMOs, TMPs, TMNs and conducting polymers, MXenes typically exhibit higher conductivity and reversible charge storage [97].

7. Exploring Strategies for Engineering Electronic Structure in MXene based electrodes

While pure MXene exhibits excellent electrochemical properties, its long-term utilization or application in commercial settings with extended lifespan can lead to inherent layer restacking, resulting in denser structures during electrode preparation due to van der Waals interactions [257]. Consequently, MXene that has been used for an extended period of time suffers from certain shortcomings compared to freshly prepared pure MXene. These drawbacks include reduced electrode material stability, an unaffected microstructure, lack of retention, relatively smaller capacitance, as well as restricted electrolyte diffusion [65]. To overcome these challenges and achieve high-performance supercapacitor applications, there is a pressing need for promising modifications. There are several methods available to alter the electronic configuration of MXene including heterostructure-based MXene, heteroatom doping-based MXene, polymer-based

MXene, MXene-based composites, and ternary composite formation. This section provides an overview of various approaches aimed at enhancing the electrochemical performance of MXene.

7.1 Heterostructure- based MXene

Heterostructures have shown tremendous potential in increasing the supercapacitors performance of MXene-based electrodes [258]. By incorporating heterostructures into MXene electrodes, several performance enhancements can be achieved. Firstly, heterostructures can enhancing the MXene electrodes surface area [259]. The combination of MXene with other materials, such as metal oxides, metal sulfide, metal selenide, metal nitride, layered double hydroxides (LDH) and carbon-based materials, creates a hierarchical structure with multiple interfaces [259-262]. These interfaces provide additional active sites for charge storage, leading to a higher capacitance and improved energy storage capacity. Secondly, heterostructures can improve the charge transfer kinetics in MXene electrodes [263]. MXenes have high electrical conductivity but sometimes suffer from limited ion diffusion due to their interlayer spacing. By introducing heterostructures, the ion diffusion pathways can be optimized, facilitating faster ion transport and reducing the resistance at the electrode-electrolyte interface [261]. Furthermore, heterostructures can enhance the structural stability of MXene electrodes. MXenes are susceptible to volume changes and mechanical degradation during repeated charge-discharge cycles [264]. By integrating MXenes with other materials in a heterostructure, the overall mechanical integrity and stability of the electrode can be improved, leading to better long-term performance and cycling stability of supercapacitors [265]. On the basis, Wang et al. [258] synthesized 1T-MoS_2/Ti_3C_2 MXene heterostructure using high magnetic field hydrothermal method for flexible symmetric supercapacitor device. The resulting composite exhibited a 3D interconnected structure, enlarged interlayer spacing, improved conductivity, and excellent structural stability. The flexible symmetric supercapacitor fabricated using two 1T-MoS_2/Ti_3C_2 MXene electrodes and PVA-H_2SO_4 electrolyte. The symmetric supercapacitor devices show excellent areal capacitance of 347 mF/cm^2 at 2 mA/cm^2 and capacitance retention of 91.1% over 20000 cycles. The device shows power density of 600 µW/cm^2 and energy density of 17.4 µW/cm^2. The outstanding rate performance observed in the 1T-MoS_2/Ti_3C_2 MXene heterostructure can be attributed to the remarkable properties of Ti_3C_2 MXene, specifically its ultrafast electron transport capability. The unique two-dimensional structure of Ti_3C_2 MXene allows for the rapid movement of electrons within its layers, enabling efficient charge storage and transfer processes. Furthermore, the 1T-MoS_2/Ti_3C_2 MXene heterostructure benefits from the strong coupling between the high-capacitance 1T-MoS_2 nanosheets and the high-rate Ti_3C_2 MXene. The integration of these two materials creates a synergistic effect, combining the enhanced energy storage capacity of 1T-MoS_2 nanosheets with the superior charge/discharge capability of Ti_3C_2 MXene. As a result, the heterostructure exhibits exceptional electrochemical performance, combining both high energy storage capacity and the ability to handle rapid charge-discharge rates. Furthermore, Liu et al. [266] synthesized carbon/$Ti_3C_2T_x$ MXene heterostructures for supercapacitor applications. The resulting electrode demonstrated high specific capacitances of 247 F/g at 0.2 A/g, along with excellent cyclic stability of 96.9% over 10,000 cycles. This remarkable cyclic stability can be attributed to the presence of heterostructures in the electrode. Moreover, Rout et al. [265] synthesized VTe_2/$Ti_3C_2T_x$ MXene heterostructures using a facile hydrothermal method for supercapacitor applications. The VTe_2/$Ti_3C_2T_x$ MXene electrode demonstrated specific capacitances of 250 F/g at 0.25 A/g. Additionally, an aqueous asymmetric supercapacitor device was fabricated using VTe_2/MXene as the cathode electrode and MoS_2/MXene as the anode electrode, with a 0.5 M K_2SO_4 electrolyte. The device exhibited excellent energy density of 46.3

Wh/kg, power density of 400 W/kg, and remarkable stability of 87% over 7000 cycles. The synergistic interplaying effects induced by the heterostructures contribute to the enhanced supercapacitance performance of the MXene electrodes. In addition, Feng et al [267]. synthesized a $Ti_3C_2T_x$ MXene/1T-WSe_2 heterostructure for micro-supercapacitors. The solid-state symmetric micro-supercapacitor device was constructed with two $Ti_3C_2T_x$ MXene/1T-WSe_2 electrodes with a PVA-KOH electrolyte. The device had specific capacitance of 355.2 F/g at 1 A/g, with a remarkable cyclic stability of 99.8% after10,000 cycles. The device had energy and power densities of 32 µWh/cm^2 and 10.7 mWh/cm^2. Satish et al. [268] successfully synthesized 2D/2D Nb_2C/Ti_3C_2 MXene heterostructures for supercapacitor applications, showcasing sustainable cyclic stability. The schematic illustration of the synthesis process of Nb_2C/Ti_3C_2 MXene heterostructures is presented in **Figure 11(a)**. The layer morphology of the heterostructures can be observed in **Figure 11(b)**. The interconnected layers of Nb_2C and Ti_3C_2 MXenes promote enhanced charge storage dynamics as well as ion diffusion pathways within the heterostructure. This interconnected structure allows for efficient transport of ions, and electrons, facilitating rapid and reversible redox reactions during the charging and discharging processes. A solid-state symmetric supercapacitor device was constructed and assessed with two Nb_2C/Ti_3C_2 MXene electrodes and a gel PVA/H_2SO_4 electrolyte, as depicted in **Figure 11(c)**. The symmetric device had energy density of 12.3 Wh/kg, as shown in **Figure 11(d).** Furthermore, the device demonstrated outstanding cyclic stability, maintaining 98% of its capacity over 50,000 cycles, as depicted in **Figure 11(e)**. The excellent cyclic stability observed in the Nb_2C/Ti_3C_2 MXene heterostructures can be attributed to several factors. The 2D/2D heterostructure design allows for enhanced charge transfer kinetics as well as the efficient utilization of the electrode materials. Additionally, interfacial interactions between Nb_2C and Ti_3C_2 MXene layers contribute to the structural integrity and prevent degradation during cycling. Furthermore, the gel PVA/H_2SO_4 electrolyte provides a stable environment for ion transport and suppresses side reactions, thereby promoting long-term stability. Furthermore, Sathish et al. [269] demonstrated the synthesis of 2D/2D MXene/boron carbon nitride (BCN) heterostructures for supercapacitor applications. The fabrication process of the MXene/BCN heterostructure is illustrated in **Figure 11(f)**. The solid-state symmetric supercapacitors fabricated and assessed using two MXene/BCN electrodes with a PVA/H_2SO_4 electrolyte. The resulting devices are depicted in **Figure 11(g)**. The MXene/BCN heterostructure exhibited outstanding capacitance performance of 245 F/g at 1 A/g. Moreover, the device demonstrated exceptional capacitance retention, maintaining 100% of its initial capacitance over an impressive 100,000 cycles. This remarkable cyclic stability indicates the long-term durability and reliability of the MXene/BCN heterostructure. In terms of energy storage, the device exhibited an excellent energy density of 22 Wh/kg and the power density of the device reached 8004 W/kg, indicating its high-power delivery capability as shown in **Figure 11(h)**. The in-situ growth of BCN nanosheets on the surfaces of MXene creates an interconnected conductive network. This network facilitates rapid electron transport throughout the electrode, reducing internal resistance and enabling high-rate charge/discharge processes. The presence of this conductive network enhances the overall capacitance as well as the energy storage capabilities of the supercapacitor. Additionally, the MXene/boron carbon nitride heterostructure exhibits a wide potential window, which refers to the range of voltages over which the supercapacitor can operate effectively. The wider potential window enables the utilization of a larger voltage range, resulting in increased energy storage capacity and higher specific capacitance. Gogotsi et al. [270] synthesized a flexible MXene/rGO heterostructures using electrostatic self-assembly. The hybrid structure achieved improved interlayer spacing and prevented restacking, resulting in better ion channels and increased active surface sites. The electrode had volumetric capacitance of 1040 F/cm^3 at 2 mV/s as well as cyclic stability of 61% over 20000 cycles. In addition, symmetric supercapcitor device exhibited energy density of 32.6 Wh/L and power density of 74.4 kW/L.

Nowadays, MXene on Transition metal double-layer hydroxides (LDH) heterostructures have emerged as highly attractive materials for supercapacitors owing to their exceptional theoretical capacitance, affordable price, as well as enabling high pseudocapacitance through increased oxidation numbers [262,271,272]. Moreover, their composition can be easily tuned, allowing for the development of novel morphologies and leveraging their outstanding physical and chemical properties [273,274]. On the basis, Wang et al. [275] investigated $V_4C_3T_x$ to develop a NiCoAl-LDH/MXene heterostructure for hybrid supercapacitors. The interconnected microstructure was achieved through in-situ formation of LDH on HF-etched MXene, forming a conductive network. The electrode exhibited capacitance of 627 C/g at 1 A/g as well as rate capacity of 300 C/g at 20 A/g. The hybrid supercapacitor fabiricated using positive electrode as a NiCoAl-LDH/MXene as well as AC negative electrode. Device had maximum energy density of 71.7 Wh/kg and power density of 20 kW/kg. The exceptional supercapacitors performance of the $V_4C_3T_x$ MXene/NiCoAl-LDH heterostructure can be attributed to its interconnected conductive network, enabling efficient ion transport and rapid charge transfer, leading to high capacitance and excellent rate capability. Similarly, Hui et al. [262] synthesized binder-free $Ti_3C_2T_x$ MXene/NiCo LDH heterostructure was synthesized on nickel foam using an in-situ electrodeposition method. The electrode exhibited capacitance of 983.6 F/g at 2 A/g. Flexible solid-state asymmetric supercapacitor constructed using MXene/NiCo LDH as the positive electrode as well as multiwalled CNTs as the negative electrode. The device had maximum energy and power densites of 36.7 Wh/kg as well as 14400 W/kg. The heterostructure provided enhanced ion/electron paths and increased active sites, leading to the larger faradaic capacitance.

DFT studies offer a profound understanding of the mechanisms behind the enhanced capacitance observed in the rosette-like V-(Ni,Co)Se_2@Nb_2CTx MXene (V-NCSN) heterostructure with abundant Se vacancies, as reported by Shen et al. [276]. The investigation begins by scrutinizing the special heterogeneous interface and vacancy structure within the V-NCSN material. Through systematic characterization and computational simulations, it becomes apparent that these structural features fundamentally modulate the electron structure of the host material. Specifically, the presence of Se vacancies alters the adsorption energy of OH^- ions, leading to a more favorable interaction with the V-NCSN electrode compared to the pristine NCSN material. This phenomenon results in an increased affinity for OH^- ions, thereby enhancing the kinetics of the V-NCSN electrode. Moreover, the unique heterostructure and vacancy-rich environment contribute synergistically to elevate the overall capacitance of the V-NCSN electrode. These findings shed light on the intricate interplay between structure and electrochemical performance in MXene-based materials, offering valuable insights for the design of high-performance energy storage devices.

Furthermore, Yang et al. [277] reported Density functional theory studies on Ni-MOF/V_2CT_x–MXene heterostructures for supercapacitor applications. They further investigated the interfacial interaction via the Ni–O–V bonds between Ni- terephthalic acid (BDC) and V_2CT_x at the heterojunction. DFT calculations on the Density of States (DOS) of Ni-BDC and MOF/MXene were carried out to explore this interaction. The calculated model structure of the heterogeneous MOF/MXene was illustrated, revealing a discontinuous DOS near the Fermi level for Ni-BDC, indicating its semiconductor behavior. Conversely, MOF/MXene showed an increased energy state near the Fermi level, suggesting improved electronic conductivity as shown in **Figure 11 (i).** To validate these theoretical findings, UV-vis absorption spectroscopy was performed. The results showed that V_2CT_x exhibited metallic properties with full frequency absorption, while MOF/MXene displayed intrinsic absorption with a redshift compared to Ni-BDC, indicating reduced bandgap and enhanced conductivity upon incorporating V_2CT_x into Ni-BDC. Interestingly, MOF/MXene exhibited even higher intrinsic conductivity, attributed to strong interfacial interactions. The results collectively demonstrate that heat treatment positively affects the construction of heterogeneous interfacial structures, leading to abundant Ni–O–V bridging bonds in MOF/MXene/NF. This enhancement in interfacial structure contributes to increased overall conductivity and higher valence state of V ions, suggesting the potential for high-performance supercapacitors using the MOF/MXene/NF electrode. Additionally, the study conducted by Shen et al. [278] investigates the electrochemical behavior and electronic properties of a heterostructure comprising $NiCo_2O_4$ and Nb_2CT_x MXene using DFT analysis. Through computational modeling, the study elucidates the chemical bond formations at the interface between Co–O bonds in $NiCo_2O_4$ and Nb_2CT_x MXene, highlighting their role in regulating the charge density crucial for redox reactions. DFT calculations reveal that the introduction of Nb_2CT_x MXene enhances the adsorption energy of OH− ions onto the composite surface, facilitating more favorable redox reactions. Analysis of the Density of States (DOS) and Partial Density of States (PDOS) indicates a significant improvement in electrical conductivity in the composite material compared to pure $NiCo_2O_4$, attributed to enhanced charge transfer performance due to the presence of Nb2CTx MXene. Further insights into orbital interactions demonstrate an enhanced state near the Fermi level after hybridization with Nb_2CT_x MXene, indicative of improved charge transfer capabilities. Additionally, charge density differences reveal electron migration from $NiCo_2O_4$ to the Nb_2CT_x MXene surface, affecting the Fermi level and electrical conductivity of the composite material. Overall, these findings highlight the beneficial effects of Nb_2CT_x MXene in enhancing the energy storage capacity and rate capability of the $NiCo_2O_4@Nb_2CT_x$ MXene composite, making it a promising candidate for applications such as supercapacitors.

7.2 Heteroatom doping

Heteroatom doping has emerged as a widely adopted strategy to increase the specific capacitance, superior stability, massive conductivity as well as it has proven particularly effective in improving the properties of MXenes [202,279]. However, their electrochemical performance can be further optimized by incorporating heteroatoms such as boron (B), nitrogen (N), phosphorus (P), and sulfur (S) into their structures [280-282]. The introduction of boron into MXenes offers several advantages. Boron doping enhances the electrical conductivity of MXenes, making them more efficient for charge transfer during electrochemical reactions [280,283]. Moreover, it improves the hydrophilicity of MXenes, promoting better interaction with the electrolyte and facilitating ion transport across the electrode-electrolyte interface. Additionally, boron doping can increase the pseudocapacitance of MXenes, resulting in enhanced energy storage capability as well as improved cycling stability [280]. Similarly, nitrogen doping has been widely employed to modify MXene properties. Nitrogen-doped MXenes exhibit enhanced electrical conductivity, mainly attributed to the introduction of electron-rich nitrogen atoms that promote charge transfer [281]. Furthermore, nitrogen doping increases the surface wettability of MXenes, allowing for better electrolyte infiltration and enhanced ion accessibility [279]. This, in turn, improves the overall electrochemical performance, especially in terms of capacitance and rate capability [284].

Phosphorus and sulfur doping have also shown promise in optimizing MXene performance [285,286]. Phosphorus-doped MXenes exhibit improved electrical conductivity due to the presence of extra electrons provided by phosphorus atoms [285]. Moreover, phosphorus doping enhances the hydrophilicity and pseudocapacitive behavior of MXenes, leading to improved charge storage capacity and electrochemical performance [282]. Similarly, sulfur doping can enhance the electrical conductivity of MXenes while also introducing additional active sites for redox reactions, thereby enhancing their pseudocapacitive behavior [286]. On the basis Tang et al. [287] synthesized N-doped m-$Ti_3C_2T_x$ using hydrothermal reaction. The specific capacitance of the material was effectively doubled through N doping, with synergistic benefits stemming from the advancements in both conductivity and pseudocapacitance. Wen et al. [279] conducted a synthesis of N-doped $Ti_3C_2T_x$ by subjecting $Ti_3C_2T_x$ to post-etch annealing in ammonia. The N-doped $Ti_3C_2T_x$ electrode demonstrated a specific capacitance of 192 F/g at 1 mV/s in a 1M H_2SO_4 electrolyte. This value is significantly higher compared to the specific capacitance of the undoped $Ti_3C_2T_x$ electrode materials, which recorded 34 F/g at the same scan rate. The presence of nitrogen (N) in N-doped MXenes demonstrates a synergistic effect that arises from two key factors: an enlarged interlayer distance and the presence of N-containing functional groups. This effect is particularly significant in N-doped $Ti_3C_2T_x$ MXene materials. In undoped $Ti_3C_2T_x$ MXenes, the contribution to capacitance comes from two sources: electrical double-layer capacitance and pseudocapacitance resulting from the oxidation of titanium (Ti) species. However, in N-doped $Ti_3C_2T_x$ electrodes, the increased interlayer spacing plays a crucial role in enhancing its capacitance. The enlarged interlayer distance in N-doped $Ti_3C_2T_x$ MXene provides several benefits. Firstly, it creates more room between the MXene layers, allowing for increased ion diffusion and improved accessibility of electrolyte ions to the electrode surface. This, in turn, enhances the electrochemical reactions and increases the charge storage capacity. Secondly, the presence of N-containing functional groups introduces additional redox-active sites, contributing to the overall pseudocapacitance of the material. The combination of an enlarged interlayer distance and N-containing functional groups in N-doped $Ti_3C_2T_x$ MXene materials leads to improved capacitance performance. This synergistic effect facilitates enhanced energy storage capabilities. Moreover, Yang et al. [288] conducted a synthesis of N-doped $Ti_3C_2T_x$ electrode materials, which demonstrated a remarkable high-capacity performance. Specifically, the N-doped $Ti_3C_2T_x$ electrode exhibited a specific capacitance of 126 F/g when tested at 2 A/g in a 6 M KOH solution. This capacitance value is significantly higher compared to the undoped $Ti_3C_2T_x$ electrode, which recorded a specific capacitance of 92 F/g under the same conditions. In addition, The N-doped $Ti_3C_2T_x$ electrode exhibited exceptional capacitance retention of 86.4% over 2000 cycles. The same research group extended their study by co-doping $Ti_3C_2T_x$ with both nitrogen (N) and sulfur (S) using thiourea as a source for both dopants [289]. This co-doping strategy resulted in a significant enhancement in the electrode performance. The co-doped $Ti_3C_2T_x$ electrode had a specific capacitance of 175 F/g at 2 mV/s in a Li_2SO_4 electrolyte. This notable improvement highlights the synergistic effect of N and S co-doping, further enhancing the electrochemical performance of the $Ti_3C_2T_x$ electrode material [289]. Yang et al. [286] conducted a study in which they synthesized nitrogen-sulfur co-doped $Ti_3C_2T_x$ MXene for supercapacitor applications. The schematic illustration of the nitrogen-sulfur MXene. The researchers also investigated the electrochemical properties of undoped $Ti_3C_2T_x$ MXene, sulfur-doped (S)- $Ti_3C_2T_x$ MXene, and nitrogen-sulfur doped (NS)- $Ti_3C_2T_x$ MXene. Based on their findings, the CV curve area of the nitrogen-sulfur doped (NS)-MXene was higher compared to both undoped $Ti_3C_2T_x$ MXene and sulfur-doped (S)- $Ti_3C_2T_x$ MXene. This suggests that the nitrogen-sulfur doped

$Ti_3C_2T_x$ MXene exhibited enhanced electrochemical performance. Furthermore, the nitrogen-sulfur doped (NS)- $Ti_3C_2T_x$ MXene demonstrated the highest specific capacitance of 495 F/g in a 1 M H_2SO_4 electrolyte. In comparison, the undoped $Ti_3C_2T_x$ MXene and sulfur-doped $Ti_3C_2T_x$ MXene (S-MXene) showed specific capacitances of 446 F/g**.** Additionally, the nitrogen-sulfur doped $Ti_3C_2T_x$ MXene exhibited superior cyclic stability performance of 98% over 6000 cycles at 50 mV/s. The enhanced electrochemical performance of the nitrogen-sulfur doped $Ti_3C_2T_x$ MXene can be attributed to changes in its electronic structure. The incorporation of nitrogen and sulfur atoms into the $Ti_3C_2T_x$ MXene lattice results in modifications in the material's physical as well as properties, which can facilitate improved ion transfer kinetics during the processes of charging and discharging. Additionally, the nitrogen and sulfur co-doping process leads to an expansion of the interlayer spacing within the MXene structure. This expanded interlayer spacing creates more available active sites within the material, which can facilitate a higher intercalation capacity. The increased number of active sites allows for more efficient adsorption and desorption of ions during the charge storage process, contributing to the improved electrochemical performance. Furthermore, Kaewpijit et al. [290] reported on the use of Mxene/N, S doped graphene electrode for supercapacitor applications. The Mxene/N, S doped graphene electrode demonstrated a maximum specific capacitance of 599.7 F/g at 1 A/g in a 6M KOH, which is three times higher than the specific capacitance of the pristine Mxene electrode (185.8 F/g at scan rate of 1 A/g). Furthermore, Que and colleagues designed a freestanding nitrogen-doped Ti_3C_2 (MD-Ti_3C_2) film through a solvothermal method using diethanolamine as a nitrogen source in methanol (MT) [291]. The addition of nitrogen elements into the 2D MXene sheets was facilitated by MT, resulting in the formation of high-quality MD-Ti_3C_2 as shown in **Figure 12 (a)**. An SEM image showcasing a fractured surface of the MD-Ti_3C_2 film suggests a relatively favorable alignment of flakes, as presented in **Figure 12(b)**. The inset, which includes SEM images, demonstrates the flexible MD-Ti_3C_2 film. The MD-Ti_3C_2 film exhibited an ultrahigh capacitance of 3123 F/cm^3 at 5 mV/s, which was significantly higher compared to the pure Ti_3C_2 capacitance of 2042.4 F/cm^3 at the same scan rate as shown in **Figure 12(c).** The MD-Ti_3C_2 electrode demonstrated excellent capacitance retention of 100% over 10,000 cycles. The enhanced conductivity, enlarged interlayer spacing, and rapid intercalation kinetics contributed to the outstanding electrochemical performance. Moreover, Pan et al. [292] synthesized nitrogen (N) as well as oxygen (O) co-doped C@Ti_3C_2 Mxene for solid-state symmetric supercapacitor devices. The synthesis process of N, O co-doped C@Ti_3C_2 is illustrated in **Figure 12(d)**. The N, O-doped C@Ti_3C_2 Mxene electrode demonstrated superior specific capacitance of 250.6 F/g at 1 A/g, which is three and a half times higher than that of the pristine Ti_3C_2 Mxene (50.1 F/g at 1 A/g). Additionally, the symmetric supercapacitor devices exhibit rectangular CV curves, as seen in **Figure 12(e)**. Notably, these devices demonstrated excellent specific capacitances of 93.9 at 1 A/g, with a superior capacitance retention of 90% over 5000 cycles, as depicted in **Figure 12(f).** The device possessed a maximum energy density of 10.8 Wh/kg and a power density of 600 W/kg, as shown in **Figure 12(g)**. The observed intercalation-pseudocapacitance in the system is primarily generated by rapid as well as the reversible surface redox reactions attributed to the presence of Ti_3C_2 and N/O functional groups in carbon materials. These phenomena are depicted in **Figure 12(h)**. The intercalation process involves the insertion of ions or molecules between the layers of the material, leading to changes in the interlayer spacing and resulting in additional capacitance. In this case, the intercalation of ions or molecules within the Ti_3C_2 layers contributes to the intercalation-pseudocapacitance effect. Furthermore, the pseudocapacitance arises from the reversible redox reactions on the surface of Ti_3C_2 and N/O functional groups in the carbon materials. These redox reactions involve the transfer of electrons and ions between the surface and the electrolyte. The fast and reversible nature of these redox reactions enables efficient charge storage and rapid energy exchange during charge-discharge cycles.

7.3. Polymer based MXenes

Polymers have indeed attracted significant attention in the field of electronics, primarily due to their intrinsic flexibility, light weight, and low cost [293,294]. However, by combining polymers with MXene compounds, the performance of materials can be significantly enhanced in multiple areas. These advancements encompass improved thermal stability [295], enhanced mechanical properties [293,295], and heightened electrical conductivity [296]. The synergistic effect of MXene and polymer composites paves the way for the development of high-performance supercapacitors with enhanced energy storage capabilities. According to the study conducted by Ling et al. [297], they discovered that by intercalating polyvinyl alcohol (PVA) between the layers of $Ti_3C_2T_x$, a remarkable volumetric capacitance of 523 F/cm^3 was achieved at a scanning rate of 2 mV/s^1. Additionally, this composite exhibited superior flexibility compared to the pure $Ti_3C_2T_x$ film, with a tensile strength of 91 MPa when PVA was loaded at 60 wt%, in contrast to the tensile strength of 22 MPa observed in the pure $Ti_3C_2T_x$ film. In addition to nonconductive polymers like PVA, conductive polymers including (i) polypyrrole (PPy), (ii) polyaniline (PANI), as well as (iii) poly(3,4-ethylenedioxythiophene) (PEDOT) have been extensively studied and combined with MXene to develop composite supercapacitor electrodes [298].

7.3.1 Polypyrrole (PPy):

In the context of supercapacitors, the utilization of polypyrrole (PPy) as the active material demonstrates a notable capacitance range, reaching between 400-500 F/cm³ [299-303]. Moreover, PPy possesses excellent mechanical flexibility, which further enhances its suitability for supercapacitor applications. Furthermore, the combination of MXene with PPy in composite materials has an additional advantage [304]. MXene is a two-dimensional material composed of nanosheets, and one challenge in utilizing MXene in composites is the restacking or aggregation of these nanosheets, which can hinder its performance. However, when MXene is combined with PPy, it has been observed that the restacking of MXene nanosheets is significantly reduced [303,305]. For instance, Gogotsi et al. [306] synthesized $Ti_3C_2T_x$/PPy through an in situ oxidant-free polymerization process of pyrrole between $Ti_3C_2T_x$ flakes. PPy chains have been intercalated as well as aligned inside $Ti_3C_2T_x$ monolayers during the synthesis process. This unique arrangement of PPy within the $Ti_3C_2T_x$ structure introduced additional electrochemically active sites and effectively suppressed the $Ti_3C_2T_x$ restacking of nanosheets, leading to the creation of an unchanging hybridized structure. The layered architecture of the $Ti_3C_2T_x$/PPy composite electrode exhibited an high capacitance of approximately 416 F/g at 5 mV/s and impressive volumetric capacitance of 1000 F/cm³ in a 1 M H_2SO_4 electrolyte. Furthermore, the composite electrode demonstrated exceptional capacitance retention, with 92% retention even after 25,000 cycles of charge-discharge testing. The high electrochemical performance and exceptional cycle life of the $Ti_3C_2T_x$/PPy composite electrode can be attributed to its unique self-assembled layered architecture, wherein aligned PPy is confined between the conductive monolayers of $Ti_3C_2T_x$. This layered structure offers several advantages that contribute to the improved performance of the electrode. Firstly, the aligned PPy chains within the $Ti_3C_2T_x$ layers enable high electronic conductivity throughout the composite electrode, facilitating efficient charge transfer and resulting in faster reversible redox reactions during the charge-discharge process. The presence of conductive PPy enhances the overall conductivity of the composite, enabling better electron transport within the electrode material. Additionally, the self-assembled layered architecture provides short diffusion pathways for ions, promoting rapid ion transport within the electrode. This enhances the overall electrochemical performance by facilitating faster ion diffusion and reducing the resistance to ion movement during the charge-discharge process. The enhanced capacitance observed in the $Ti_3C_2T_x$ /PPy composite electrode is a result of the synergistic effects of two key factors. Firstly, the PPy between the $Ti_3C_2T_x$ layers increases interlayer spacing, creating more room for ion adsorption and enhancing the overall capacitance of the electrode. Secondly, surface redox processes of both PPy as well as MXene contribute to overall capacitance by providing additional electrochemically active sites for charge storage. Moreover, Ma et al. [307] developed a flexible textile-based electrode using electrochemically depositing PPy onto a cotton textile coated with $Ti_3C_2T_x$. The $Ti_3C_2T_x$/PPy exhibited a significantly higher capacitance compared to the pristine $Ti_3C_2T_x$ MXene electrode (114 F/g). Specifically, the $Ti_3C_2T_x$ /PPy composite electrode demonstrated a higher capacitance of 343.2 F/g. Furthermore, the solid-state symmetrical supercapacitors device fabricates using two MXene–PPy electrode with H_2SO_4/PVA gel electrolyte. MXene–PPy textiles device exhibited maximum energy density of 1.30 mW h/g and power density of 41.1 mW/g. This improvement in capacitance can be attributed to the synergistic effects of the $Ti_3C_2T_x$ and PPy in the composite electrode. The $Ti_3C_2T_x$ coating provides a conductive framework and increased surface area, enabling efficient charge storage. Meanwhile, the electrochemically deposited PPy enhances the conductivity and contributes to additional charge storage through redox reactions. Furthermore, Pumera et al. [308] synthesized a composite of MXene Ti_3C_2 nanosheets as well as ppy-carboxymethylcellulose nanospheres (Ti_3C_2@PPy-

CMC) for use in wearable flexible supercapacitors. Sweat was used as the electrolyte. The process involved creating symmetrical flexible supercapacitors by layering two Ti_3C_2@PPy-CMC nanosheet electrodes in opposite directions, separated by a separator (as depicted in **Figure 13(a)).** This sweat-rechargeable setup was then incorporated into a patch configuration, where flexible supercapacitors were directly attached to a commercially available medical patch (as shown in **Figure 13(b)**). The practical application of the Ti_3C_2@PPy-CMC composite-coated fabric electrode entails assembling symmetrically configured flexible supercapacitors. This assembly process utilizes an artificial sweat electrolyte. The electrochemical performance of the flexible supercapacitors patch was evaluated under varying sweat electrolyte exposure levels. It was attached to fabric and operated for durations of 30, 45, and 60 minutes, showing partial wetting after 30 minutes and full wetting after 60 minutes. The galvanostatic charge-discharge (GCD) profile **(Figure 13c inset)** highlighted the relationship between exercise time, discharge time, and sweat concentration, with increasing discharge time during running. The patch demonstrated lower specific capacitance initially, but at 45 and 60 minutes, specific capacitance rose to 12.2 F/g as well as 19.3 F/g, respectively (**Figure 13c)**. In intense sweating, the fabricated patch achieved peak energy density and power density of 0.43 Wh/kg at 93 W/kg depicted in **Figure13(d).** Under partial sweating, it achieved E of 71 mWh/kg at 1 A/g. The Ti_3C_2@PPy-CMC flexible supercapacitors' performance in real sweat electrolyte surpassed previous reports. Additionally, two interconnected flexible supercapacitors were fully wetted during extended runs. When charged to 1.6 V, they powered a red LED for 7 seconds **(Figure 13e),** showcasing the patch's capability using real sweat electrolyte. With its lightweight, flexible nature, easy integration onto clothing, and enhanced wearer comfort, the flexible supercapacitors power patch holds promise for wearable applications. The flexible supercapacitors patch was placed on various body areas: fingers, foot sole, and wrist. After a 45-minute jog with finger and foot sole attachment, foot sole's CV curve showed slightly lower current density due to fewer sweat glands. Higher gland density in fingers led to quicker sweat secretion. Wrist, with minimal secretion, had much lower current density due to insufficient sweat to wet the patch. GCD profiles (**Figures 13(f))** showed specific capacitance values: finger - 14.08 F/g, foot sole - 22.3 F/g, wrist - 9.04 F/g. For skin comfort assessment, the flexible supercapacitors patch was worn for 4 hours, maintaining color despite sweat, and no skin inflammation upon removal, credited to sweat-absorbing textile and microporous medical features

7.3.2 Polyaniline (PANI)

The PANI/MXene composite demonstrates superior electrochemical performance primarily attributed to two key factors: the high conductivity and interconnectivity of the redox-active PANI and the synergy effect between the components [309,310]. Firstly, the high conductivity (0.5-5 S/cm) of PANI contributes to efficient charge transfer within the composite electrode, enabling rapid redox reactions and improved electrochemical performance [310]. The conducting polymer PANI facilitates the movement of electrons, enhancing the overall conductivity of the composite material [311]. Secondly, the interconnectivity of the redox-active PANI within the MXene structure plays a crucial role in achieving superior electrochemical performance [309]. The PANI is intimately integrated with the MXene, forming a well-dispersed and interconnected network [311]. This interconnectivity maximizes the utilization of the redox-active PANI, leading to enhanced charge storage capacity and improved overall electrochemical performance [309,311]. In recent times, PANI has gained significant attention and has been widely utilized for the preparation of MXene-based supercapacitor composite materials [311,312]. On the basis, Wang et al. [313] synthesized PANI/V_2C MXene for supercapacitor device performances.

The PANI/V_2C MXene electrode demonstrated a maximum specific capacitance of 337.5 F/g at 1 A/g. The asymmetric supercapacitor device has been manufactured utilizing PANI/V_2C MXene as the positive electrode, active carbon as the negative electrode, and H_2SO_4/PVA gel electrolyte. The asymmetric supercapacitor device exhibited a maximum energy density of 12.25 Wh/kg and a power density of 415.38 W/kg, with a capacitance retention of 97.6% over 10,000 cycles. Additionally, Fu et al. [309] presented a novel composite electrode consisting of graphene encapsulated $Ti_3C_2T_x$ MXene intercalated with PANI chains. PANI chains were used to electrostatically assemble graphene and $Ti_3C_2T_x$ nanosheets during the assembly process. The resulting electrode demonstrated excellent electrochemical performance. $Ti_3C_2T_x$ MXene/ PANI electrode exhibited a gravimetric capacitance of 635 F/g at 1 A/g in a 1 M H_2SO_4, corresponding to a volumetric capacitance of 1143 F/cm^3. The electrodes show outstanding capacitance retention of 97.54% over 10000 cycles. The excellent supercapacitor device performance of the composite electrode due to the PANI chains were strongly intercalated within the multi-layered $Ti_3C_2T_x$, promoting enhanced charge storage capabilities. In a related study, Lin et al. [311] successfully synthesized an electrode for supercapacitor applications by combining $Ti_3C_2T_x$ MXene with PANI. The resulting $Ti_3C_2T_x$ MXene/polyaniline composite exhibited a specific capacitance of 496.5 F/g at a current density of 1 A/g in 1M H_2SO_4 electrolyte. This specific capacitance was notably higher than that of the pure MXene electrode (38.2 F/g at 0.5 A/g) and the PANI electrode (295.1 F/g at 1 A/g). Moreover, the $Ti_3C_2T_x$ MXene/polyaniline electrode demonstrated outstanding capacitance retention, reaching 91.6% over the course of 5000 cycles. This substantial increase in capacitance, ten times higher than that of the pristine MXene, can be attributed to the efficient transport of ions and electrons, as well as the heightened electrochemical activity of the $Ti_3C_2T_x$/PANI composite compared to the pristine MXene material. In a related study, Liu et al.

[314] fabricated a flexible solid-state symmetric supercapacitor device by integrating PANI into a $Ti_3C_2T_x$ MXene electrode(I-PANI/ MXene). The synthesis process of the PANI/$Ti_3C_2T_x$ MXene electrode is depicted in the **Figure 13(g)**. The PANI/$Ti_3C_2T_x$ MXene electrode exhibited significantly enhanced volumetric capacitance, reaching 1360 F/cm^3, along with a higher gravimetric capacitance of 385 F/g. These values outperform those of the pristine MXene material. The improved electrochemical characteristics of the I-PANI/MXene electrode can be attributed to the ice-assisted PANI intercalation mechanism. This mechanism effectively reduces the self-restacking tendency of MXene, leading to increased interlayer spacing as depicted in the **Figure 13(h)**. As a result, a more accessible surface is formed, promoting rapid ion diffusion and transport throughout the charge/discharge cycle. Moreover, a symmetric supercapacitor was fabricated using pairs of I-PANI/MXene film electrodes and PVA–H_2SO_4 gel-based electrolyte and separator, as depicted in **Figure 13(i).** The device showed a remarkable highest specific capacitance of 103 F/g at 1 A/g in a PVA/H_2SO_4 gel electrolyte. Furthermore, the electrode demonstrated excellent capacitance retention of 93% over 1000 cycles when subjected to various bending angles, including 0˚, 30˚, 90˚, and 180˚. Additionally, the device exhibited energy and power densities of 13.1 Wh/kg and 425 W/kg, respectively as depicted in **Figure 13(k)-(l)**. The superior capacitance performance of PANI and MXene arises from their excellent conductivities, which synergistically enhance the charge transfer of the redox reactions at the contact interface. This synergy also contributes to achieving an ultra-high rate capability. The minimal incorporation of PANI within/between MXene layers serves to preserve MXene's high energy storage characteristics while also preventing direct contact between oxygen and MXene. As a result, this configuration leads to both massive capacitance as well as superior capacitance retention for the I-PANI/MXene electrode.

7.3.3 Poly(3,4-ethylenedioxythiophene) (PEDOT)

PEDOT:Polystyrene sulfonate (PEDOT:PSS) has gained recognition as a promising material for supercapacitors due to its advantageous features, including a large voltage operating window**,** swift electrochemical reaction, as well as superb film-forming features [299]. To further enhance the supercapacitor performance, researchers have investigated the combination of PEDOT with MXenes materials. The incorporation of MXenes into PEDOT:PSS composites has demonstrated a notable effect on the interlayer spacing between MXene layers [315]. This expansion of interlayer spacing results in increased exposure of electroactive surfaces, leading to enhanced supercapacitance performance. By utilizing MXenes as additives, the PEDOT-based supercapacitors exhibit improved supercapacitors performance. On the basis, Qin et al. [315] fabricated a flexible solid-state supercapacitor through $Mo_{1.33}C$ MXene as well as PEDOT: poly(styrenesulfonic acid) (PSS). The active electrodes of the supercapacitor were composed of aligned layer composite films, which were formed by vacuum filtration of $Mo_{1.33}C$ MXene and a PEDOT: PSS-based solution. The $Mo_{1.33}C$ MXene/PEDOT: PSS electrode exhibited a high specific capacitance of 568 F/cm^3 at 0.5 A/cm^3, which is higher than the capacitance of the pristine $Mo_{1.33}C$ MXene electrode (301 F/cm^3 at 0.5 A/cm^3). The solid-state $Mo_{1.33}C$ MXene/PEDOT: PSS device demonstrated superior stability of 90% over 10,000 cycles, whereas the pristine $Mo_{1.33}C$ MXene electrode showed a retention of only 49% over the same cycle count. Moreover, the device possesses an energy and power densities of 24.72 mWh/cm^3, 19,470 mW/cm^3 respectiverly. The improved capacitance and stability observed in the system can be attributed to the synergistic effect resulting from two key factors: the expanded interlayer spacing observed in $Mo_{1.33}C$ MXene layers is a result of the introduction of conductive PEDOT, along with surface redox processes involving both PEDOT and MXene. By incorporating conductive PEDOT into the $Mo_{1.33}C$ MXene structure, the interlayer spacing between MXene layers is expanded. This increased spacing provides more room for electrolyte ions to access the electrode surface, facilitating improved ion diffusion and enhancing the overall capacitance of the system. Additionally, the surface redox processes of both PEDOT and MXene contribute to the enhanced performance. PEDOT, being a conductive polymer, undergoes redox reactions at its surface, enabling efficient charge transfer. Simultaneously, the MXene surface also participates in redox processes, further enhancing the overall electrochemical performance. Simillaerly, Li et al. [316] synthesized $Ti_3C_2T_x$ MXene/PEDOT:PSS specifically for supercapacitor applications. The $Ti_3C_2T_x$ MXene/PEDOT:PSS electrode demonstrated the highest volumetric capacitance, reaching 1065 F/cm^3 at a scanning rate of 2 mV/s in a 1M H_2SO_4 electrolyte. This volumetric capacitance was notably higher compared to the pure $Ti_3C_2T_x$ MXene, which achieved 952 F/cm^3 at the same scanning rate. Moreover, the researchers fabricated asymmetric supercapacitor devices by employing $Ti_3C_2T_x$ MXene/PEDOT: PSS as the negative electrode and rGO as the positive electrode, with a PTFE membrane serving as the separator. Remarkably, the device electrode exhibited a high energy density of 23 mW h/cm^3 and a power density of 7659 mW/cm^3. The superior supercapacitor performance of the $Ti_3C_2T_x$ MXene/PEDOT: PSS electrode can be attributed to two factors. First, the PEDOT: PSS acted as a pillar between $Ti_3C_2T_x$ nanosheets, which increased the exposure of electroactive surfaces and reduced ion diffusion pathways. This facilitated enhanced electrochemical reactions and improved the overall capacitance. Second, PEDOT: PSS served as a conductive bridge, enabling the formation of multidimensional electronic transport channels. These channels accelerated the electrochemical reaction process, leading to higher power density. Moreover, Razal et al. [317] synthesized $Ti_3C_2T_x$ MXene with doped PEDOT (Poly(3,4-ethylenedioxythiophene)) using the wet-spinning method. In this approach, doped PEDOT served as both an active electrode as well as binder. With the conductive PEDOT: PSS filling the gaps between the $Ti_3C_2T_x$ nanosheets, resulting in a high conductivity of approximately 1489 S/cm. This conductivity enhancement was attributed to the efficient electrical pathways provided by PEDOT: PSS within the $Ti_3C_2T_x$ matrix. The electrode exhibited an impressive cyclic stability of 96% even over undergoing repeated tensile strain of 100%. This indicates the excellent mechanical stability and durability of the supercapacitor, making it suitable for flexible and stretchable applications. Furthermore, the flexible supercapacitor demonstrated favorable electrochemical performance delivering an energy and power densities of 7.13 W h/cm^3 and 8249 mW/cm^3.

Typically, MXene/conductive polymer are synthesized by mixing a MXene colloidal suspension with organic monomers and allowing polymerization to occur on the surface of MXene flakes [318,319]. This method is widely used because it's straightforward and flexible for large-scale production. In some cases, the polymerization of certain polymers can take place in a MXene colloidal suspension without the need for additional oxidants [320]. In terms of electrochemical performance, MXene/conductive polymer materials exhibit high capacitance and good cycle life [321]. This is caused by conductive polymers intercalating into the MXene layers, which increases the MXene interlayer spacing and creates conductive pathways for charge percolation. As a result, the pseudocapacitance is increased [321,322]. In terms of mechanical characteristics, the molecular-level interaction between MXene and polymers significantly enhances the mechanical robustness as well as flexibility of hybrid films composed of MXene and polymers [323]. Nevertheless, throughout the in situ polymerization of organic monomers in MXene suspension, the oxidation conditions as well as oxidants used in the process may cause the oxidation of MXene [324]. It is necessary to develop oxidation-free methods that are simple and efficient to overcome this issue. Furthermore, the polymer additive's content frequently affects the MXene's mechanical attributes, electrochemical properties, and electrical conductivity. Therefore, it is important to optimize the ratio of MXene to the combined polymer to achieve the desired properties for practical applications [304].

7.4. MXene based composites and ternary composites

Composite materials are engineered materials made by combining two or more different materials to create a new material with enhanced properties [325]. The constituents of a composite material remain separate and distinct, and they are combined on a macroscopic scale. For instance, Rizwan and colleagues successfully developed a ZrO_2-V_2CT_X MXene composite with potential applications in supercapacitors [326]. The synthesis process of the ZrO_2-V_2CT_X MXene composite. The composite electrode exhibited a CV curve pattern similar to that of the delaminated V_2CT_X, but with an increased area, indicating improved capacitive performance due to the presence of zirconia (ZrO_2). The incorporation of zirconia enhances the diffusion kinetics within the composite, providing accessible sites for cation-driven pseudo capacitance. This composite electrode displayed remarkable performance, boasting a capacitance of 1200 F/g at 5 mV/s in 3 M H_2SO_4. Notably, this capacitance is more than double the capacitance exhibited by the pristine MXene**.** The composite electrode demonstrated superior cyclic stability of 97% over 10,000 at 1 A/g charge-discharge cycles as compared pristine**.** The electrode possesses with energy density of 15.39 W/kg and a power density of 4000 Wh/kg. These improved supercapacitor performance characteristics can be attributed to the incorporation of zirconia (ZrO_2) into the MXene structure, which creates accessible diffusion sites and enhances diffusion kinetics during charge storage. Moreover, Zahra et al. [327] synthesized a V_2CT_x MXene- CNT composite electrode for supercapacitor applications. The composite electrode exhibited a maximum gravimetric capacitance of 576 F/g at 200 mV/s in a 1 M KOH electrolyte, which is two times higher compared to the capacitance of pristine V_2CT_x MXene, which was 230.5 F/g at 200 mV/s. Moreover, the composite electrode maintained a capacitance retention of 94% over 10,000 cycles. The incorporation of CNTs in the V_2CT_x MXene electrode enhanced conductivity and structural stability, resulting in a significantly higher specific capacitance compared to the pristine MXene electrode. Zhou et al. [328] developed a $Ti_3C_2T_x$ MXene-reduced graphene oxide (RGO) composite electrode for stretchable supercapacitors, demonstrating remarkable electrochemical performance and robustness even under extreme strains. The morphology of the MXene-RGO composite is depicted in **Figure 14(a)**. Field Emission Scanning Electron Microscope images demonstrate that the composite films with wrinkles and ridges maintain their structural integrity even when uniaxial prestrains are applied, as shown in **Figure 14(b).** The biaxially stretchable MXene-RGO electrode exhibited significant local deformation while maintaining its structural integrity during stretching. In comparison to the MXene/RGO composite electrodes, pure MXene supercapacitor electrodes demonstrate significantly diminished electrochemical performance under substantial deformations. They become highly distorted (resistive) when scan rate rises to 50 mV/s, confirming the substantial resistance caused by MXene film cracking. When a uniaxial strain is applied to the electrode, the distance between cracked MXene flake pieces increases, resulting in further reduction of the film conductivity. MXene-RGO composite electrode displayed excellent electrochemical performance, as evidenced by the preservation of square-shaped cyclic voltammetry curves under different strains, is depicted in **Figure 14(c)**. The specific capacitance of the electrode was minimally affected by applied strain but decreased with increasing current density. The electrode had maximum specific capacitance 36 mF/cm^2 at 0.5 A/g. Moreover, symmetric solid-state supercapacitors device was fabricated using MXene-RGO composite electrodes and a PVA-H_2SO_4 gel electrolyte, as depicted in **Figure 14(d)**. These devices exhibited capacitive behavior and stable electrochemical performance even under different strains. Charge-discharge tests confirmed the dominance of the electrochemical double layer as the primary charge storage mechanism, as depicted in **Figure 14(e)**. The specific capacitance remained consistent across various strain states, with minimal variation during stretching-relaxation cycles, as illustrate in **Figure 14(f)**. The supercapacitor device demonstrated excellent electrochemical stability, maintaining 85% of its initial capacitance over 10,000 cycles. The exceptional performance of the MXene/RGO composite can be attributed to several factors. Firstly, the hybrid film possessed a small mechanical modulus, enabling it to withstand mechanical strain without incurring structural damage. Secondly, the strong intersheet interactions within the composite maintained its electrical conductivity. Lastly, the large nanoflake size of RGO contributed to enhanced electrochemical properties. Collectively, these characteristics result in a composite material with high capacitance, mechanical stretchability, and stable electrochemical performance, making it well-suited for applications in wearable and stretchable electronics.

Enhancing the supercapacitor device performance of MXenes can be achieved by engineering their electronic structure through various methods, including, heteroatom doping, polymer hybrids, heterostructure formation and the development of ternary composites. **Table 2** presents a comprehensive summary of the performance of supercapacitor devices, as derived from the available literature.

The current advancements in MXene-based materials for enhancing electrochemical performance, particularly in supercapacitor applications, exhibit significant potential but are accompanied by several notable shortcomings. While heterostructure integration, heteroatom doping, and polymer composites show promising results in improving capacitance, conductivity, and stability, the scalability of these methods remains a concern due to their reliance on complex synthesis processes and costly precursors. Additionally, the precise control required over synthesis conditions poses challenges for reproducibility and standardization across research efforts. Moreover, the long-term stability and durability of MXene-based electrodes, crucial for practical applications, require further investigation. To address these shortcomings, streamlined synthesis methods, standardized protocols, and exploration of sustainable precursors could enhance scalability, reproducibility, and sustainability. Comprehensive studies focusing on long-term stability are essential to assess practical viability and develop strategies for enhancing MXene-based energy storage technologies. By addressing these challenges and implementing proposed solutions, MXene-based supercapacitors could move closer to commercialization, offering a promising solution for various energy storage needs.

8. Structural stability of MXene based electrodes after electrochemical testing

MXene-based electrodes have garnered significant attention in the field of supercapacitor technology due to their excellent electrochemical performance [329]. To ensure MXene electrodes' long-term dependability and durability, it is imperative to evaluate their structural stability following electrochemical testing. During electrochemical cycling, MXene-based electrodes undergo repeated charge and discharge processes, leading to stress and strain on their structures [330]. The structural stability of MXene electrodes refers to their ability to maintain their original morphology, composition, and interlayer spacing throughout these cycles [244,331]. Studies have shown that MXene materials, such as titanium carbide ($Ti_3C_2T_x$), exhibit remarkable structural stability even after extensive electrochemical testing [332]. The unique 2D layered structure of MXenes, combined with their high conductivity and large interlayer spacing, enables efficient ion diffusion and minimizes the volume changes during cycling, contributing to their structural robustness [100]. Additionally, the strong atomic bonding within MXene layers and the interaction between MXene and current collectors provide enhanced mechanical stability, reducing the likelihood of electrode degradation or delamination [73,333,334]. However, it is worth noting that the structural stability of MXene-based electrodes can be influenced by various factors, such as the specific MXene composition, the choice of electrolyte, and the cycling conditions [100]. Therefore, comprehensive characterization techniques, including X-ray diffraction (XRD), scanning electron microscopy (SEM), energy-dispersive X-ray (EDX), Raman spectra and transmission electron microscopy (TEM), are employed to evaluate the structural integrity of MXene electrodes before and after electrochemical testing. By ensuring the structural stability of MXene-based electrodes, researchers can advance the development of high-performance supercapacitors with extended cycle life and improved energy storage capabilities.

In the study conducted by Chen et al. [244], it was observed that the V_2CT_x MXene electrode exhibited remarkable structural stability even after undergoing extensive electrochemical testing. The electrode maintained its excellent structural integrity after s 100,000 GCD cycles. This is clearly demonstrated by the well-preserved morphology of the V_2CT_x MXene electrode, as depicted in **Figure 15(a)**. These findings indicate the superior stability of this electrode material, suggesting its potential for long-term and durable energy storage applications. Similarly, Nasrin et al. [268] conducted an electrochemical test to evaluate the structural stability of Nb_2C/Ti_3C_2 MXene electrodes. The electrodes exhibited remarkable stability, as evidenced by their capacitance retention of 98% after undergoing 50,000 charging and discharging cycles at a rate of 2 A/g in a PVA/H_2SO_4 electrolyte. Upon examining the morphology of the electrode surface after the extensive cycling, the researchers found no discernible changes. The surface of the electrodes remained intact and exhibited no visible signs of degradation or damage. This observation suggests that the material maintained its structural integrity throughout the electrochemical testing. The researchers further analyzed the crystallinity of the sample using techniques such as XRD. The XRD analysis demonstrated that there were no major alterations in the intensity of diffraction peaks or peak positions compared to the pristine material as shown in **Figure 15(b)**. This finding indicates that the crystalline structure of the Nb_2C/Ti_3C_2 MXene electrodes remained unaltered even after 50,000 cycles. The absence of intensity changes or peak shifting in the XRD pattern provides strong evidence for the structural robustness of the material. Moreover, Pathak et al. conducted a study on $Ti_3C_2T_x$ MXene@porous carbon nanofiber (PCNF) composites, investigating their structural stability after undergoing 10,000 charge-discharge cycles at a current density of 2 A/g [335]. The results demonstrated that the $Ti_3C_2T_x$ MXene@PCNF electrodes exhibited a preserved structure and remained stable throughout the cycling process. The FESEM images of the $Ti_3C_2T_x$ MXene@PCNF electrodes and control electrodes after the electrochemical test revealed a conserved morphology, displaying no noticeable deformations or changes (as depicted in **Figure 15(c)**). Additionally, EDX analysis indicated a similar elemental distribution before and after the electrochemical tests, further supporting the structural stability of the material. Furthermore, the XRD patterns obtained before and after the stability test exhibited a high degree of consistency, indicating that the crystal structure of the electrodes remained largely unaffected. The Raman spectra, as depicted in **Figure 15(d)**, also provided additional evidence of the material's stability, as no significant differences were observed before and after the stability test. Furthermore, Shao and colleagues conducted a study on $Ti_3C_2T_x$ MXene electrodes and found that the crystal structure exhibited stability throughout the electrochemical testing process, including cycling in acidic electrolyte [336]. They observed that the lattice parameter, which represents the interatomic spacing within the crystal lattice, remained consistent with a value of 20.7 Å both before and after cycling. This finding indicates that the MXene electrodes maintained their structural integrity and did not undergo significant changes in interlayer spacing or lattice arrangement during the electrochemical cycling process. Li et al. [337] observed in their study that the (0002) peak of the $Ti_3C_2T_x$ material weakened and broadened after 15,000 cycles, suggesting an increase in resistance due to defects. Scanning Electron Microscopy images revealed rougher edges on $Ti_3C_2T_x$ nanosheets after the cycles, while the overall structure remained unchanged. Additionally, Ag nanoparticles agglomerated, resulting in an increased size and causing a nonuniform distribution. This led to decreased diffusion and a fading capacitance. In their comprehensive investigation, Hu et al. [305] meticulously detailed their XPS and FESEM examinations of $Ti_3C_2T_x$/PPy following an extensive 20,000 cycles at 1 mA/cm^2 current density in a 0.5 M H_2SO_4 electrolyte. Remarkably, the morphology and structure of $Ti_3C_2T_x$/PPy demonstrated exceptional stability, exhibiting no signs of degradation or shifts in chemical composition throughout the continuous charge and discharge cycles. This finding underscores the robustness and integrity of the material's configuration under the demanding conditions of electrochemical cycling. Zhao and co-authors noted the absence of dissolution during the electrochemical test [236]. By contrasting XRD patterns pre and post 5000 cycles, they identified a noteworthy shift towards a larger angle in the (002) peak of $Nb_4C_3T_x$. This alteration suggests a reduction in interlayer spacing, pointing to the extraction of TMAOH as a key driver for capacitance loss. This process is coupled with layer collapse and subsequent re-stacking. The notion of decreased interlayer distance is additionally backed by SEM images.

While the recent progress in MXene electrode stability, as evidenced by various studies, holds promise for durable energy storage applications, several shortcomings warrant attention.

Despite the overall structural integrity maintained throughout extensive cycling, observations of capacity fade and increased resistance due to defects, as noted by Li et al. [337], raise concerns about long-term performance. Additionally, the agglomeration of nanoparticles, as highlighted in the same study, leads to non-uniform distribution and decreased diffusion, ultimately impacting capacitance. Furthermore, the reduction in interlayer spacing and subsequent collapse and restacking, as reported by Zhao et al. [236], pose challenges to sustained electrochemical performance. To address these issues, research efforts could focus on surface modification techniques to mitigate defect formation, alternative conductive additives to prevent nanoparticle agglomeration, and the exploration of electrolyte options or surface treatments to minimize interlayer interactions, thereby preserving electrode integrity and enhancing long-term stability. These strategies could pave the way for the practical utilization of MXene electrodes in energy storage devices with improved reliability and performance over extended cycling periods.

9. MXenes-Based Electrodes for Practical Applications in Improving Human Life

The development of MXene-based flexible smart wearable supercapacitors for enhancing human lifestyle is an exciting and rapidly evolving area of research [338,339]. These flexible wearable supercapacitors have the potential to address the energy storage needs of portable and flexible wearable electronic devices, such as smartwatches, fitness trackers, and other e-textiles [339]. A specific subfield of interest is the integration of conformable electronics with traditional soft goods, leading to the creation of self-chargeable smart wristbands and other innovative wearables [340]. Furthermore, electronic textiles, or e-textiles, involve the incorporation of electronic components and functionality into textiles and clothing. MXene-based materials offer several advantages for these applications, such as lightweight, high flexibility, conformable electronics, high electrical conductivity, and fast charging and discharging [341].

A flexible self-chargeable smart wristband based on MXene supercapacitors could potentially harvest energy from the wearer's movements or ambient environmental sources, offering a sustainable and convenient power source for electronic functionalities [342,343]. As research in this field progresses, it is likely that MXene-based materials will play a crucial role in the development of advanced and efficient wearable energy storage solutions, contributing to the evolution of smart textiles and enhancing the overall quality of human life [344-346]. Researchers and engineers continue to explore innovative ways to improve the performance, scalability, and integration of MXene-based devices into everyday wearables. On the basis, Weng et al [347] developed flexible MXene-bacterial cellulose (BC) composite films with high capacitance (346 mF cm^{-2}), employing bacterial cellulose as a crosslinking agent. The lightweight MXene- bacterial cellulose (BC) composite films were synthesized through vacuum filtration, as depicted in **Figure 16(a)**. The researchers proposed a self-chargeable supercapacitor integrated into a smart wristband, designed to harness human sweat for power, thereby offering a promising solution for self-powered wearables. The smart wristband features innovative self-rechargeable supercapacitors, comprising four interconnected units arranged in a series, accompanied by a pedometer and a comfortable wrist strap. Strategically designed filter papers within the wristband absorb perspiration from the wearer's skin, as shown in **Figure 16(b)**. The device starts in an initial off-state (**Figure 16c),** and after a few minutes of jump rope activity by the volunteer (**Figure 16d**), the self-charging supercapacitor absorbs sweat, activating the pedometer (**Figure 16e**). As the volunteer walks (**Figure 16f**), the pedometer accurately records the number of steps taken, highlighting the self-powered functionality of the smart wristband (**Figure 16g**). This real-world application underscores the effectiveness of MXene-BC composite films in creating practical and self-charging wearable electronics suitable for everyday use, marking a significant advancement in the field of wearable technology. Furthermore, Gogotsi et al. [339] reported a noteworthy development in textile-based supercapacitor devices, featuring a high areal loading of $Ti_3C_2T_x$ and designed for integration in wearable electronics to meet real-world power requirements. Their device utilized a stacked supercapacitor design (see **Figure 16h**), where two electrodes were separated by porous cotton fabric. In the '2.Electrodes' configuration, electrodes were placed side by side. Additionally, two interdigitated designs ('I.2' and 'I.1') were employed to minimize ionic resistance in two dimensions, eliminating the need for a separator. The researchers demonstrated the practicality of their approach by creating a textile supercapacitor with 5 cells, showcasing a 6 V voltage window. This setup delivered significant energy density (0.401 mW h/cm^2) and successfully powered a temperature monitoring system for an impressive duration of 96 minutes. This demonstration underscores the potential applications of flexible supercapacitors in smart garments and peripheral electronics, as illustrated in **Figure 16(i)**. The ability to provide sustained power for real-world functions highlights the promising role of these textile-based electrochemical capacitor devices in the realm of wearable and flexible electronics. Recently, Researchers have successfully developed 2D MXene-based supercapacitors using advanced printing techniques. In their study, Xu et al. [348] utilized screen printing to construct a coplanar asymmetric microscale hybrid device (MHD) based on MXene. Notably, $Ti_3C_2T_x$ MXene nanolayers functioned as the negative electrode, while Co-Al layered double hydroxide (LDH) nanolayers were employed as the positive electrode. The development process involved a meticulous two-step screen printing technique. The resulting microdevice exhibited impressive features, including a notable energy density of 8.84 Wh/cm^2 and exceptional cyclic stability, maintaining 92% capacitance even after 10,000 cycles. The researchers showcased the practical application of this innovative device by integrating it with a flexible force sensor fabricated on paper and PET flexible substrates. This integration transformed the MHD into a portable power source unit, facilitating heart rate monitoring by detecting subtle vibrations from the finger arteries. Moreover, the researchers highlighted the device's capability to be directly attached to human body skin. The implications of this technological advancement are significant, offering valuable contributions to the improvement of human life. The developed 2D MXene-based supercapacitors and their versatile applications, from energy storage to health monitoring, showcase the potential for transformative impact in various fields.

Despite the rapid advancements in MXene-based flexible wearable supercapacitors, several limitations persist within the current progress. While MXene materials offer lightweight and high conductivity properties ideal for wearable electronics, challenges such as energy harvesting efficiency and scalability need addressing. For instance, the reliance on human sweat or ambient environmental sources for energy harvesting, as proposed in the self-chargeable smart wristband developed by Weng et al. [347], may face limitations in practical implementation due to variable sweat production rates and environmental conditions. Additionally, while the integration of MXene into wearable textiles, as demonstrated by Gogotsi et al. [339], shows promise, challenges regarding manufacturing scalability and durability remain unresolved. Moreover, despite impressive achievements in energy density and cyclic stability, as showcased by Xu et al. [348] with their 2D MXene-based supercapacitors, the translation of lab-scale prototypes to mass production and commercial viability poses a significant hurdle. To address these shortcomings, future research efforts should focus on optimizing energy harvesting mechanisms, improving manufacturing scalability, and enhancing device durability to realize the full potential of MXene-based wearable supercapacitors. Additionally, collaboration between researchers, engineers, and industry stakeholders will be crucial in overcoming these challenges and accelerating the adoption of MXene-based wearable energy storage solutions, ultimately enhancing the quality of human life through innovative wearable technologies.

10. Conclusions and perspective

MXenes possess the potential to revolutionize high-performance energy storage devices due to their excellent electrical conductivity, intriguing layered structure, hydrophilic surface, mechanical durability, outstanding catalytic reactivity, outstanding stability, and remarkable energy density. Even though MXenes offer numerous advantages and have made significant strides in both production and application, there are still certain challenges that require further investigation. In particular, this review primarily focuses on the recent progress achieved in MXene based electrode materials for supercapacitors. It delves into topics such as the impact of various electrolytes on MXene electrodes, techniques for fabricating devices, the electrochemical behavior exhibited, and strategies for enhancing performance through modifications. Additionally, the study delves into the enduring structural stability of MXene electrodes after electrochemical testing. Future studies should investigate the following research and innovation directions for MXene-based supercapacitors:

1. Despite the numerous strategies employed for MXene synthesis, the challenge of achieving a high yield of MXenes persists, and the underlying cause behind this issue remains elusive. Furthermore, the conventional etching techniques utilized in the synthesis process pose several safety concerns. These obstacles collectively impede the scalability and commercial viability of MXene production.
2. The electrolyte is a crucial component of supercapacitors, providing ionic conductivity and charge compensation. The potential window of the electrolyte greatly affects the operating voltage of supercapacitors, impacting energy density. Balancing a wider potential window

with high ionic conductivity is a significant challenge in developing electrolytes that enhance both properties without compromising performance.

3. Most MXene electrodes exhibit a constrained potential range, usually between 0.5 and 1V, when employed in aqueous electrolytes, thereby limiting their practical applicability. Despite the broader potential range observed in MXene electrodes when used with organic electrolytes, they face obstacles such as sluggish ion transport rates and limited capacitance. Addressing these challenges requires additional efforts, including expanding the potential range of MXene electrodes in aqueous electrolytes and enhancing the ion conductivity of organic electrolytes.
4. Overcoming the challenge of increasing MXene's resistance to oxidation remains a significant obstacle, given its direct impact on the long-term cycling performance of supercapacitor electrodes based on MXene. Potential solutions to address this issue could involve surface modifications and storage under controlled conditions of low temperatures or inert atmospheres.
5. MXenes exhibit low crystallinity and are prone to oxidation in testing environments. Additionally, understanding the structural changes and electrochemical processes of MXene-based electrodes across cycles is crucial. Hence, employing in situ characterization techniques like SEM, TEM, electrochemical Raman spectroscopy, and X-ray photoelectron spectroscopy can facilitate a deeper analysis of composite materials. These methods are essential for comprehending the intricate relationship between material composition, structure, and properties of MXene-based electrodes. Furthermore, further theoretical exploration of MXene materials is imperative. Experimental findings should be

corroborated through theoretical investigations, underscoring the importance of integrating theoretical research with experimental testing.

6. Research articles frequently explore both symmetric and asymmetric supercapacitors. The rise in popularity of flexible electronics, known for their slimness, lightweight nature, and adaptability, has fueled the demand for flexible devices capable of maintaining substantial energy storage and consistent capacitance even during bending and distortion. Hybrid supercapacitors play a pivotal role in this context, as they combine high energy density as well as specific capacitance, effectively bridging gap between conventional supercapacitors and batteries.
7. The supercapacitor is paramount to meeting the evolving demands of flexible and portable printed electronics. Overcoming production challenges necessitates the exploration of innovative active electrode materials, and the emergence of printable MXene materials holds great promise in addressing limitations associated with other 2D materials. MXenes, with their unique physical and chemical properties, stand out as potential game-changers in the realm of printed electronics. Although research in this area is still in its nascent stages, the current findings suggest that MXenes could revolutionize printed electronics, offering not only efficiency but also a cost-effective solution for the development of future electronic devices. Acknowledging the ongoing challenges, this avenue of research signifies a compelling direction for the continued evolution of electronic technologies.
8. Wearable supercapacitors harnessing MXene technology represent a remarkable stride in biomedical engineering, offering a plethora of possibilities for transformative applications in healthcare and biotechnology. The distinctive features of MXene materials, such as their inherent flexibility, lightweight nature, and biocompatibility, position them as compelling

options for powering wearable devices, ushering in a paradigm shift in healthcare delivery. These supercapacitors boast advantages such as high energy density and outstanding electrochemical performance, making them well-suited for integration into wearable devices, ensuring sustained power and comfortable use. Despite these advantages, challenges related to scalability, stability, integration with other components, and cost-effectiveness must be addressed. Further research is imperative to refine manufacturing processes, enhance stability, ensure seamless compatibility with other components, and reduce production costs. As ongoing research and development endeavors persist in refining MXene-based technologies, a promising future unfolds, with wearable devices poised to significantly enhance patient outcomes, enable remote monitoring, and revolutionize the landscapes of biomedicine and healthcare.

9. To facilitate the translation from laboratory-scale demonstrations to practical applications, it is imperative to prioritize the development of scalable methods for MXene synthesis and electrode fabrication techniques. This transition is pivotal in harnessing the full potential of MXene supercapacitors for viable energy storage solutions in real-world scenarios.
10. Examine the ecological consequences of MXene-derived supercapacitors, encompassing both their production methods and the disposal procedures at the end of their lifecycle. It's crucial to explore sustainable techniques and recycling practices to reduce their environmental footprint.
11. In addition to the supercapacitor, there is lot more to explore and validate MXene as nanofillers in polymer based dielectric energy storage capacitor. This area is unexplored using MXene as 2D filler materials. MXene as a 2D nanofiller in polymer matrix shows excellent properties, and reported to be enhanced the dielectric constant to 5-fold on PVDF

based polymer with 15 wt% of 2D $Ti_3C_2T_x$ nanosheets as fillers. This is quite surprising for such a high enhancement of dielectric constant from 40 to 10,0000 with incorporation of small amount of 2D MXene. But, due to the high conductivity the dielectric loss shows significantly high. High dielectric constant and high breakdown field strength are required to use a dielectric material for high-density energy storage devices according to the formula Storage energy density $U_d \sim \frac{1}{2}\varepsilon_o\varepsilon_r E_{BD}^2$, where ε_o is the dielectric constant of free space and ε_r is the dielectric constant of the dielectric material. E_{BD} is the breakdown electric field strength. A capacitor to be used as high-density energy storage device dielectric constant and breakdown field strength are two major components to be enhanced and at the same time dielectric loss need to be minimized. Thus, a proper engineering method to incorporate MXene as a filler in the polymer need to be developed to minimize the loss and enhance the energy storage performance to envision potential application of MXene based dielectric materials for next generation of high-density energy storage devices.

This review emphasizes the significance of investigating novel MXenes as possible anode electrode replacements for supercapacitor devices. In particular, heterostructures show promise because of their exceptional conductivity as well as wide electrochemical operating range**.** Moreover, the advancement of MXene-based supercapacitors relies on the crucial development of binder-free electrodes. The purpose of this review is to establish a connection between past research and future directions, bridging the existing knowledge gap and identifying areas that require further investigation.

Declaration of competing interest

The author declares no conflicts of interest.

Data availability

Upon request, data will be made available

Acknowledgements

The authors SAK and KPK extend their thanks to the Department of Physics at the National Dong Hwa University in Hualien 97401, Taiwan. NRP acknowledged the funding support from the Princeton Alliance for Collaborative Research and Innovation (PACRI) Grant #PACRI-JSU-02 and NSF HBCU-UP Excellence in Research NSF-DMR-1900692 and DoD Grant #G634E27. SAK and NRP acknowledges the funding support by the U.S. Department of Energy, Office of Science, Office of Basic Energy Sciences program under Award Number DE-SC0024072.

Tables

Table 1. A comprehensive comparison of MXene based electrodes in three-electrode systems.

Sr. No.	**Electrode**	**BET surface area (m^2/g)**	**Electrolyte**	**Potential window (V)**	**Specific capacitance (C_s)**	**Retention (No. of cycles**	**Ref.**
1	Ti_2CT_x	10.59	1 M H_2SO_4	−0.2 to 0.6 V	262 F/g at 1 A/g	88.79% after 10000 cycles at 10 A/g	[309]
2	$Ti_3C_2T_x$	32	1M H_2SO_4	0 to 0.4	499 F/g at 2 mV/s	100% after 10000 cycles at 10 A/g	[349]
3	$Ti_3C_2T_x$/Ag	107	1M H_2SO_4	−0.95 to −0.25 V	332.2 mF/cm^2 at 2 mV/s	78.2% after 15000 cycles at 50 mV/s	[337]
4	$Ti_3C_2T_x$/RGO	-	2 M KOH	0 to -0.6	154.3 F/g at 2 A/g	85% after 6000 cycles at 4 A/g	[350]
5	$Ti_3C_2T_x$/CNTs	-	1 M $MgSO_4$	0 to -0.8	390 F/cm^3 at 2 mV/s	100 % after 10000 cycles at 5 A/g	[351]
6	ak-$Ti_3C_2T_x$/carbon cloth	-	1M H_2SO_4	0.4 to-0.4	312 mF/cm^2 at 1 mA/ cm^2	97% after 8000 cycles	[352]
7	$Ti_3C_2T_x$ aerogel	108	3 M H_2SO_4	0.2 to -0.6 V	438 F/g at 10 mV/s	90 % after 20000 cycles	[353]
8	N doped $Ti_3C_2T_x$	368.8	1M NaCl	0 to 1	514 F/cm^3 at 2 mV/s	99.75 % after 2000 cycles at 0.5 A/g	[354]
9	$Ti_3C_2T_x$/rGO	-	1 M H_2SO_4	0 to 1	233 F/g at 1A/g	91 % after 10000 cycles at 1A/g	[355]
10	$Ti_3C_2T_x$/PPy	-	1 M H_2SO_4	−0.2 to 0.35 V	416 F/g at 5 mV/s	92% after 25000 cycles at 100 mV/s	[306]
11	$Ti_3C_2T_x$/PPy	-	0.5 M H_2SO_4	0 to 0.5 V	406 F/g at 1 mA/cm^2	100% after 20000 cycles at 1 mA/cm^2	[305]
12	$Ti_3C_2T_x/MoO_3$	37.28	1 M KOH	−1.0 to −0.3 V	151 F/g at 2 mV/s	93.7% after 8000	[356]

						cycles at 1 A/g	
13	$Nb_4C_3T_x$	-	1M H_2SO_4	-1.0 to 0	1075 F/cm^3 at 5 mV/s	76.13% after 5000 cycles at 2 A/g	[236]
14	$Nb_4C_3T_x$	-	1M Li_2SO_4	-0.8 to 0	177 F/g at 5mV/s	90% after 10,000 cycles at 2A/g	[237]
15	Nb_2CT_x	-	1 M $LiSO_4$	0 to-0.6	154 F/g at 5 mV/s	10% after 2000 cycles at 100 mV/s	[212]
16	Ni-Nb_2C	18.02	1 M PVA/ H_2SO_4	0.4 to -0.2	666 F/g at 5mV/s	81% after 10000 cycles	[357]
17	Nb_2CT_x/CNT	-	1M H_2SO_4	0.2 to -0.4	186 F/g at 2 mV/s	80.3 % after 5000 cycles	[235]
18	$V_4C_3T_x$	31.35	1M H_2SO_4	0.15 to - 0.35	209 F/g at 2 mV/s	97.23% after 10,000 cycles at 10 A/g	[240]
19	V_2C MXene	-	1M H_2SO_4	0 to -1.2	487 F/g at 2 mV/s	99% after 10000 cycles at 10A/g	[238]
20	V_4C_3 MXenes	-	1M H_2SO_4	0.4 to -0.4	330 F/g at 5 mV/s	90 % after 3000 cycles at 1 V/s	[158]
21	V_2CT_x	-	Seawater electrolyte	-0.8 to -0.3	181 F/g at 0.2 A/g	98.1% after 5000 cycles at 2A/g	[206]
22	V_2C MXene	-	1M Na_2SO_4	-0.3 V to - 0.9 V	164 F/g at 2 mV/s	90% after 10,000 cycles at 5 A/g	[243]
23	V_2NT_x	-	3.5 KOH	0 to -1.0	112.8 F/g at 1.85 mA/cm^2	96% after 10000 cycles at 5 mA/cm^2	[213]
24	V_2CT_x	-	2M $ZnSO_4$	0.3 to -0.9	481 F/g at 1 A/g.	84% after 60000 cycles at 10 A/g	[244]
25	Mo_2CT_x	19.5	1M H_2SO_4	0.3 to-0.3	79.14 F/g at 0.3 A/g	98% after 5000 cycles at 5 A/g	[214]
26	$Mo_{1.33}C$ MXene	-	5 M LiCl	0.1 to -1.2	217 F/g at 2 mV/s	85% after 7000	[70]

						cycles at 10 A/g	
27	$Mo_{1.33}CT_z$	-	5 M LiCl	0.5 to -1.2	681.5 F/cm^3 at 2mV/s	109% after 40000 cycles at 10 mA/cm^2	[199]
28	$Mo_{1.33}CT_z$	-	1M $MnSO_4$	0 to 1.1	185 F/g at 2mV/s	>90% after 10000 cycles at 10 A/g	[253]
29	Ta_4C_3 MXene	6.599	0.1 M H_2SO_4	0 to 1.6	481 F/g at 5 mV/s	89% after 2000 cycles	[254]

Table 2. Comparing the performance of MXene based electrodes in supercapacitor devices

Sr. No.	Positive electrode	Negative electrode	Electrolyte	Potential window (V)	Specific capacitance (C_s)	Energy density	Power density	Retention (No. of cycles)	Ref.
1	MnO_2	$Ti_3C_2T_x$/Ag	1 M Na_2SO_4	0 to 1.9	246.2 at 2mA/cm^2	121.4 µW h/cm^2	17 395 µW/cm^2	82% after 10000 cycles at 10 mA/cm^2	[337]
2	rGO/$Ti_3C_2T_x$	rGO/$Ti_3C_2T_x$	PVA/KOH	0 to 0.7	405.5 F/g at 1 A/g	63 mWh/cm^3	2786 mW /cm^3	100 % after 10000 cycles at 5 A/g	[358]
3	$Ti_3C_2T_x$/ rGO	$Ti_3C_2T_x$/ rGO	3 M H_2SO_4	0 to 1	1040 F/cm^3 at 2 mV/s	32.6 Wh/L	74.4 kW/L	-	[270]
4	$Ti_3C_2T_X$/Ni-Fe oxide	$Ti_3C_2T_X$/Ni-Fe oxide		0 to 0.8	328.35 mF/cm^2 at 0.2 mA/cm^2	76.8 mW h/cm^3	0.4 W/cm^3	90.88% after 10000 cycles At 1 mA/cm^2	[359]
5	rGO-PDDA/Ti3C2Tx MXene	rGO-PDDA/Ti3C2Tx MXene	ACN-PC-PMMA-$LiCF_3SO_3$	0 to 1.2 V	40.8 mF/cm^2 at 0.02 mA/cm^2	8.2 µWh/cm^2	630.1 µW/cm^2	75% after 5000 cycles	[360]
6	$Ti_3C_2T_x$ nanosheets/$Ti_3C_2T_x$ quantum dots/RGO fiber	$Ti_3C_2T_x$ nanosheets/PEDOT: PSS fiber	PVA/H_2SO_4	0 to 1.5 V	542 F/c^3 at 0.25 A/cm^3	16.6 mWh/cm^3	450 mW/cm^3	96.6 % after 5000 cycles at 10 mV/s	[361]
7	$Ti_3C_2T_x$/ rGO-AD	$Ti_3C_2T_x$/ rGO-AD	PVA/H_3PO_4	0 to 0.8V	645 F/cm^3 at 1.0 A/cm^3	13.0 mWh/cm^3	1992 mW/cm^3	75.3% after 20000 cycles at 8.6 A/cm^3	[362]
8	N-doped d-$Ti_3C_2T_x$/ rGO	N-doped d-$Ti_3C_2T_x$/ rGO	PVA/H_2SO_4	0 to 0.6V	247 F/g at 1 A/g	15.7 Wh/kg	3738.7 W/kg	>90% after 1000 cycles at 5 A g^{-1}	[363]
9	Graphene-encapsulated Ti_2CT_x@PANI	Graphene	1 M H_2SO_4	0 to 1.8	94.5 F/g at 1 A/g	42.3 Wh kg^{-1}	18 000 W kg^{-1}	94.25% after 10000 cycles at 10 A/g	[309]
10	$Mo_{1.33}C$ MXene/PEDOT: PSS	$Mo_{1.33}C$ MXene/PEDOT: PSS		0 to 0.6	568 F/cm^3 at 0.5 mV/s	250.1 mWh/cm^3	32.9 W/cm^3	90 % after 10000 cycles at 5 A/cm^3	[315]

11	Nb_2C/Ti_3C_2 MXene	Nb_2C/Ti_3C_2 MXene	PVA/ H_2SO_4	0 to 1.2	211 F/g at 0.3 A/g	38.5 W h/kg	3840 W/kg	98% after 50000 cycles at 2A/g	[268]
12	AC	Nb_2CT_x/CNT	1M H_2SO_4	0 to 1.5	51 F/g at 2 mV/s	154.1 μWh/cm^2	74843.1μW/cm^2	73.3% after 2000 cycles at 5 A/g	[235]
13	$Ti_3C_2T_x/Nb_2CT_x$	$Ti_3C_2T_x/Nb_2CT_x$	PVA–H_2SO_4	0 to 0.7	81 F/g at 5 mV/s	5.5 mW h/g	141.4 mW/g	94% after 10 000 cycles at 2 A/g	[364]
14	AC	Co_3O_4-Nb_2CT_x	6 M KOH	-1.0 to 0.8	-	60.3 Wh/kg	670 W/kg	93% after 1000 cycles at 5 A/g	[365]
15	AC	perovskite $NaNbO_3$/f-Nb_2CT_x	1 M $LiPF_6$	1 to 4	82 F/g at 0.05 A/g	241 Wh/kg	125.0 W/kg	75.1% after 4000 cycles at 1.0 A/g	[366]
16	Mn_3O_4	V_2NT_x	3.5 KOH	-1.0 to 0.8	112.8 F/g at 1.85 mA/cm^2	15.66 W h/kg	3748.4 W/kg	96% after 10000 cycles at 5 mA/cm^2	[213]
17	AC	V_2CT_x	2M $ZnSO_4$	0 to 1.8	76 F/g at 1 A/g	13.4 kW/kg	17 Wh/kg	79% after 100,000 cycles at 10 A/g	[244]
18	Mo_2CT_x	Mo_2CT_x	PVA/H_2SO_4	0 to 0.6	64.74 F/g at 0.2 A/g	16.0 Wh/L	1449.1 W/L	89.2% after 10,000 cycles at 1 A/g	[214]
19	Mn_xO_n	$Mo_{1.33}C$ MXene	5M LiCl	0 to 2	38 F/g at 2 mV/s	19 Wh/kg	1.08 W/kg	92% after 10,000 at 10 A/g	[70]
20	$Mo_{1.33}CT_z$	$Mo_{1.33}CT_z$	19.5 LiCl	0 to 1.4	140 F/cm^3 at 2 mV/s	41.3 mWh/cm^3	165.2 mW/cm^3	84.8% after 20,000 cycles at 10 A/cm^2	[199]
21	$Mo_{1.33}CT_z$	$Mo_{1.33}CT_z$	0.5 M K_2SO_4	0 to 1.1	24 F/g at 2 mV/s	0.0128 Wh/cm^3	0.9 W/cm^3	82% after 5000 cycles at 100 mV/s	[253]

Figures

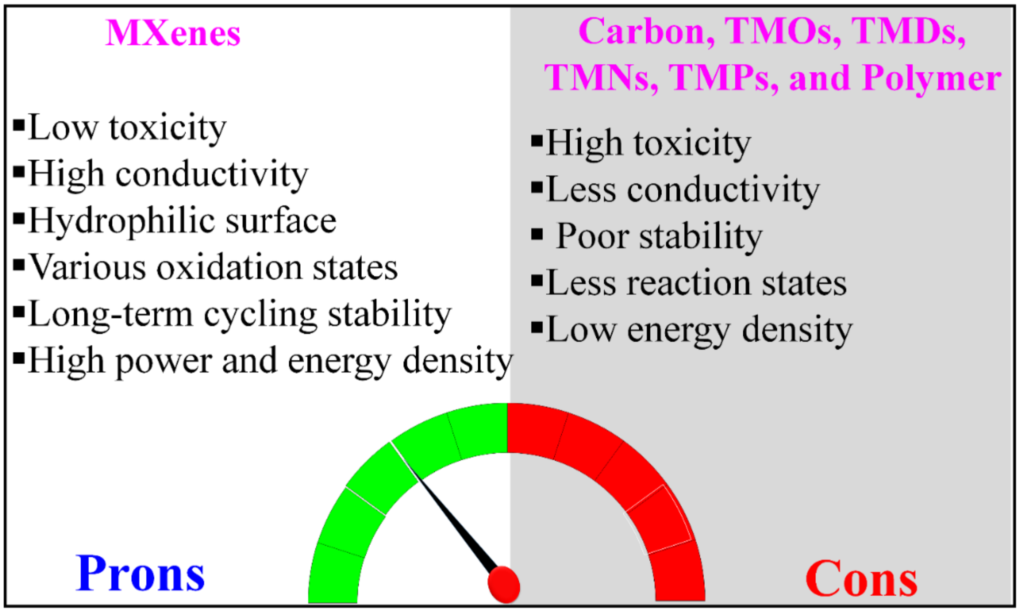

Figure 1. Schematic representation of the prons of Mxenes and the cons of Carbon, TMOs, TMDs, TMNs, TMPs, and Polymers.

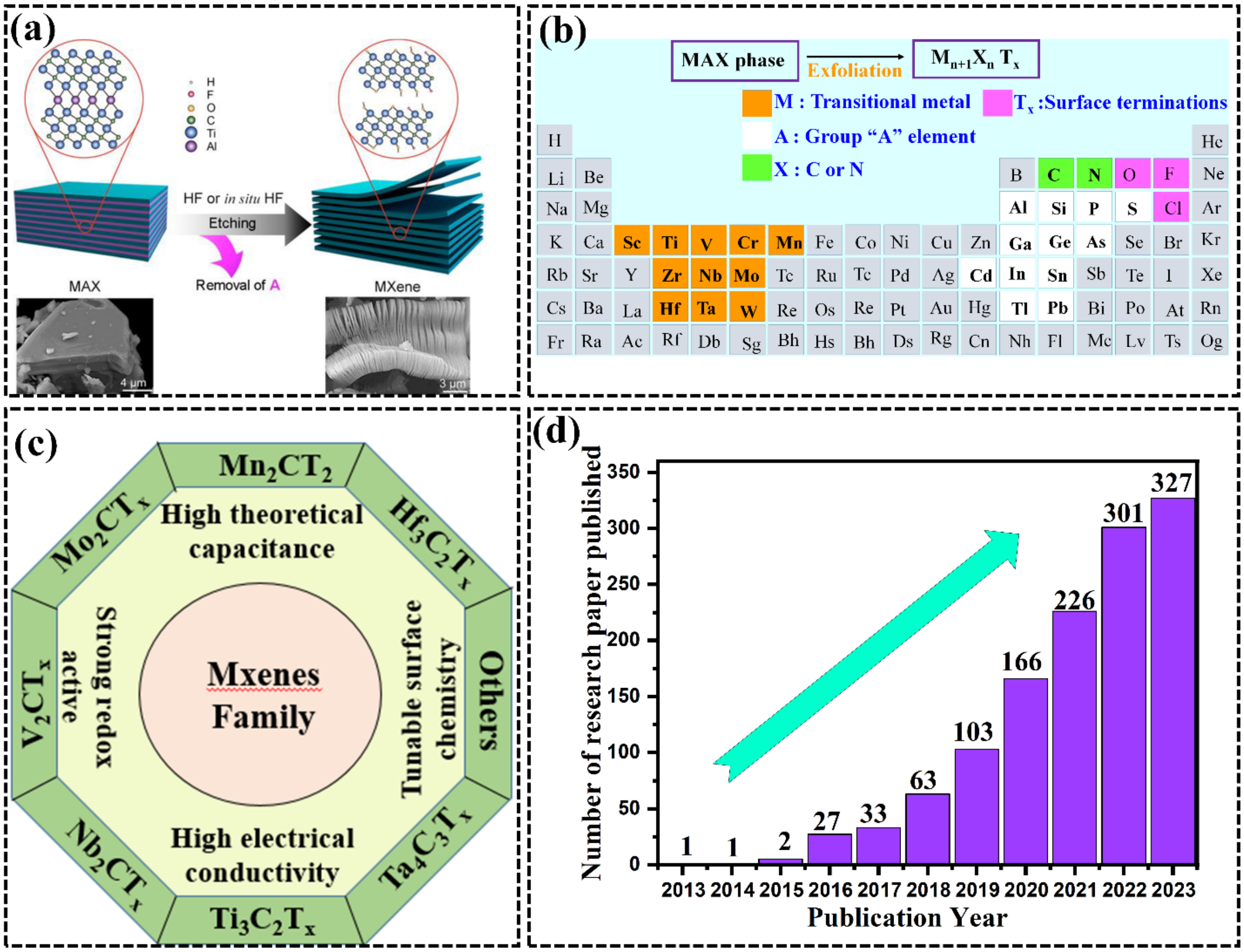

Figure 2. (a) Schematic representation of the procedure involving the etching and delamination of MXene [42,43]. Copy @ Elsevier 2019. Copy@ American Chemical Society 2014. (b) Arrangement of potential constituent elements of MXene in the periodic table. (c) Schematic representation for specific interesting MXene properties. (d) Recently reported research articles on MXene-based materials for supercapacitor applications from Web of Science.

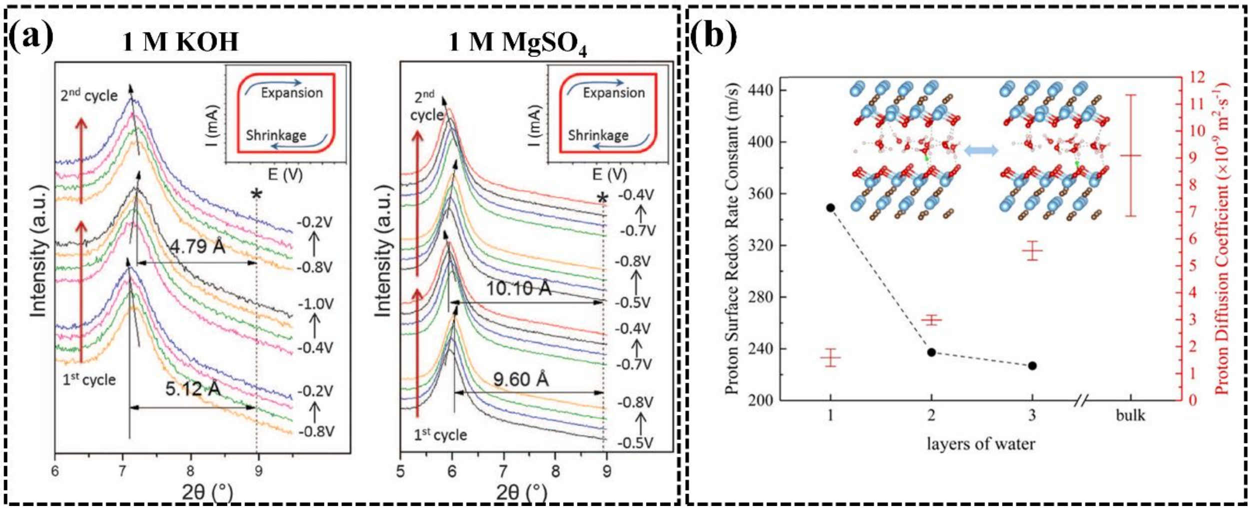

Figure 3. (a) Exploring the structure of Ti$_3$C$_2$T$_x$ multilayers using electrochemical in situ X-Ray Diffraction. The vertical dashed lines show where the (0002) peak for the Ti$_3$C$_2$T$_x$ electrodes started before being placed in a cell. The slanted arrows point to the direction of the shift in the (0002) peak. The smaller pictures show the cycling direction and how the c lattice parameters change during cycling. In both KOH and MgSO$_4$ electrolytes, the size decreases during cathodic polarization [211]. Copy @ American Association for the Advancement of Science 2013. (b) Correlation between water layer confinement and declining rate constants in proton surface redox [112]. Copy@ American Chemical Society 2018.

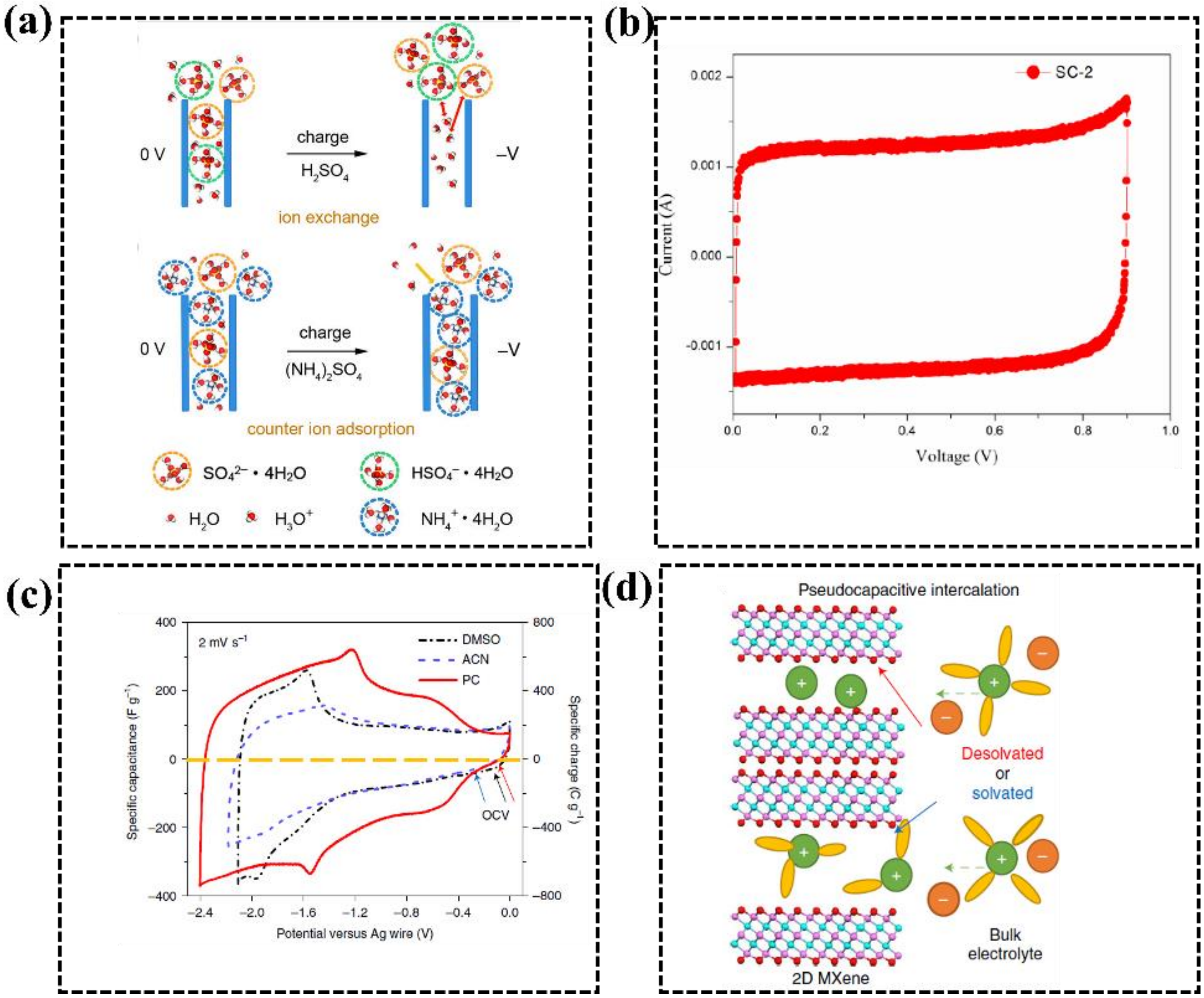

Figure 4 (a) $Ti_3C_2T_x$ negative electrode exhibits distinct charge storage mechanisms based on the electrolyte used: ion exchange occurs in H_2SO_4 electrolyte, while counterion adsorption takes place in $(NH_4)_2SO_4$ electrolyte [128]. Copy @ American Chemical Society 2016. (b) Cyclic voltammogram plots depicting the behavior of Ta-based MXene at a scan rate of 1 mV/s in a KOH electrolyte. copy@ springer 2015. (c) Cyclic voltammetry analysis of $Ti_3C_2T_x$ MXene conducted in three different organic electrolytes, using a scan rate of 2 mV/s [116]. Copy@ Nature 2019. (d) Schematic illustration the configuration of a supercapacitor utilizing a 2D MXene material (pink for Ti, cyan for C, red for O) as the negative electrode, showcasing both solvated and desolvated states and the electrolyte components are represented as follows: green for cations, orange for anions, and yellow for solvent molecules [116]. Copy@ Nature 2019.

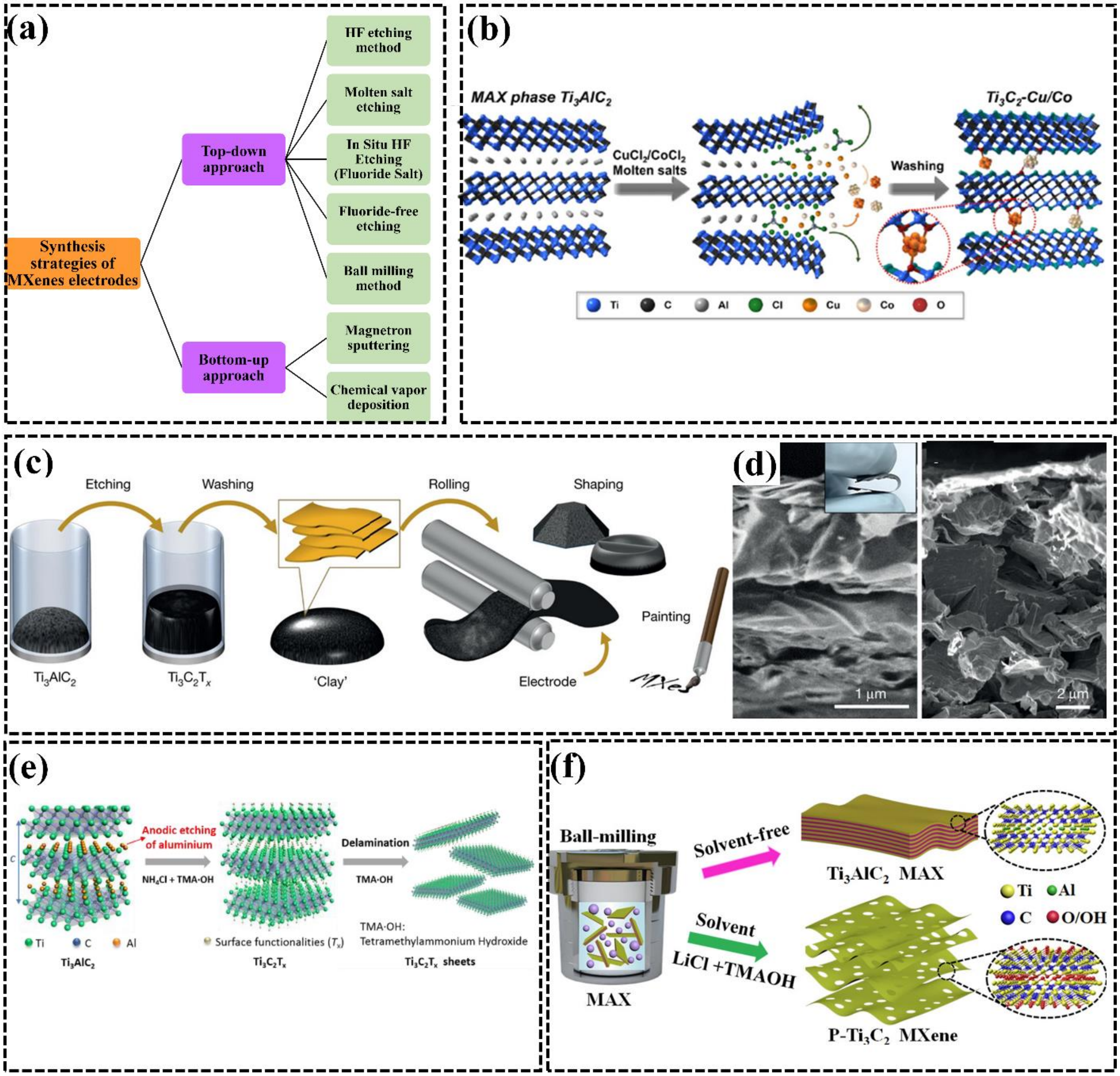

Figure 5. (a) Approaches for MXene electrode fabrication using both top-down and bottom-up methods. (b) Preparation process of Ti_3C_2 MXene-Cu/Co hybrids using molten salt etching technique [161]. Copy @ Wiley-VCH 2021. (c) The MAX phase undergoes acid and fluoride salt etching (step 1), followed by water washing to remove byproducts and adjust pH (step 2), resulting in clay-like sediment for film formation (step 3), molding into conductive objects upon drying (step 4), or dilution for substrate coating (step 5). (d) Scanning electron microscope image depicts a fracture surface of a roughly 4-µm-thick rolled film, exhibiting layer shearing; the inset illustrates the film's flexibility. Fracture surface of a thicker rolled film (approximately 30 µm) exposes less favorable alignment of flakes within the film's interior [163]. Copy@ Springer Nature 2014. (e) synthesis process of $Ti_3C_2T_x$ through fluoride-free etching technique $Ti_3C_2T_x$. (f) Schematic illustration of synthesis of Ti_3C_2 MXene using a chemical ball-milling method [174]. Copy @ American Chemical Society 2020.

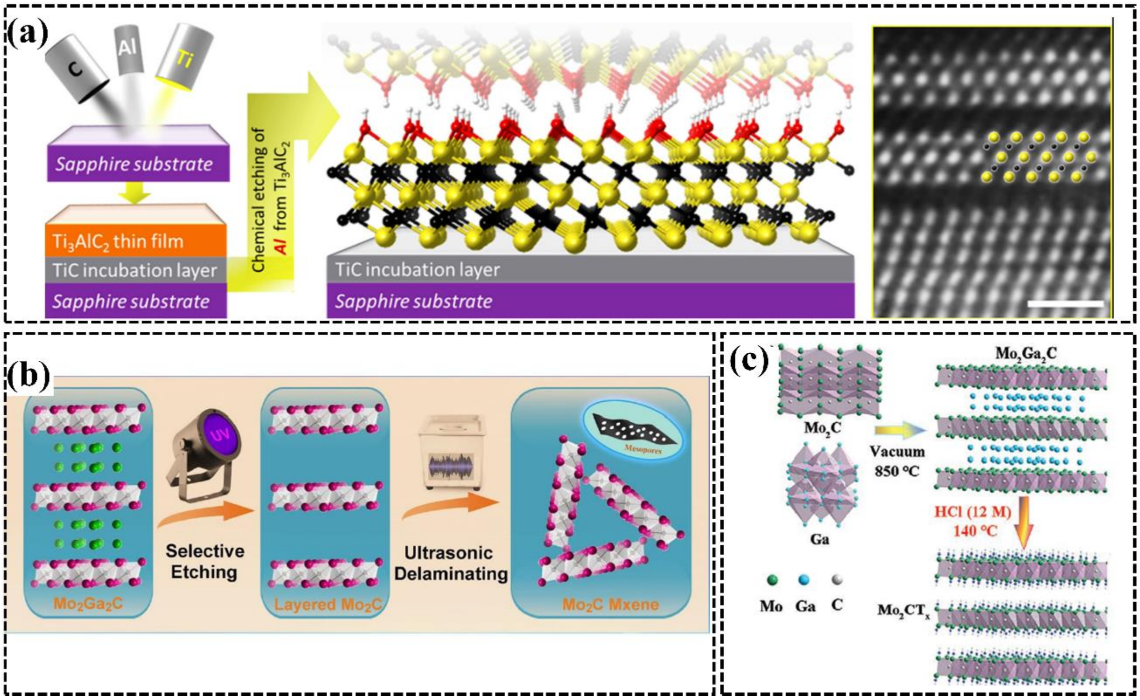

Figure 6. (a) Illustration depicts the Magnetron sputtering process, which involves depositing Ti, Al, and C. This leads to the formation of a TiC incubation layer, only a few nanometers thick, on a sapphire substrate oriented along (0001). Following this, a layer of Ti_3AlC_2 is subsequently deposited atop the TiC layer. The arrangement of OH-terminated Ti_3C_2 after the selective etching of Al from Ti_3AlC_2, featuring Ti, C, O, and H atoms with distinct colors, while an inset in a scanning transmission electron microscopy image showcases the Wiener filter-treated initial two layers of $Ti_3C_2T_x$, accompanied by a 1 nm scale bar for reference [181]. Copy @ American Chemical Society 2014. (b) Diagrammatic representation of the fabrication of a 2D mesoporous Mo_2C MXene through the process of selective etching induced by ultraviolet (UV) light [190]. Copy @ Elsevier 2020. (c) Illustration depicting the process of fabricating fluoride-free Mo_2CT_x through the exclusive use of an HCl-assisted hydrothermal etching strategy [191]. Copy @ Wiley-VCH 2021.

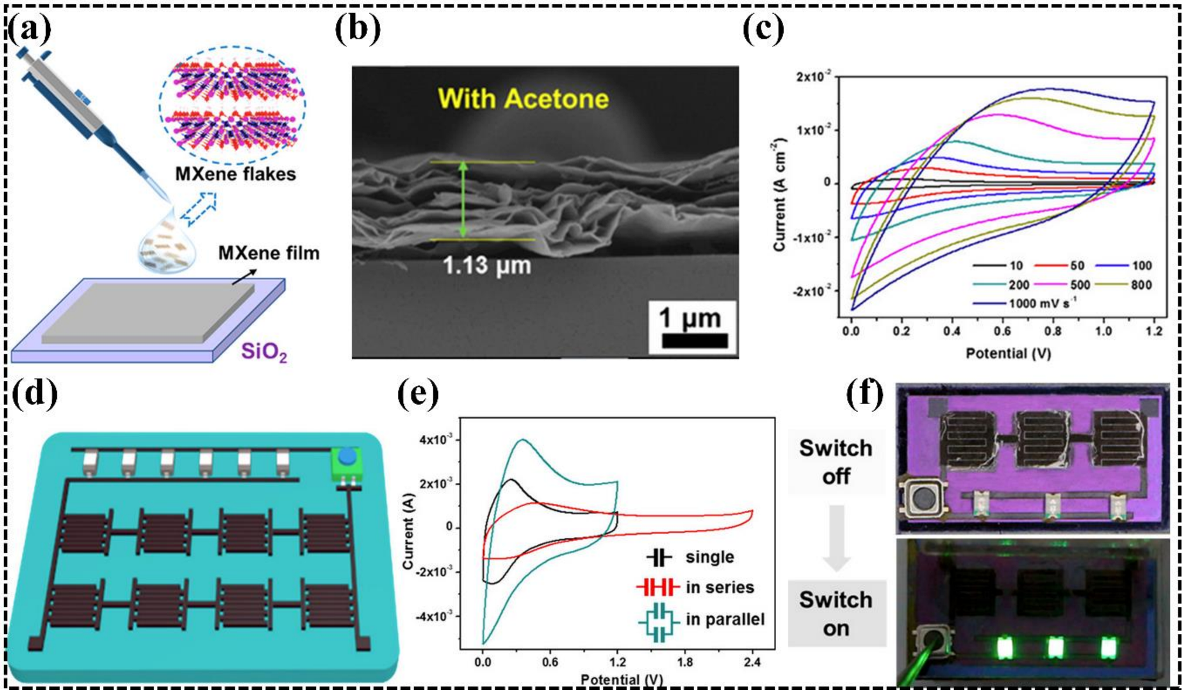

Figure 7. (a) The schematic illustration depicting the creation process of the MXene-SiO_2 electrode using a method involving drop-coating and natural sedimentation. (b) SEM images displaying a cross-sectional view of the MXene-SiO_2 electrode. (c) Cyclic voltammetry plots obtained by varying the scan rates from 10 to 1000 mV/s for the microsupercapacitor-W/A. (d) Visual representation depicting the creation process of integrated Si-based electronics using the laser etching technique. (e) Cyclic voltammetry profiles obtained under different conditions: when the microsupercapacitors are individually tested, connected in series, and connected in parallel. (f) A visual image captured digitally, showcasing the comprehensive device featuring three microsupercapacitors connected in series, three chip LEDs, and a one-inching switch. When activated, the device is capable of functioning continuously for approximately 30 seconds [228]. Copy @ American Chemical Society 2022.

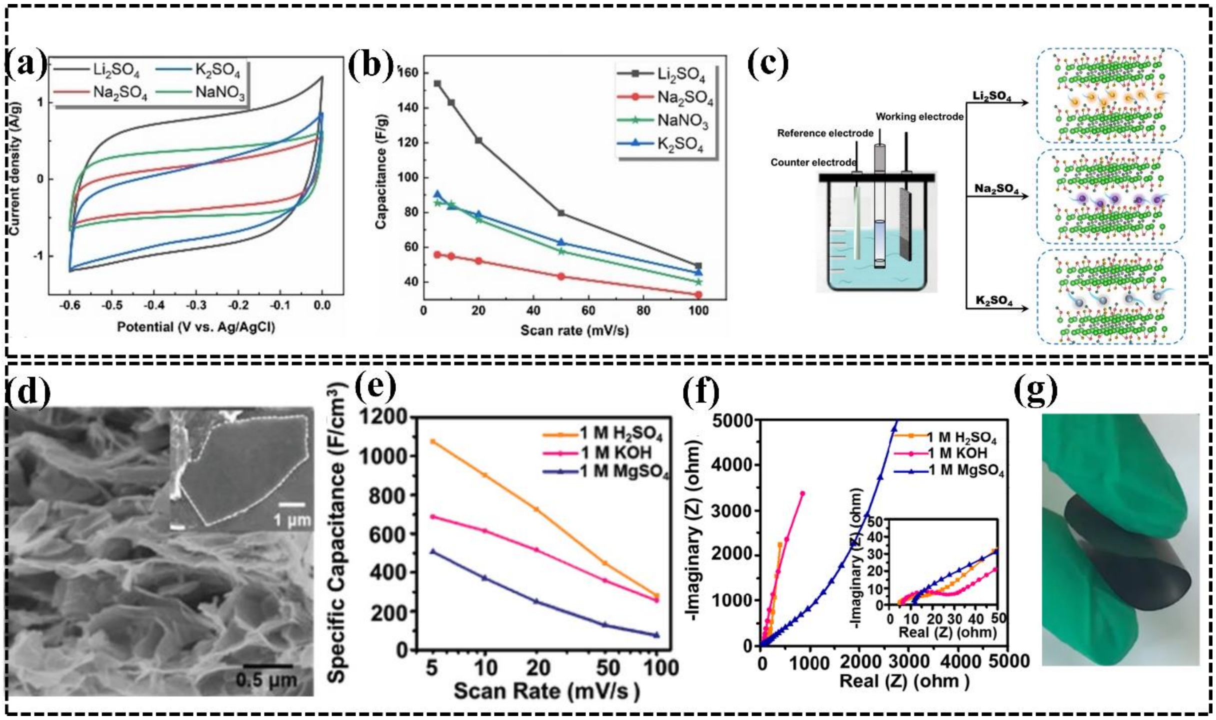

Figure 8. (a) Comparison of cyclic voltammetry profiles for Nb_2CT_x electrodes across various electrolyte solutions. (b) Evaluating the specific capacitance at different scan rates within diverse electrolyte media. (c) Visual representation depicting the process of intercalating various cations between layers of Nb_2CT_x [212]. Copy@ Wiley-VCH 2021. (d) Cross-sectional SEM image of a $Nb_4C_3T_x$ film (with an inset displaying an SEM image of an individual flake). (e) Specific capacitance values obtained from the corresponding cyclic voltammetry curves. (f) Nyquist plots for $Nb_4C_3T_x$ films in three different electrolytes. (g) Digital photograph of flexible $Nb_4C_3T_x$ [236] Copy@ Wiley-VCH 2020.

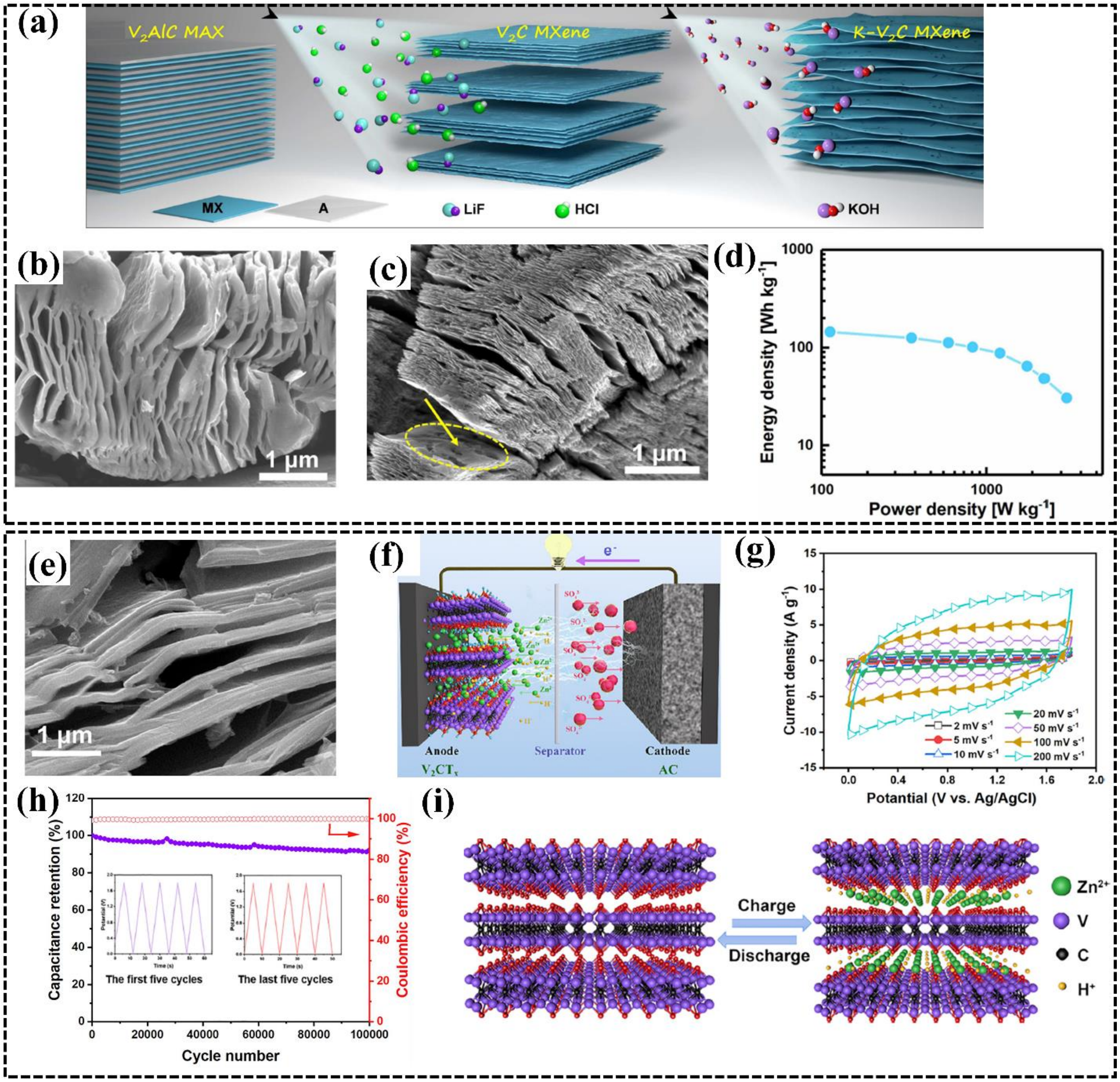

Figure 9. (a) Diagrammatic representation of the K–V_2C preparation process. SEM pictures showing (b) V_2C MXenes, and (c) K–V_2C MXenes. (d) The Ragone graph representing the performance of the K–V_2C//$K_xMnFe(CN)_6$ device [242]. Copy @ Elsevier 2019. (e) Scanning Electron Microscope pictures of V_2CT_x MXene. (f) Diagrammatic representation of the V_2CT_x//AC asymmetric supercapacitor device. (g) cyclic voltammetry curves of the device at varying scan rates. (h) Extended cycling stability of the V_2CT_x//AC device at 10 A/g (insert: Charge-Discharge Curves of the initial and the last five cycles). (i) Illustration depicting potential charge storage mechanisms within V_2CT_x MXene [244]. Copy @ Elsevier 2022.

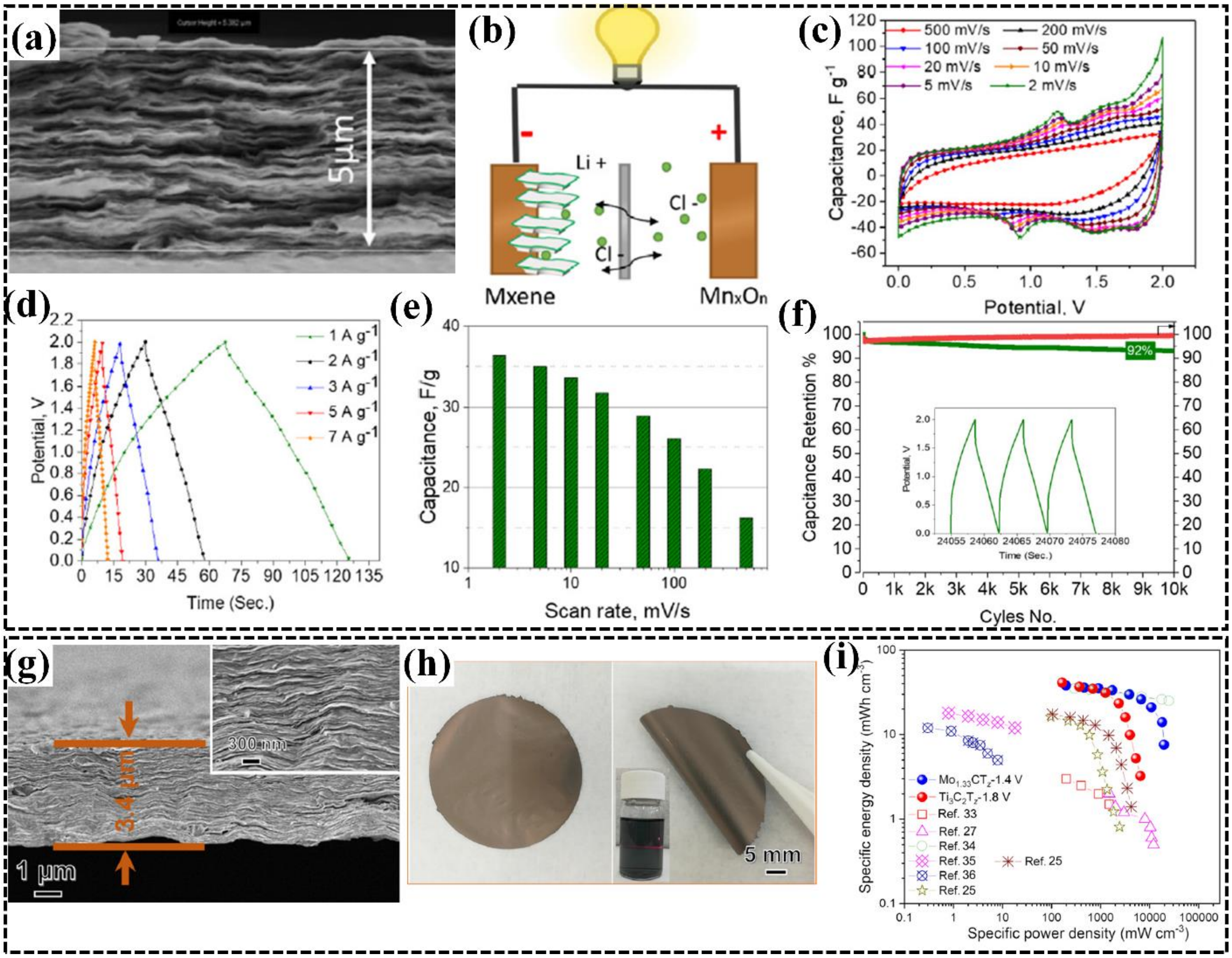

Figure 10. (a) Scanning Electron Microscope cross-sectional image of the $Mo_{1.33}C$ MXene film. (b) Diagrammatic representation of the design for the MXene//Mn_xO_n asymmetric supercapacitor device. (c) Cyclic Voltammetry plots of the MXene//Mn_xO_n device recorded at various scan rates (ranging from 2 mV/s to 500 mV/s). (d) Charge and discharge profiles of the MXene//Mn_xO_n device at varying current densities. (e) Gravimetric capacitance values of the MXene//Mn_xO_n device measured at different scan rates. (f) Capacitance retention and coulombic efficiency data for the asymmetric supercapacitor device, with an inset displaying the charge/discharge curves at a current density of 10 A/g [70]. Copy @ Elsevier 2021. (h) Images displaying the pliability of $Mo_{1.33}CT_z$ films, with the inset capturing the Tyndall effect. (i) Ragone plot illustrating the performance of $Mo_{1.33}CT_z$ MXene symmetric supercapacitor device [199]. Copy @ Elsevier 2022.

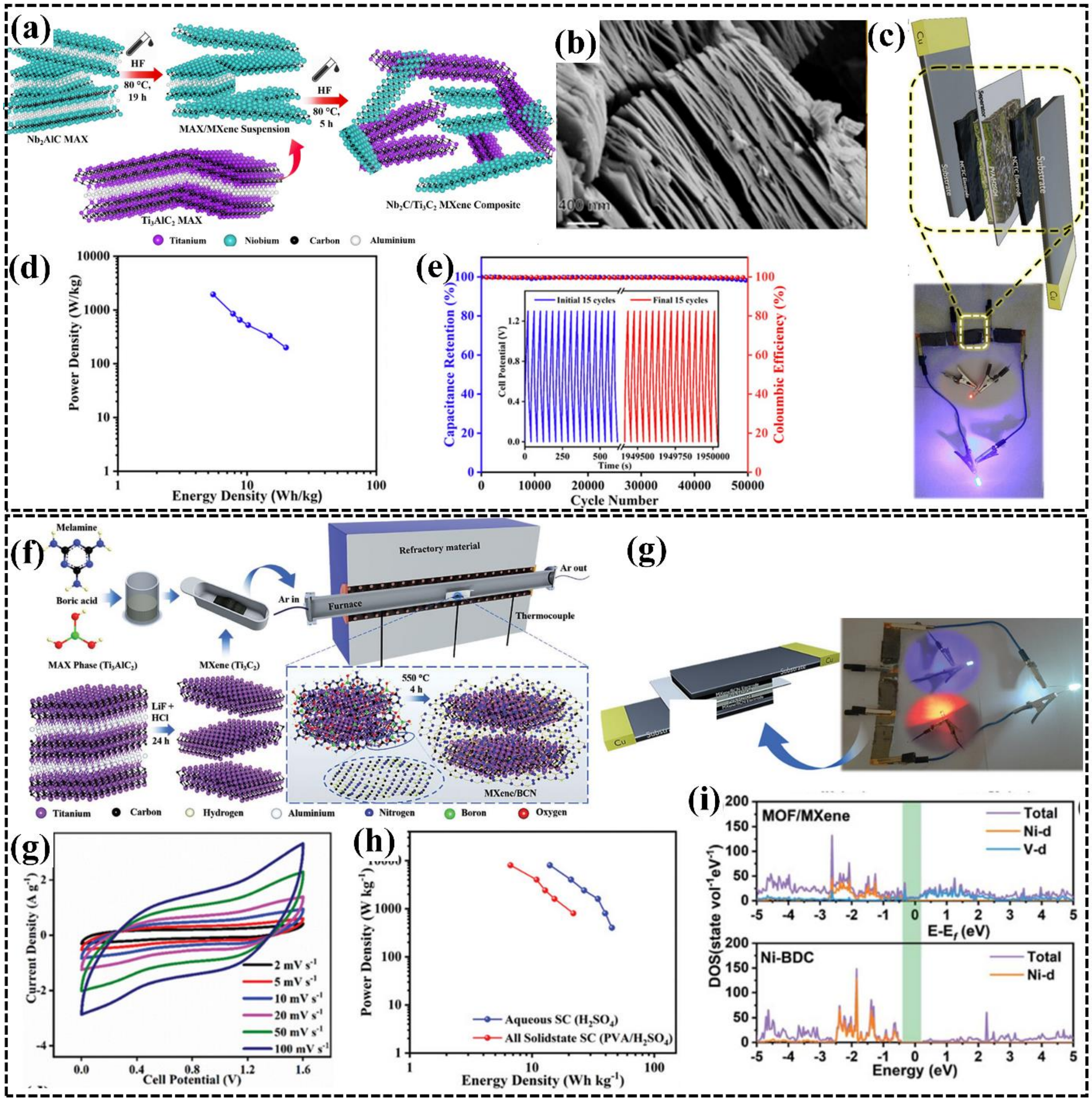

Figure 11. (a) Fabrication process of the synthesis of the Nb_2C/Ti_3C_2 MXene heterointerface through an in situ selective acid etching approach. (b) Field Emission Scanning Electron Microscope image of the Nb_2C/Ti_3C_2 heterointerface. (c) An exploded diagram of the solid-state symmetric supercapacitors device along with an inset showing the Nb_2C/Ti_3C_2 MXene heterointerface solid-state device illuminating a green LED. (d) The Ragone plot illustrating the performance of the all-solid-state device featuring the Nb_2C/Ti_3C_2 MXene heterointerface supercapacitor. (e) cycling stability of the all-solid-state Nb_2C/Ti_3C_2 MXene heterointerface over 50,000 cycles, evaluated at a current density of 2 A/g [268]. Copy @ American Chemical Society 2022. (f) Illustrative representation of the synthesis and creation process of the MXene/BCN nanocomposite through the direct pyrolysis method. (g) Schematic representation of the solid-state model and an inset demonstrating the functional MXene/BCN heterostructure solid-state supercapacitor illuminating various LEDs. (h) The Ragone plot illustrating the energy density vs.

power density performance comparison between the aqueous and all-solid-state MXene/BCN heterostructure supercapacitor devices [269]. Copy @ Wiley-VCH 2022. (i) Computed Density of States (DOS) for Ni-BDC and MOF/MXene [277]. Copy@ Royal Society of Chemistry 2023.

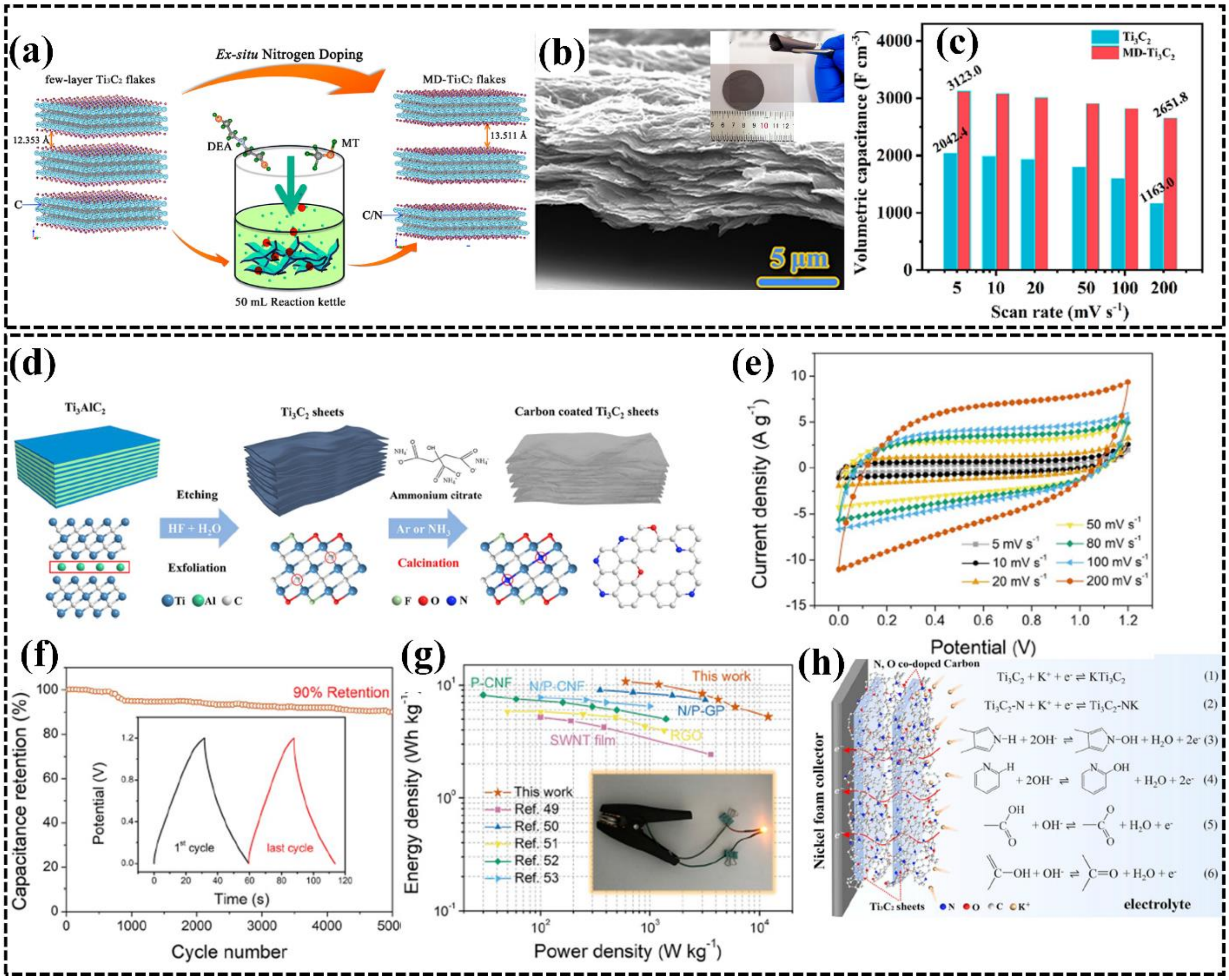

Figure 12. (a) The schematic diagram depicts the solvothermal process generating few-layer Ti_3C_2 flakes with nitrogen assistance, followed by ex situ nitrogen doping to introduce various nitrogen species in N-doped Ti_3C_2 (MD-Ti_3C_2) flakes. (b) Scanning Electron Microscope (SEM) imagery displays a cross-sectional perspective of the MD-Ti_3C_2 film, accompanied by an additional inset depicting photographs of the MD-Ti_3C_2 film with a diameter of 40 mm. (c) Volumetric capacitances of electrodes were measured at different scan rates [291]. Copy@ American Chemical Society 2020. (d) Representation depicts the synthesis procedure and the underlying reaction mechanism of N, O co-doped C@Ti_3C_2 composites. (e) The cyclic voltammetry responses of the device at different scan rates, all maintained at a voltage of 1.2 V. (f) A Ragone chart presents the performance characteristics of the device, with an inset showcasing supercapacitor device illuminating an orange LED. (h) Illustrative diagram depicts the structure of N, O co-doped coated Ti_3C_2, along with its corresponding reaction equation during the charge-discharge process [292]. Copy@ Elsevier 2019.

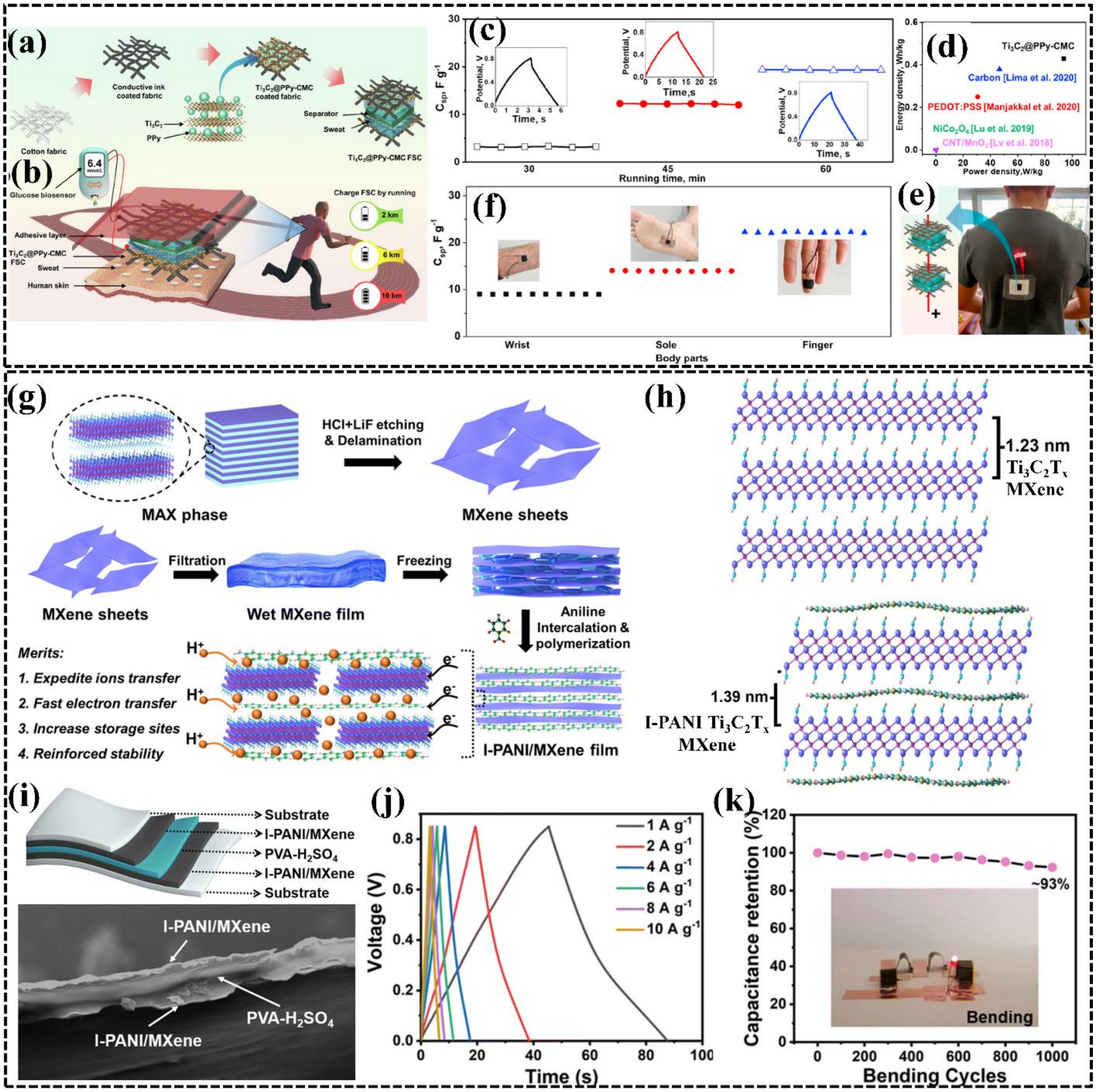

Figure 13. (a) Synthesis process of process of Ti_3C_2@PPy-CMC flexible supercapacitors. (b) schematic presentation of the skin-adhering flexible supercapacitor patch incorporating Ti_3C_2@PPy-CMC composite, utilizing the energy from human perspiration during physical activity. (c) Variation of specific capacitance in relation to the volume of sweat electrolyte produced during various running durations. (d) Ragone plot displaying a comparison between the performance of the Flexible Supercapacitor using sweat electrolyte, as well as previously documented instances of sweat electrolyte-based Flexible Supercapacitor. (e) Photograph of a tandem setup featuring Ti_3C_2@PPy-CMC Flexible Supercapacitor patches, which are powering a light emitting diode (LED) following extended running sessions. (f) Specific capacitance behavior observed when the Flexible Supercapacitor patch is affixed directly to the fingertip, the sole of the foot, and the wrist. Copy@ Elsevier [308]. (g) Schematic representation demonstrating the process of producing a single-layered MXene, as well as the creation of an MXene film with PANI

intercalation facilitated by ice (I-PANI/MXene). (h) Diagram depicting the layered configurations of pristine MXene and I-PANI/MXene electrodes. (i) schematic diagram of a symmetric supercapacitor device utilizing the I-PANI/MXene film, along with a scanning electron microscope image of the symmetric supercapacitor device separated by a PVA-H_2SO_4 gel electrolyte. (j) GCD curves depicting the performance of a supercapacitor device. (k) Percentage of capacitance retention after 1000 bends, featuring an LED illuminated by four SSC devices connected in series, both in flat and bent states [314]. Copy@ Royal Society of Chemistry 2023.

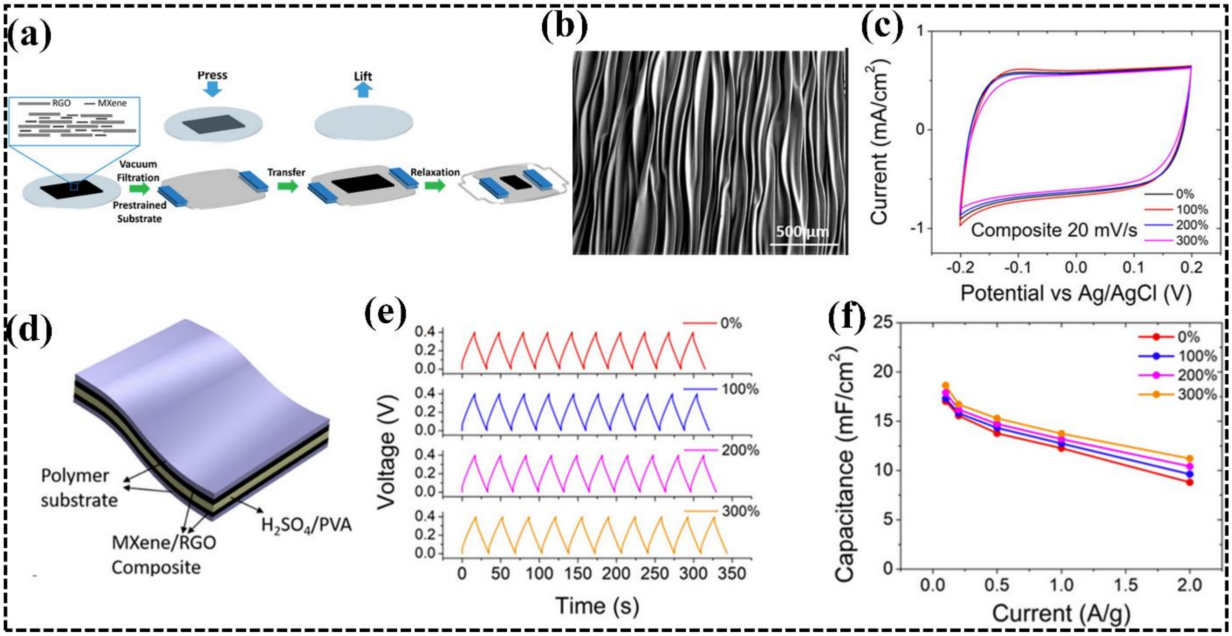

Figure 14. (a) Diagrammatic representation of the manufacturing procedure for a flexible electrode composed of a $Ti_3C_2T_x$ MXene/RGO composite thin film. (b) Scanning Electron Microscopy depiction of the surface structure of a $Ti_3C_2T_x$ MXene/RGO composite thin film (approximately 1 μm thickness) produced through the application of a uniaxial prestrain of 300%. (c) Cyclic Voltammetry plots of a $Ti_3C_2T_x$ MXene/RGO electrode recorded with a scan rate of 20 mV/s, varying with different levels of tensile strains (ranging from 0% to 300%). (d) Schematic representation of the $Ti_3C_2T_x$ MXene/RGO composite symmetric supercapacitor device. (e) Galvanostatic Charge-Discharge profiles of the flexible supercapacitor tested under varying strains and recorded at a constant current of 0.5 A/g. (f) Specific capacitance of the flexible supercapacitor assessed at different levels of strain and various charge/discharge current densities [328]. Copy@ American Chemical Society 2022.

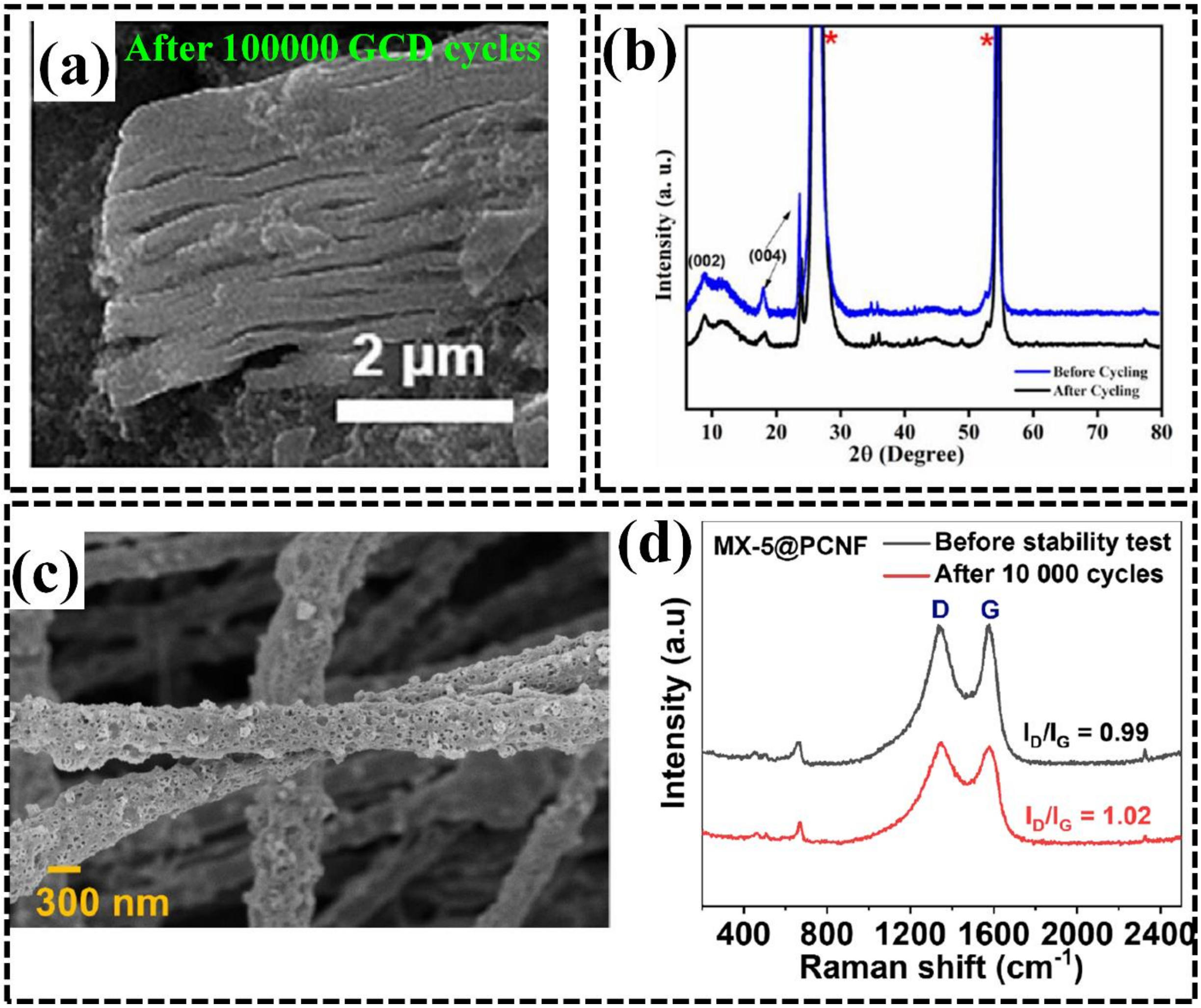

Figure 15. (a) The scanning electron microscopy images illustrate the V_2CT_x//AC asymmetric supercapacitor device after 100,000 cycles of testing conducted in a 2 M $ZnSO_4$ electrolyte [244]. Copy @ Elsevier 2022. (b) The X-ray diffraction pattern of the solid-state device's electrode film made from Nb_2C/Ti_3C_2 MXene after experiencing 5000 cycles of charge and discharge tests [268]. Copy @ American Chemical Society 2022. (c) FESEM images of $Ti_3C_2T_x$ MXene@PCNF after undergoing a stability test of 10,000 cycles. (d) Raman spectra of $Ti_3C_2T_x$ MXene@PCNF before and after a stability test of 10,000 cycles [335]. Copy @ Royal Society of Chemistry 2023.

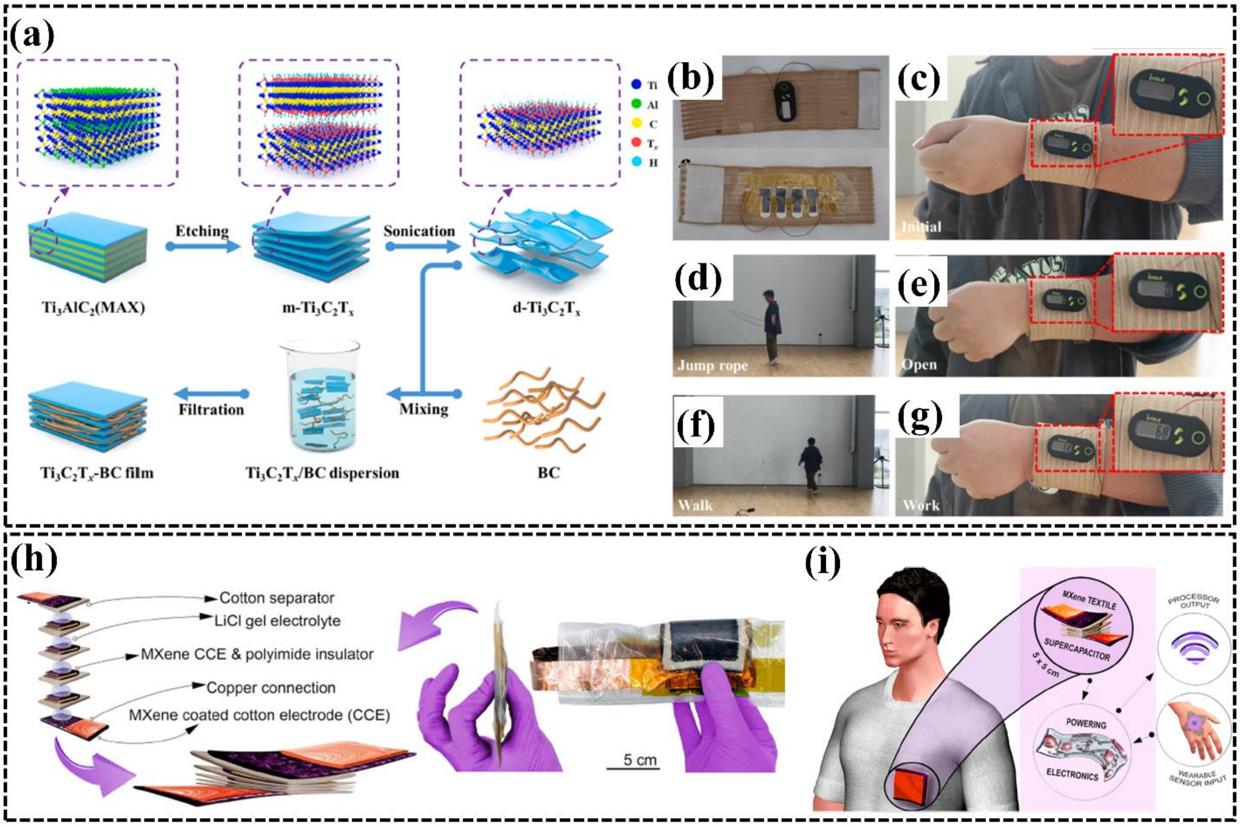

Figure 16. (a) Schematic Depictions Illustrating the Manufacturing Steps Involved in Producing MXene-BC Composite Films. (b-c) Visual representations of the self-chargeable smart wristband. (d-g) Images showcasing the functionality of the self-powered step metering feature of the smart wristband [347]. Copy @ Elsevier 2023. (h) Diagram and Photograph of a 6 V 'Stacked' Supercapacitor Encased in a Vacuum-Sealed Bag. (i) Essential Metrics for Textile Supercapacitor Integration in Flexible Energy Storage Systems and Collaboration with Peripheral Electronics: A Case Study with a $Ti_3C_2T_x$ MXene Textile Supercapacitor Featuring a 5 × 5 cm^2 Footprint Powering Programmable Electronics [339]. Copy @ Royal Society of Chemistry 2023.

References

[1] M.R. Islam, S. Afroj, K.S. Novoselov, N. Karim, Smart Electronic Textile-Based Wearable Supercapacitors. *Advanced Science* 9, 2203856 (2022)

[2] Y.W. Na, J.Y. Cheon, J.H. Kim, Y. Jung, K. Lee, J.S. Park, J.Y. Park, K.S. Song, S.B. Lee, T. Kim, S.J. Yang, All-in-one flexible supercapacitor with ultrastable performance under extreme load. *Science Advances* 8, eabl8631 (2022)

[3] Z. Zhao, K. Xia, Y. Hou, Q. Zhang, Z. Ye, J. Lu, Designing flexible, smart and self-sustainable supercapacitors for portable/wearable electronics: from conductive polymers. *Chemical Society Reviews* 50, 12702-12743 (2021)

[4] T. Kedara Shivasharma, R. Sahu, M.C. Rath, S.J. Keny, B.R. Sankapal, "Exploring tin oxide based materials: A critical review on synthesis, characterizations and supercapacitive energy storage". *Chemical Engineering Journal* 477, 147191 (2023)

[5] Z. Zhu, T. Jiang, M. Ali, Y. Meng, Y. Jin, Y. Cui, W. Chen, Rechargeable Batteries for Grid Scale Energy Storage. *Chemical Reviews* 122, 16610-16751 (2022)

[6] M. Chafiq, A. Chaouiki, Y.G. Ko, Advances in COFs for energy storage devices: Harnessing the potential of covalent organic framework materials. *Energy Storage Materials* 63, 103014 (2023)

[7] F. Wang, S. Wang, F. Tian, F. Wang, X. Xia, Q. Zhang, Z. Pang, X. Yu, G. Li, H.-Y. Hsu, S. Hu, L. Ji, Q. Xu, Y. Zhao, X. Zou, X. Lu, Advances in molten-salt-assisted synthesis of 2D MXenes and their applications in electrochemical energy storage and conversion. *Chemical Engineering Journal* 470, 144185 (2023)

[8] A.K. Tareen, K. Khan, M. Iqbal, Y. Zhang, J. Long, A. Mahmood, N. Mahmood, Z. Xie, C. Li, H. Zhang, Recent advance in two-dimensional MXenes: New horizons in flexible batteries and supercapacitors technologies. *Energy Storage Materials* 53, 783-826 (2022)

[9] S.A. Kadam, R.S. Kate, V.M. Peheliwa, S.A. Shingate, C.C. Sta. Maria, Y.-R. Ma, A comprehensive review on transition metal nitrides electrode materials for supercapacitor: Syntheses, electronic structure engineering, present perspectives and future aspects. *Journal of Energy Storage* 72, 108229 (2023)

[10] S. Samantaray, D. Mohanty, I.M. Hung, M. Moniruzzaman, S.K. Satpathy, Unleashing recent electrolyte materials for next-generation supercapacitor applications: A comprehensive review. *Journal of Energy Storage* 72, 108352 (2023)

[11] J. Castro-Gutiérrez, A. Celzard, V. Fierro, Energy Storage in Supercapacitors: Focus on Tannin-Derived Carbon Electrodes. *Frontiers in Materials* 7, (2020)

[12] P.K. Panda, A. Grigoriev, Y.K. Mishra, R. Ahuja, Progress in supercapacitors: roles of two dimensional nanotubular materials. *Nanoscale Advances* 2, 70-108 (2020)

[13] B.K. Kim, S. Sy, A. Yu, J. Zhang, Electrochemical Supercapacitors for Energy Storage and Conversion, Handbook of Clean Energy Systems, pp. 1-25.

[14] J. Wen, B. Xu, Y. Gao, M. Li, H. Fu, Wearable technologies enable high-performance textile supercapacitors with flexible, breathable and wearable characteristics for future energy storage. *Energy Storage Materials* 37, 94-122 (2021)

[15] Y. Gogotsi, R.M. Penner, Energy Storage in Nanomaterials – Capacitive, Pseudocapacitive, or Battery-like? *ACS Nano* 12, 2081-2083 (2018)

[16] J. Cherusseri, D. Pandey, J. Thomas, Symmetric, Asymmetric, and Battery-Type Supercapacitors Using Two-Dimensional Nanomaterials and Composites. *Batteries & Supercaps* 3, 860-875 (2020)

[17] R. Kumar, S. Sahoo, E. Joanni, R.K. Singh, K.K. Kar, Microwave as a Tool for Synthesis of Carbon-Based Electrodes for Energy Storage. *ACS Applied Materials & Interfaces* 14, 20306-20325 (2022)

[18] H. Zhang, F. Zhang, Y. Wei, Q. Miao, A. Li, Y. Zhao, Y. Yuan, N. Jin, G. Li, Controllable Design and Preparation of Hollow Carbon-Based Nanotubes for Asymmetric Supercapacitors and Capacitive Deionization. *ACS Applied Materials & Interfaces* 13, 21217-21230 (2021)

[19] P. More, S.A. Kadam, Y.-R. Ma, Y.-R. Chen, N. Tarwal, Y. Navale, A. Salunkhe, V. Patil, Spray Synthesized Mn-doped CuO Electrodes for High Performance Supercapacitor. *ChemistrySelect* 7, e202202504 (2022)

[20] S.A. Kadam, G.T. Phan, D.V. Pham, R.A. Patil, C.-C. Lai, Y.-R. Chen, Y. Liou, Y.-R. Ma, Doping-free bandgap tunability in Fe_2O_3 nanostructured films. *Nanoscale Advances* 3, 5581-5588 (2021)

[21] F. Lv, H. Ma, L. Shen, Y. Jiang, T. Sun, J. Ma, X. Geng, A. Kiran, N. Zhu, Wearable Helical Molybdenum Nitride Supercapacitors for Self-Powered Healthcare Smartsensors. *ACS Applied Materials & Interfaces* 13, 29780-29787 (2021)

[22] A. Bagheri, S. Bellani, H. Beydaghi, M. Eredia, L. Najafi, G. Bianca, M.I. Zappia, M. Safarpour, M. Najafi, E. Mantero, Z. Sofer, G. Hou, V. Pellegrini, X. Feng, F. Bonaccorso, Functionalized Metallic 2D Transition Metal Dichalcogenide-Based Solid-State

Electrolyte for Flexible All-Solid-State Supercapacitors. *ACS Nano* 16, 16426-16442 (2022)

[23] S.A. Thomas, S.A. Kadam, Y.-R. Ma, A. Aravind, Photocatalytic Degradation of Malachite Green Dye Using Zinc Sulfide Nanostructures. *ChemistrySelect* 6, 10015-10024 (2021)

[24] S.S. Pujari, S.A. Kadam, Y.-R. Ma, S.B. Jadhav, S.S. Kumbhar, S.B. Bhosale, J.L. Gunjakar, C.D. Lokhande, U.M. Patil, Hydrothermally synthesized nickel copper phosphate thin film cathodes for high-performance hybrid supercapacitor devices. *Journal of Energy Storage* 52, 105037 (2022)

[25] S.S. Pujari, S.A. Kadam, Y.-R. Ma, S.B. Jadhav, S.S. Kumbhar, S.B. Bhosale, V.V. Patil, J.L. Gunjakar, C.D. Lokhande, U.M. Patil, A binder-free facile synthetic approach for amorphous, hydrous nickel copper phosphate thin film electrode preparation and its application as a highly stable cathode for hybrid asymmetric supercapacitors. *Sustainable Energy & Fuels* 6, 5608-5620 (2022)

[26] T. Ye, Y. Zou, W. Xu, T. Zhan, J. Sun, Y. Xia, X. Zhang, D. Yang, Poorly-crystallized poly(vinyl alcohol)/carrageenan matrix: Highly ionic conductive and flame-retardant gel polymer electrolytes for safe and flexible solid-state supercapacitors. *Journal of Power Sources* 475, 228688 (2020)

[27] J. Zhan, A.F.M. El-Mahdy, Redox-Active Benzodithiophene-4,8-dione-Based conjugated microporous polymers for High-Performance faradaic supercapacitor energy storage. *Chemical Engineering Journal* 473, 145124 (2023)

[28] A.G. Olabi, Q. Abbas, M.A. Abdelkareem, A.H. Alami, M. Mirzaeian, E.T. Sayed, Carbon-Based Materials for Supercapacitors: Recent Progress, Challenges and Barriers, Batteries, 2023.

[29] M. Hu, H. Zhang, T. Hu, B. Fan, X. Wang, Z. Li, Emerging 2D MXenes for supercapacitors: status, challenges and prospects. *Chemical Society Reviews* 49, 6666-6693 (2020)

[30] L. Maria Jose, S. Anna Thomas, A. Aravind, Y.-R. Ma, S. Anil Kadam, Effect of Ni doping on the adsorption and visible light photocatalytic activity of ZnO hexagonal nanorods. *Inorganic Chemistry Communications* 147, 110208 (2023)

[31] S.A. Kadam, L.M. Jose, N.S. George, S. Sreehari, D.A. Nayana, D. Van Pham, K.P. Kadam, A. Aravind, Y.-R. Ma, Recent progress in transition metal nitride electrodes for supercapacitor, water splitting, and battery applications. *Journal of Alloys and Compounds* 976, 173083 (2024)

[32] G. Lu, X. Xing, J. Zhang, X. Xu, X. Zhang, H. Liu, J. Fan, B. Zhang, Rational design of cobalt ion chelated quasi-monolayer $Ti_3C_2T_x$ MXene with abundant surface loading for high-performance asymmetric supercapacitor. *Colloids and Surfaces A: Physicochemical and Engineering Aspects* 671, 131694 (2023)

[33] W. Yang, Z. Yang, J. Wang, W. Lu, W. Wang, A bean catching double pigeons: Sonication assisted modification of Nb_2C MXenes composites by O-doping porous biomass-carbons for supercapacitors and zinc-ion batteries. *Journal of Energy Storage* 65, 107334 (2023)

[34] I. Ali, M. Yousaf, I.H. Sajid, M.W. Hakim, S. Rizwan, Reticulation of 1D/2D Mo_2TiC_2 MXene for excellent supercapacitor performance. *Materials Today Chemistry* 34, 101766 (2023)

[35] Z. Otgonbayar, S. Yang, I.-J. Kim, W.-C. Oh, Recent advances in 2D MXene and solid state electrolyte for energy storage applications: Comprehensive review. *Chemical Engineering Journal* 472, 144801 (2023)

[36] X. He, S. Koo, E. Obeng, A. Sharma, J. Shen, J.S. Kim, Emerging 2D MXenes for antibacterial applications: Current status, challenges, and prospects. *Coordination Chemistry Reviews* 492, 215275 (2023)

[37] R. Wang, W. Young Jang, W. Zhang, C. Venkata Reddy, R.R. Kakarla, C. Li, V.K. Gupta, J. Shim, T.M. Aminabhavi, Emerging two-dimensional (2D) MXene-based nanostructured materials: Synthesis strategies, properties, and applications as efficient pseudo-supercapacitors. *Chemical Engineering Journal* 472, 144913 (2023)

[38] Z. Shi, R. Khaledialidusti, M. Malaki, H. Zhang, MXene-Based Materials for Solar Cell Applications, Nanomaterials, 2021.

[39] A. Bhat, S. Anwer, K.S. Bhat, M.I.H. Mohideen, K. Liao, A. Qurashi, Prospects challenges and stability of 2D MXenes for clean energy conversion and storage applications. *npj 2D Materials and Applications* 5, 61 (2021)

[40] B. Zhao, D. Shen, Z. Zhang, P. Lu, M. Hossain, J. Li, B. Li, X. Duan, 2D Metallic Transition-Metal Dichalcogenides: Structures, Synthesis, Properties, and Applications. *Advanced Functional Materials* 31, 2105132 (2021)

[41] A.K. Geim, K.S. Novoselov, The rise of graphene. *Nature Materials* 6, 183-191 (2007)

[42] M. Naguib, O. Mashtalir, J. Carle, V. Presser, J. Lu, L. Hultman, Y. Gogotsi, M.W. Barsoum, Two-Dimensional Transition Metal Carbides. *ACS Nano* 6, 1322-1331 (2012)

[43] M.-S. Cao, Y.-Z. Cai, P. He, J.-C. Shu, W.-Q. Cao, J. Yuan, 2D MXenes: Electromagnetic property for microwave absorption and electromagnetic interference shielding. *Chemical Engineering Journal* 359, 1265-1302 (2019)

[44] G. Deysher, C.E. Shuck, K. Hantanasirisakul, N.C. Frey, A.C. Foucher, K. Maleski, A. Sarycheva, V.B. Shenoy, E.A. Stach, B. Anasori, Y. Gogotsi, Synthesis of Mo_4VAlC_4 MAX Phase and Two-Dimensional Mo_4VC_4 MXene with Five Atomic Layers of Transition Metals. *ACS Nano* 14, 204-217 (2020)

[45] F. Shahzad, A. Iqbal, H. Kim, C.M. Koo, 2D Transition Metal Carbides (MXenes): Applications as an Electrically Conducting Material. *Advanced Materials* 32, 2002159 (2020)

[46] J. Björk, J. Halim, J. Zhou, J. Rosen, Predicting chemical exfoliation: fundamental insights into the synthesis of MXenes. *npj 2D Materials and Applications* 7, 5 (2023)

[47] Y. Wang, Z. Niu, Y. Dai, P. Mu, J. Li, Two-dimensional nanomaterial MXenes for efficient gas separation: a review. *Nanoscale* 15, 4170-4194 (2023)

[48] U. Khan, Y. Luo, L.B. Kong, W. Que, Synthesis of fluorine free MXene through lewis acidic etching for application as electrode of proton supercapacitors. *Journal of Alloys and Compounds* 926, 166903 (2022)

[49] Y.-L. Liu, C. Zhang, L. Guo, Q. Zeng, R. Wang, H. Chen, Q. Zhang, Q. Zeng, Synergistically adsorbing and reducing Uranium from water by a novel nano zero-valent copper/MXene 0D/2D nanocomposite. *Water Research* 245, 120666 (2023)

[50] L. Liu, H. Zschiesche, M. Antonietti, B. Daffos, N.V. Tarakina, M. Gibilaro, P. Chamelot, L. Massot, B. Duployer, P.-L. Taberna, P. Simon, Tuning the Surface Chemistry of MXene

to Improve Energy Storage: Example of Nitrification by Salt Melt. *Advanced Energy Materials* 13, 2202709 (2023)

[51] H. Hwang, S. Byun, S. Yuk, S. Kim, S.H. Song, D. Lee, High-rate electrospun $Ti_3C_2T_x$ MXene/carbon nanofiber electrodes for flexible supercapacitors. *Applied Surface Science* 556, 149710 (2021)

[52] H. Shi, P. Zhang, Z. Liu, S. Park, M.R. Lohe, Y. Wu, A. Shaygan Nia, S. Yang, X. Feng, Ambient-Stable Two-Dimensional Titanium Carbide (MXene) Enabled by Iodine Etching. *Angewandte Chemie International Edition* 60, 8689-8693 (2021)

[53] M. Naguib, V.N. Mochalin, M.W. Barsoum, Y. Gogotsi, 25th Anniversary Article: MXenes: A New Family of Two-Dimensional Materials. *Advanced Materials* 26, 992-1005 (2014)

[54] T. Su, X. Ma, J. Tong, H. Ji, Z. Qin, Z. Wu, Surface engineering of MXenes for energy and environmental applications. *Journal of Materials Chemistry A* 10, 10265-10296 (2022)

[55] J. Choi, M.S. Oh, A. Cho, J. Ryu, Y.-J. Kim, H. Kang, S.-Y. Cho, S.G. Im, S.J. Kim, H.-T. Jung, Simple Approach to Enhance Long-Term Environmental Stability of MXene Using Initiated Chemical Vapor Deposition Surface Coating. *ACS Nano* 17, 10898-10905 (2023)

[56] F. Shahzad, M. Alhabeb, C.B. Hatter, B. Anasori, S. Man Hong, C.M. Koo, Y. Gogotsi, Electromagnetic interference shielding with 2D transition metal carbides (MXenes). *Science* 353, 1137-1140 (2016)

[57] H. Yu, Y. Wang, Y. Jing, J. Ma, C.-F. Du, Q. Yan, Surface Modified MXene-Based Nanocomposites for Electrochemical Energy Conversion and Storage. *Small* 15, 1901503 (2019)

[58] N. Liu, Q. Li, H. Wan, L. Chang, H. Wang, J. Fang, T. Ding, Q. Wen, L. Zhou, X. Xiao, High-temperature stability in air of $Ti_3C_2T_x$ MXene-based composite with extracted bentonite. *Nature Communications* 13, 5551 (2022)

[59] F. Cao, Y. Zhang, H. Wang, K. Khan, A.K. Tareen, W. Qian, H. Zhang, H. Ågren, Recent Advances in Oxidation Stable Chemistry of 2D MXenes. *Advanced Materials* 34, 2107554 (2022)

[60] P. Ganguly, M. Harb, Z. Cao, L. Cavallo, A. Breen, S. Dervin, D.D. Dionysiou, S.C. Pillai, 2D Nanomaterials for Photocatalytic Hydrogen Production. *ACS Energy Letters* 4, 1687-1709 (2019)

[61] L.-f. Hong, R.-t. Guo, Y. Yuan, X.-y. Ji, Z.-s. Li, Z.-d. Lin, W.-g. Pan, Recent progress of two-dimensional MXenes in photocatalytic applications: a review. *Materials Today Energy* 18, 100521 (2020)

[62] A. Sherryna, M. Tahir, Role of Ti_3C_2 MXene as Prominent Schottky Barriers in Driving Hydrogen Production through Photoinduced Water Splitting: A Comprehensive Review. *ACS Applied Energy Materials* 4, 11982-12006 (2021)

[63] M. Arslanoglu, B. Yuan, R. Panat, O.B. Ozdoganlar, 3D Assembly of MXene Networks using a Ceramic Backbone with Controlled Porosity. *Advanced Materials* 35, 2304757 (2023)

[64] Z. Cao, H. Hu, D. Ho, Micro-Redoxcapacitor: A Hybrid Architecture Out of the Notorious Energy-Power Density Dilemma. *Advanced Functional Materials* 32, 2111805 (2022)

[65] F. Song, G. Li, Y. Zhu, Z. Wu, X. Xie, N. Zhang, Rising from the horizon: three-dimensional functional architectures assembled with MXene nanosheets. *Journal of Materials Chemistry A* 8, 18538-18559 (2020)

[66] J. Pang, R.G. Mendes, A. Bachmatiuk, L. Zhao, H.Q. Ta, T. Gemming, H. Liu, Z. Liu, M.H. Rummeli, Applications of 2D MXenes in energy conversion and storage systems. *Chemical Society Reviews* 48, 72-133 (2019)

[67] Z. Cao, G. Liang, D. Ho, C. Zhi, H. Hu, Interlayer Injection of Low-Valence Zn Atoms to Activate MXene-Based Micro-Redox Capacitors With Battery-Type Voltage Plateaus. *Advanced Functional Materials* 33, 2303060 (2023)

[68] Y. Wang, Y. Wang, Recent progress in MXene layers materials for supercapacitors: High-performance electrodes. *SmartMat* 4, e1130 (2023)

[69] J. Xu, J. You, L. Wang, Z. Wang, H. Zhang, MXenes serving aqueous supercapacitors: Preparation, energy storage mechanism and electrochemical performance enhancement. *Sustainable Materials and Technologies* 33, e00490 (2022)

[70] A.E. Ghazaly, W. Zheng, J. Halim, E.N. Tseng, P.O. Persson, B. Ahmed, J. Rosen, Enhanced supercapacitive performance of $Mo_{1.33}C$ MXene based asymmetric supercapacitors in lithium chloride electrolyte. *Energy Storage Materials* 41, 203-208 (2021)

[71] T. Jiang, Y. Wang, G.Z. Chen, Electrochemistry of Titanium Carbide MXenes in Supercapacitor. *Small Methods* 7, 2201724 (2023)

[72] A.E. Ghazaly, H. Ahmed, A.R. Rezk, J. Halim, P.O.Å. Persson, L.Y. Yeo, J. Rosen, Ultrafast, One-Step, Salt-Solution-Based Acoustic Synthesis of Ti_3C_2 MXene. *ACS Nano* 15, 4287-4293 (2021)

[73] R. Akhter, S.S. Maktedar, MXenes: A comprehensive review of synthesis, properties, and progress in supercapacitor applications. *Journal of Materiomics* 9, 1196-1241 (2023)

[74] M.R. Lukatskaya, S. Kota, Z. Lin, M.-Q. Zhao, N. Shpigel, M.D. Levi, J. Halim, P.-L. Taberna, M.W. Barsoum, P. Simon, Y. Gogotsi, Ultra-high-rate pseudocapacitive energy storage in two-dimensional transition metal carbides. *Nature Energy* 2, 17105 (2017)

[75] Y. Xia, T.S. Mathis, M.-Q. Zhao, B. Anasori, A. Dang, Z. Zhou, H. Cho, Y. Gogotsi, S. Yang, Thickness-independent capacitance of vertically aligned liquid-crystalline MXenes. *Nature* 557, 409-412 (2018)

[76] C. Zhang, B. Anasori, A. Seral-Ascaso, S.-H. Park, N. McEvoy, A. Shmeliov, G.S. Duesberg, J.N. Coleman, Y. Gogotsi, V. Nicolosi, Transparent, Flexible, and Conductive 2D Titanium Carbide (MXene) Films with High Volumetric Capacitance. *Advanced Materials* 29, 1702678 (2017)

[77] X. Xu, L. Yang, W. Zheng, H. Zhang, F. Wu, Z. Tian, P. Zhang, Z. Sun, MXenes with applications in supercapacitors and secondary batteries: A comprehensive review. *Materials Reports: Energy* 2, 100080 (2022)

[78] Y. Bao, Y. Liu, Y. Kuang, D. Fang, T. Li, 3D-printed highly deformable electrodes for flexible lithium ion batteries. *Energy Storage Materials* 33, 55-61 (2020)

[79] V.K.A. Muniraj, M.K. Srinivasa, H.D. Yoo, Flexible supercapacitors toward wearable energy storage devices. *Bulletin of the Korean Chemical Society* 44, 125-136 (2023)

[80] L.-Q. Yao, Y. Qin, X.-C. Li, Q. Xue, F. Liu, T. Cheng, G.-J. Li, X. Zhang, W.-Y. Lai, High-efficiency stretchable organic light-emitting diodes based on ultra-flexible printed embedded metal composite electrodes. *InfoMat* 5, e12410 (2023)

[81] Y. Wang, X. Wang, X. Li, Y. Bai, H. Xiao, Y. Liu, R. Liu, G. Yuan, Engineering 3D Ion Transport Channels for Flexible MXene Films with Superior Capacitive Performance. *Advanced Functional Materials* 29, 1900326 (2019)

[82] T.-H. Chang, T. Zhang, H. Yang, K. Li, Y. Tian, J.Y. Lee, P.-Y. Chen, Controlled Crumpling of Two-Dimensional Titanium Carbide (MXene) for Highly Stretchable, Bendable, Efficient Supercapacitors. *ACS Nano* 12, 8048-8059 (2018)

[83] R.S. Kate, S.A. Khalate, R.J. Deokate, Overview of nanostructured metal oxides and pure nickel oxide (NiO) electrodes for supercapacitors: A review. *Journal of Alloys and Compounds* 734, 89-111 (2018)

[84] M.Z. Ansari, S.A. Ansari, S.-H. Kim, Fundamentals and recent progress of Sn-based electrode materials for supercapacitors: A comprehensive review. *Journal of Energy Storage* 53, 105187 (2022)

[85] S.A. Kadam, K.P. Kadam, C.C. Sta. Maria, Y.-R. Ma, A.C. Molane, S.A. Lolage, V.B. Patil, P.D. More, Microporous α-Fe_2O_3@NiO Heterostructures Synthesized for Enhanced Supercapacitor Performance. *ChemistrySelect* 9, e202302376 (2024)

[86] B. Pal, S. Yang, S. Ramesh, V. Thangadurai, R. Jose, Electrolyte selection for supercapacitive devices: a critical review. *Nanoscale Advances* 1, 3807-3835 (2019)

[87] S. Ahankari, D. Lasrado, R. Subramaniam, Advances in materials and fabrication of separators in supercapacitors. *Materials Advances* 3, 1472-1496 (2022)

[88] L. Ding, N. Yan, S. Zhang, R. Xu, T. Wu, F. Yang, Y. Cao, M. Xiang, Separator impregnated with polyvinyl alcohol to simultaneously improve electrochemical performances and compression resistance. *Electrochimica Acta* 403, 139568 (2022)

[89] M. Winter, R.J. Brodd, What Are Batteries, Fuel Cells, and Supercapacitors? *Chemical Reviews* 104, 4245-4270 (2004)

[90] S. Lehtimäki, A. Railanmaa, J. Keskinen, M. Kujala, S. Tuukkanen, D. Lupo, Performance, stability and operation voltage optimization of screen-printed aqueous supercapacitors. *Scientific Reports* 7, 46001 (2017)

[91] S. Zhang, N. Pan, Supercapacitors Performance Evaluation. *Advanced Energy Materials* 5, 1401401 (2015)

[92] B.A. Ali, N.K. Allam, A first-principles roadmap and limits to design efficient supercapacitor electrode materials. *Physical Chemistry Chemical Physics* 21, 17494-17511 (2019)

[93] X. Wang, S. Kajiyama, H. Iinuma, E. Hosono, S. Oro, I. Moriguchi, M. Okubo, A. Yamada, Pseudocapacitance of MXene nanosheets for high-power sodium-ion hybrid capacitors. *Nature Communications* 6, 6544 (2015)

[94] M. Boota, Y. Gogotsi, MXene—Conducting Polymer Asymmetric Pseudocapacitors. *Advanced Energy Materials* 9, 1802917 (2019)

[95] H. Tang, Q. Hu, M. Zheng, Y. Chi, X. Qin, H. Pang, Q. Xu, MXene–2D layered electrode materials for energy storage. *Progress in Natural Science: Materials International* 28, 133-147 (2018)

[96] X. Liu, Y. Qiu, D. Jiang, F. Li, Y. Gan, Y. Zhu, Y. Pan, H. Wan, P. Wang, Covalently grafting first-generation PAMAM dendrimers onto MXenes with self-adsorbed AuNPs for use as a functional nanoplatform for highly sensitive electrochemical biosensing of cTnT. *Microsystems & Nanoengineering* 8, 35 (2022)

[97] A. Djire, A. Bos, J. Liu, H. Zhang, E.M. Miller, N.R. Neale, Pseudocapacitive Storage in Nanolayered Ti_2NT_x MXene Using Mg-Ion Electrolyte. *ACS Applied Nano Materials* 2, 2785-2795 (2019)

[98] M.Z. Iqbal, M.W. Khan, S. Siddique, S. Aftab, MXenes: An exotic material for hybrid supercapacitors and rechargeable batteries. *Journal of Energy Storage* 56, 105914 (2022)

[99] Y. Gogotsi, Q. Huang, MXenes: Two-Dimensional Building Blocks for Future Materials and Devices. *ACS Nano* 15, 5775-5780 (2021)

[100] M.P. Bilibana, Electrochemical properties of MXenes and applications. *Advanced Sensor and Energy Materials* 2, 100080 (2023)

[101] Y. Wang, M. Liu, Z. Wang, Q. Gu, B. Liu, C. Zhao, J. Zhang, S. Xu, M. Lu, H. Li, B. Zhang, Interlayer environment engineered MXene: Pre-intercalated Zn^{2+} ions as intercalants renders the modulated Li storage. *Journal of Energy Chemistry* 68, 306-313 (2022)

[102] J. Park, Y. Kim, H. Bark, P.S. Lee, Recent Progress in MXene-Based Electrochemical Actuators and Capacitors. *Small Structures* n/a, 2300520 (2024)

[103] L. Cui, C. Zhang, MXenes as conductive and mechanical additives in energy storage devices. *EnergyChem* 100110 (2023)

[104] H. Liu, Z. Xin, B. Cao, B. Zhang, H.J. Fan, S. Guo, Versatile MXenes for Aqueous Zinc Batteries. *Advanced Science* n/a, 2305806 (2023)

[105] A. Burke, R&D considerations for the performance and application of electrochemical capacitors. *Electrochimica Acta* 53, 1083-1091 (2007)

[106] X. Zang, J. Wang, Y. Qin, T. Wang, C. He, Q. Shao, H. Zhu, N. Cao, Enhancing Capacitance Performance of $Ti_3C_2T_x$ MXene as Electrode Materials of Supercapacitor: From Controlled Preparation to Composite Structure Construction. *Nano-Micro Letters* 12, 77 (2020)

[107] K. Ghosh, S. Ng, P. Lazar, A.K.K. Padinjareveetil, J. Michalička, M. Pumera, 2D Germanane-MXene Heterostructures for Cations Intercalation in Energy Storage Applications. *Advanced Functional Materials* n/a, 2308793 (2023)

[108] M.R. Lukatskaya, O. Mashtalir, C.E. Ren, Y. Dall'Agnese, P. Rozier, P.L. Taberna, M. Naguib, P. Simon, M.W. Barsoum, Y. Gogotsi, Cation intercalation and high volumetric capacitance of two-dimensional titanium carbide. *Science* 341, 1502-1505 (2013)

[109] M.D. Levi, M.R. Lukatskaya, S. Sigalov, M. Beidaghi, N. Shpigel, L. Daikhin, D. Aurbach, M.W. Barsoum, Y. Gogotsi, Solving the Capacitive Paradox of 2D MXene using Electrochemical Quartz-Crystal Admittance and In Situ Electronic Conductance Measurements. *Advanced Energy Materials* 5, 1400815 (2015)

[110] M.A. Kosnan, M.A. Azam, N.E. Safie, R.F. Munawar, A. Takasaki, Recent Progress of Electrode Architecture for MXene/MoS_2 Supercapacitor: Preparation Methods and Characterizations, Micromachines, 2022.

[111] Y. Dall'Agnese, M.R. Lukatskaya, K.M. Cook, P.-L. Taberna, Y. Gogotsi, P. Simon, High capacitance of surface-modified 2D titanium carbide in acidic electrolyte. *Electrochemistry Communications* 48, 118-122 (2014)

[112] N. Shpigel, M.D. Levi, S. Sigalov, T.S. Mathis, Y. Gogotsi, D. Aurbach, Direct Assessment of Nanoconfined Water in 2D Ti_3C_2 Electrode Interspaces by a Surface Acoustic Technique. *Journal of the American Chemical Society* 140, 8910-8917 (2018)

[113] Y. Sun, C. Zhan, P.R.C. Kent, M. Naguib, Y. Gogotsi, D.-e. Jiang, Proton Redox and Transport in MXene-Confined Water. *ACS Applied Materials & Interfaces* 12, 763-770 (2020)

[114] H. Shao, K. Xu, Y.-C. Wu, A. Iadecola, L. Liu, H. Ma, L. Qu, E. Raymundo-Piñero, J. Zhu, Z. Lin, P.-L. Taberna, P. Simon, Unraveling the Charge Storage Mechanism of $Ti_3C_2T_x$ MXene Electrode in Acidic Electrolyte. *ACS Energy Letters* 5, 2873-2880 (2020)

[115] N.S. George, S. Anil Kadam, S. Sreehari, L. Maria Jose, Y. Ron Ma, A. Aravind, Inquest on photocatalytic and antibacterial traits of low composition Cu doped ZnO nanoparticles. *Chemical Physics Letters* 815, 140351 (2023)

[116] X. Wang, T.S. Mathis, K. Li, Z. Lin, L. Vlcek, T. Torita, N.C. Osti, C. Hatter, P. Urbankowski, A. Sarycheva, M. Tyagi, E. Mamontov, P. Simon, Y. Gogotsi, Influences from solvents on charge storage in titanium carbide MXenes. *Nature Energy* 4, 241-248 (2019)

[117] Y.A. Kumar, C.J. Raorane, H.H. Hegazy, T. Ramachandran, S.C. Kim, M. Moniruzzaman, 2D MXene-based supercapacitors: A promising path towards high-performance energy storage. *Journal of Energy Storage* 72, 108433 (2023)

[118] Y. Long, Y. Tao, T. Shang, H. Yang, Z. Sun, W. Chen, Q.-H. Yang, Roles of Metal Ions in MXene Synthesis, Processing and Applications: A Perspective. *Advanced Science* 9, 2200296 (2022)

[119] G. Sharma, E. Muthuswamy, M. Naguib, Y. Gogotsi, A. Navrotsky, D. Wu, Calorimetric Study of Alkali Metal Ion (K^+, Na^+, Li^+) Exchange in a Clay-Like MXene. *The Journal of Physical Chemistry C* 121, 15145-15153 (2017)

[120] P. Bärmann, R. Nölle, V. Siozios, M. Ruttert, O. Guillon, M. Winter, J. Gonzalez-Julian, T. Placke, Solvent Co-intercalation into Few-layered $Ti_3C_2T_x$ MXenes in Lithium Ion Batteries Induced by Acidic or Basic Post-treatment. *ACS Nano* 15, 3295-3308 (2021)

[121] P. Ma, D. Fang, Y. Liu, Y. Shang, Y. Shi, H.Y. Yang, MXene-Based Materials for Electrochemical Sodium-Ion Storage. *Advanced Science* 8, 2003185 (2021)

[122] X. Gao, X. Du, T.S. Mathis, M. Zhang, X. Wang, J. Shui, Y. Gogotsi, M. Xu, Maximizing ion accessibility in MXene-knotted carbon nanotube composite electrodes for high-rate electrochemical energy storage. *Nature Communications* 11, 6160 (2020)

[123] F. Kamarulazam, S. Bashir, S. Ramesh, K. Ramesh, Emerging trends towards MXene-based electrolytes for electrochemical applications. *Materials Science and Engineering: B* 290, 116355 (2023)

[124] J. Yin, K. Wei, J. Zhang, S. Liu, X. Wang, X. Wang, Q. Zhang, Z. Qin, T. Jiao, MXene-based film electrode and all-round hydrogel electrolyte for flexible all-solid supercapacitor with extremely low working temperature. *Cell Reports Physical Science* 3, 100893 (2022)

[125] X. Zhao, C. Dall'Agnese, X.-F. Chu, S. Zhao, G. Chen, Y. Gogotsi, Y. Gao, Y. Dall'Agnese, Electrochemical Behavior of $Ti_3C_2T_x$ MXene in Environmentally Friendly Methanesulfonic Acid Electrolyte. *ChemSusChem* 12, 4480-4486 (2019)

[126] D. Gandla, F. Zhang, D.Q. Tan, Advantage of Larger Interlayer Spacing of a $Mo_2Ti_2C_3$ MXene Free-Standing Film Electrode toward an Excellent Performance Supercapacitor in a Binary Ionic Liquid–Organic Electrolyte. *ACS Omega* 7, 7190-7198 (2022)

[127] X. Tang, D. Zhou, P. Li, X. Guo, C. Wang, F. Kang, B. Li, G. Wang, High-Performance Quasi-Solid-State MXene-Based Li–I Batteries. *ACS Central Science* 5, 365-373 (2019)

[128] M. Hu, Z. Li, T. Hu, S. Zhu, C. Zhang, X. Wang, High-Capacitance Mechanism for $Ti_3C_2T_x$ MXene by in Situ Electrochemical Raman Spectroscopy Investigation. *ACS Nano* 10, 11344-11350 (2016)

[129] G. Bergman, E. Ballas, Q. Gao, A. Nimkar, B. Gavriel, M.D. Levi, D. Sharon, F. Malchik, X. Wang, N. Shpigel, D. Mandler, D. Aurbach, Elucidation of the Charging Mechanisms and the Coupled Structural–Mechanical Behavior of $Ti_3C_2T_x$ (MXenes) Electrodes by In Situ Techniques. *Advanced Energy Materials* 13, 2203154 (2023)

[130] C. Zhan, M. Naguib, M. Lukatskaya, P.R.C. Kent, Y. Gogotsi, D.-e. Jiang, Understanding the MXene Pseudocapacitance. *The Journal of Physical Chemistry Letters* 9, 1223-1228 (2018)

[131] Y. Tang, J. Zhu, C. Yang, F. Wang, Enhanced Capacitive Performance Based on Diverse Layered Structure of Two-Dimensional Ti_3C_2 MXene with Long Etching Time. *Journal of The Electrochemical Society* 163, A1975 (2016)

[132] J. Fu, L. Li, D. Lee, J.M. Yun, B.K. Ryu, K.H. Kim, Enhanced electrochemical performance of $Ti_3C_2T_x$ MXene film based supercapacitors in H2SO4/KI redox additive electrolyte. *Applied Surface Science* 504, 144250 (2020)

[133] Y. Gao, L. Wang, Z. Li, Y. Zhang, B. Xing, C. Zhang, A. Zhou, Electrochemical performance of Ti_3C_2 supercapacitors in KOH electrolyte. *Journal of Advanced Ceramics* 4, 130-134 (2015)

[134] R. Syamsai, P. Kollu, S. Kwan Jeong, A. Nirmala Grace, Synthesis and properties of 2D-titanium carbide MXene sheets towards electrochemical energy storage applications. *Ceramics International* 43, 13119-13126 (2017)

[135] Y.-Y. Peng, B. Akuzum, N. Kurra, M.-Q. Zhao, M. Alhabeb, B. Anasori, E.C. Kumbur, H.N. Alshareef, M.-D. Ger, Y. Gogotsi, All-MXene (2D titanium carbide) solid-state microsupercapacitors for on-chip energy storage. *Energy & Environmental Science* 9, 2847-2854 (2016)

[136] Y. Dall'Agnese, P. Rozier, P.-L. Taberna, Y. Gogotsi, P. Simon, Capacitance of two-dimensional titanium carbide (MXene) and MXene/carbon nanotube composites in organic electrolytes. *Journal of Power Sources* 306, 510-515 (2016)

[137] K.R. Seddon, Ionic Liquids for Clean Technology. *Journal of Chemical Technology & Biotechnology* 68, 351-356 (1997)

[138] Z. Said, P. Sharma, N. Aslfattahi, M. Ghodbane, Experimental analysis of novel ionic liquid-MXene hybrid nanofluid's energy storage properties: Model-prediction using modern ensemble machine learning methods. *Journal of Energy Storage* 52, 104858 (2022)

[139] L. Sun, K. Zhuo, Y. Chen, Q. Du, S. Zhang, J. Wang, Ionic Liquid-Based Redox Active Electrolytes for Supercapacitors. *Advanced Functional Materials* 32, 2203611 (2022)

[140] M. Pandey, K. Deshmukh, A. Raman, A. Asok, S. Appukuttan, G.R. Suman, Prospects of MXene and graphene for energy storage and conversion. *Renewable and Sustainable Energy Reviews* 189, 114030 (2024)

[141] N. Jäckel, B. Krüner, K.L. Van Aken, M. Alhabeb, B. Anasori, F. Kaasik, Y. Gogotsi, V. Presser, Electrochemical in Situ Tracking of Volumetric Changes in Two-Dimensional Metal Carbides (MXenes) in Ionic Liquids. *ACS Applied Materials & Interfaces* 8, 32089-32093 (2016)

[142] N.C. Osti, M.W. Thompson, K.L. Van Aken, M. Alhabeb, M. Tyagi, J.-K. Keum, P.T. Cummings, Y. Gogotsi, E. Mamontov, Humidity Exposure Enhances Microscopic Mobility in a Room-Temperature Ionic Liquid in MXene. *The Journal of Physical Chemistry C* 122, 27561-27566 (2018)

[143] N. Osti, M. Thompson, K. Van Aken, M. Alhabeb, M. Tyagi, J.-K. Keum, P. Cummings, Y. Gogotsi, E. Mamontov, Humidity Exposure Enhances Microscopic Mobility in a Room-Temperature Ionic Liquid in MXene. *The Journal of Physical Chemistry C* 122, (2018)

[144] C. Likitaporn, M. Okhawilai, P. Kasemsiri, J. Qin, P. Potiyaraj, H. Uyama, High electrolyte uptake of MXene integrated membrane separators for Zn-ion batteries. *Scientific Reports* 12, 19915 (2022)

[145] S. Nahirniak, A. Ray, B. Saruhan, Challenges and Future Prospects of the MXene-Based Materials for Energy Storage Applications, Batteries, 2023.

[146] P. Das, Z.-S. Wu, MXene for energy storage: present status and future perspectives. *Journal of Physics: Energy* 2, 032004 (2020)

[147] J.-J. Zhu, A. Hemesh, J.J. Biendicho, L. Martinez-Soria, D. Rueda-Garcia, J.R. Morante, B. Ballesteros, P. Gomez-Romero, Rational design of MXene/activated carbon/polyoxometalate triple hybrid electrodes with enhanced capacitance for organic-electrolyte supercapacitors. *Journal of Colloid and Interface Science* 623, 947-961 (2022)

[148] N. Kitchamsetti, A.L.F. de Barros, Recent Advances in MXenes Based Composites as Photocatalysts: Synthesis, Properties and Photocatalytic Removal of Organic Contaminants from Wastewater. *ChemCatChem* 15, e202300690 (2023)

[149] L. Zhang, W. Song, H. Liu, H. Ding, Y. Yan, R. Chen, Influencing Factors on Synthesis and Properties of MXene: A Review, Processes, 2022.

[150] K. Khan, A.K. Tareen, M. Iqbal, I. Hussain, A. Mahmood, U. Khan, M.F. Khan, H. Zhang, Z. Xie, Recent advances in MXenes: a future of nanotechnologies. *Journal of Materials Chemistry A* 11, 19764-19811 (2023)

[151] L. Verger, C. Xu, V. Natu, H.-M. Cheng, W. Ren, M.W. Barsoum, Overview of the synthesis of MXenes and other ultrathin 2D transition metal carbides and nitrides. *Current Opinion in Solid State and Materials Science* 23, 149-163 (2019)

[152] L. Jiang, D. Zhou, J. Yang, S. Zhou, H. Wang, X. Yuan, J. Liang, X. Li, Y. Chen, H. Li, 2D single- and few-layered MXenes: synthesis, applications and perspectives. *Journal of Materials Chemistry A* 10, 13651-13672 (2022)

[153] T.S. Kvashina, N.F. Uvarov, M.A. Korchagin, Y.L. Krutskiy, A.V. Ukhina, Synthesis of MXene Ti_3C_2 by selective etching of MAX-phase Ti_3AlC_2. *Materials Today: Proceedings* 31, 592-594 (2020)

[154] K.P. Loh, MXenes Are Still Hot. *Chemistry of Materials* 35, 8771-8773 (2023)

[155] N.K. Chaudhari, H. Jin, B. Kim, D. San Baek, S.H. Joo, K. Lee, MXene: an emerging two-dimensional material for future energy conversion and storage applications. *Journal of Materials Chemistry A* 5, 24564-24579 (2017)

[156] N. Iqbal, U. Ghani, W. Liao, X. He, Y. Lu, Z. Wang, T. Li, Synergistically engineered 2D MXenes for metal-ion/Li–S batteries: Progress and outlook. *Materials Today Advances* 16, 100303 (2022)

[157] M. Naguib, M. Kurtoglu, V. Presser, J. Lu, J. Niu, M. Heon, L. Hultman, Y. Gogotsi, M.W. Barsoum, Two-Dimensional Nanocrystals Produced by Exfoliation of Ti_3AlC_2. *Advanced Materials* 23, 4248-4253 (2011)

[158] R. Syamsai, A.N. Grace, Synthesis, properties and performance evaluation of vanadium carbide MXene as supercapacitor electrodes. *Ceramics International* 46, 5323-5330 (2020)

[159] M. Li, J. Lu, K. Luo, Y. Li, K. Chang, K. Chen, J. Zhou, J. Rosen, L. Hultman, P. Eklund, P.O.Å. Persson, S. Du, Z. Chai, Z. Huang, Q. Huang, Element Replacement Approach by

Reaction with Lewis Acidic Molten Salts to Synthesize Nanolaminated MAX Phases and MXenes. *Journal of the American Chemical Society* 141, 4730-4737 (2019)

[160] M. Tang, J. Li, Y. Wang, W. Han, S. Xu, M. Lu, W. Zhang, H. Li, Surface Terminations of MXene: Synthesis, Characterization, and Properties. *Symmetry* 14, 2232 (2022)

[161] Y. Bai, C. Liu, T. Chen, W. Li, S. Zheng, Y. Pi, Y. Luo, H. Pang, MXene-Copper/Cobalt Hybrids via Lewis Acidic Molten Salts Etching for High Performance Symmetric Supercapacitors. *Angewandte Chemie International Edition* 60, 25318-25322 (2021)

[162] H. Alnoor, A. Elsukova, J. Palisaitis, I. Persson, E.N. Tseng, J. Lu, L. Hultman, P.O.Å. Persson, Exploring MXenes and their MAX phase precursors by electron microscopy. *Materials Today Advances* 9, 100123 (2021)

[163] M. Ghidiu, M.R. Lukatskaya, M.-Q. Zhao, Y. Gogotsi, M.W. Barsoum, Conductive two-dimensional titanium carbide ‘clay’ with high volumetric capacitance. *Nature* 516, 78-81 (2014)

[164] F. Liu, A. Zhou, J. Chen, J. Jia, W. Zhou, L. Wang, Q. Hu, Preparation of Ti_3C_2 and Ti_2C MXenes by fluoride salts etching and methane adsorptive properties. *Applied Surface Science* 416, 781-789 (2017)

[165] A. Sinha, K. Ma, H. Zhao, 2D $Ti_3C_2T_x$ flakes prepared by in-situ HF etchant for simultaneous screening of carbamate pesticides. *Journal of Colloid and Interface Science* 590, 365-374 (2021)

[166] N. Anjum, O. Ekuase, V. Eze, O.I. Okoli, Ti-based MXenes for Energy Storage Application: Structure, Properties, Processing Parameters and Stability. *ECS Journal of Solid State Science and Technology* 11, (2022)

[167] L. Wang, H. Zhang, B. Wang, C. Shen, C. Zhang, Q. Hu, A. Zhou, B. Liu, Synthesis and electrochemical performance of $Ti_3C_2T_x$ with hydrothermal process. *Electronic Materials Letters* 12, 702-710 (2016)

[168] C.E. Shuck, K. Ventura-Martinez, A. Goad, S. Uzun, M. Shekhirev, Y. Gogotsi, Safe Synthesis of MAX and MXene: Guidelines to Reduce Risk During Synthesis. *ACS Chemical Health & Safety* 28, 326-338 (2021)

[169] M.R. Lukatskaya, S.-M. Bak, X. Yu, X.-Q. Yang, M.W. Barsoum, Y. Gogotsi, Probing the Mechanism of High Capacitance in 2D Titanium Carbide Using In Situ X-Ray Absorption Spectroscopy. *Advanced Energy Materials* 5, 1500589 (2015)

[170] T. Li, L. Yao, Q. Liu, J. Gu, R. Luo, J. Li, X. Yan, W. Wang, P. Liu, B. Chen, W. Zhang, W. Abbas, R. Naz, D. Zhang, Fluorine-Free Synthesis of High-Purity $Ti_3C_2T_x$ (T=OH, O) via Alkali Treatment. *Angewandte Chemie International Edition* 57, 6115-6119 (2018)

[171] S. Yang, P. Zhang, F. Wang, A.G. Ricciardulli, M.R. Lohe, P.W.M. Blom, X. Feng, Fluoride-Free Synthesis of Two-Dimensional Titanium Carbide (MXene) Using A Binary Aqueous System. *Angewandte Chemie International Edition* 57, 15491-15495 (2018)

[172] J. Joy, A. Krishnamoorthy, A. Tanna, V. Kamathe, R. Nagar, S. Srinivasan, Recent Developments on the Synthesis of Nanocomposite Materials via Ball Milling Approach for Energy Storage Applications, Applied Sciences, 2022.

[173] M.M. Nair, A.C. Iacoban, F. Neaţu, M. Florea, Ş. Neaţu, A comparative overview of MXenes and metal oxides as cocatalysts in clean energy production through photocatalysis. *Journal of Materials Chemistry A* 11, 12559-12592 (2023)

[174] N. Xue, X. Li, M. Zhang, L. Han, Y. Liu, X. Tao, Chemical-Combined Ball-Milling Synthesis of Fluorine-Free Porous MXene for High-Performance Lithium Ion Batteries. *ACS Applied Energy Materials* 3, 10234-10241 (2020)

[175] X. Su, J. Zhang, H. Mu, J. Zhao, Z. Wang, Z. Zhao, C. Han, Z. Ye, Effects of etching temperature and ball milling on the preparation and capacitance of Ti_3C_2 MXene. *Journal of Alloys and Compounds* 752, 32-39 (2018)

[176] S. Venkateshalu, M. Shariq, B. Kim, M. Patel, K.S. Mahabari, S.-I. Choi, N.K. Chaudhari, A.N. Grace, K. Lee, Recent advances in MXenes: beyond Ti-only systems. *Journal of Materials Chemistry A* 11, 13107-13132 (2023)

[177] J.T. Gudmundsson, Physics and technology of magnetron sputtering discharges. *Plasma Sources Science and Technology* 29, 113001 (2020)

[178] J. Halim, I. Persson, E.J. Moon, P. Kühne, V. Darakchieva, P.O.Å. Persson, P. Eklund, J. Rosen, M.W. Barsoum, Electronic and optical characterization of 2D Ti_2C and Nb_2C (MXene) thin films. *Journal of Physics: Condensed Matter* 31, 165301 (2019)

[179] R. Su, H. Zhang, D.J. O’Connor, L. Shi, X. Meng, H. Zhang, Deposition and characterization of Ti2AlC MAX phase and Ti_3AlC thin films by magnetron sputtering. *Materials Letters* 179, 194-197 (2016)

[180] C. Azina, B. Tunca, A. Petruhins, B. Xin, M. Yildizhan, P.O.Å. Persson, J. Vleugels, K. Lambrinou, J. Rosen, P. Eklund, Deposition of MAX phase-containing thin films from a $(Ti,Zr)_2AlC$ compound target. *Applied Surface Science* 551, 149370 (2021)

[181] J. Halim, M.R. Lukatskaya, K.M. Cook, J. Lu, C.R. Smith, L.-Å. Näslund, S.J. May, L. Hultman, Y. Gogotsi, P. Eklund, M.W. Barsoum, Transparent Conductive Two-

Dimensional Titanium Carbide Epitaxial Thin Films. *Chemistry of Materials* 26, 2374-2381 (2014)

[182] G. Li, J. Liu, F. Wang, H. Nie, R. Wang, K. Yang, B. Zhang, J. He, Third-Order Nonlinear Optical Response of Few-Layer MXene Nb_2C and Applications for Square-Wave Laser Pulse Generation. *Advanced Materials Interfaces* 8, 2001805 (2021)

[183] J. Jeon, Y. Yang, H. Choi, J.-H. Park, B.H. Lee, S. Lee, MXenes for future nanophotonic device applications. *Nanophotonics* 9, 1831-1853 (2020)

[184] V. Thirumal, R. Yuvakkumar, P.S. Kumar, G. Ravi, S.P. Keerthana, D. Velauthapillai, Facile single-step synthesis of MXene@CNTs hybrid nanocomposite by CVD method to remove hazardous pollutants. *Chemosphere* 286, 131733 (2022)

[185] A. Zamhuri, G.P. Lim, N.L. Ma, K.S. Tee, C.F. Soon, MXene in the lens of biomedical engineering: synthesis, applications and future outlook. *BioMedical Engineering OnLine* 20, 33 (2021)

[186] C. Xu, L. Wang, Z. Liu, L. Chen, J. Guo, N. Kang, X.-L. Ma, H.-M. Cheng, W. Ren, Large-area high-quality 2D ultrathin Mo_2C superconducting crystals. *Nature Materials* 14, 1135-1141 (2015)

[187] X.-H. Zha, J. Zhou, P. Eklund, X. Bai, S. Du, Q. Huang, Non-MAX Phase Precursors for MXenes, in: B. Anasori, Y. Gogotsi (Eds.), 2D Metal Carbides and Nitrides (MXenes): Structure, Properties and Applications, Springer International Publishing, Cham, 2019, pp. 53-68.

[188] L. Gao, C. Li, W. Huang, S. Mei, H. Lin, Q. Ou, Y. Zhang, J. Guo, F. Zhang, S. Xu, H. Zhang, MXene/Polymer Membranes: Synthesis, Properties, and Emerging Applications. *Chemistry of Materials* 32, 1703-1747 (2020)

[189] J. Zhou, X. Zha, X. Zhou, F. Chen, G. Gao, S. Wang, C. Shen, T. Chen, C. Zhi, P. Eklund, S. Du, J. Xue, W. Shi, Z. Chai, Q. Huang, Synthesis and Electrochemical Properties of Two-Dimensional Hafnium Carbide. *ACS Nano* 11, 3841-3850 (2017)

[190] J. Mei, G.A. Ayoko, C. Hu, J.M. Bell, Z. Sun, Two-dimensional fluorine-free mesoporous Mo2C MXene via UV-induced selective etching of Mo_2Ga_2C for energy storage. *Sustainable Materials and Technologies* 25, e00156 (2020)

[191] C. Wang, H. Shou, S. Chen, S. Wei, Y. Lin, P. Zhang, Z. Liu, K. Zhu, X. Guo, X. Wu, P.M. Ajayan, L. Song, HCl-Based Hydrothermal Etching Strategy toward Fluoride-Free MXenes. *Advanced Materials* 33, 2101015 (2021)

[192] Q. Wang, J. Yan, Z. Fan, Carbon materials for high volumetric performance supercapacitors: design, progress, challenges and opportunities. *Energy & Environmental Science* 9, 729-762 (2016)

[193] I. Shown, A. Ganguly, L.-C. Chen, K.-H. Chen, Conducting polymer-based flexible supercapacitor. *Energy Science & Engineering* 3, 2-26 (2015)

[194] M. Huang, F. Li, F. Dong, Y.X. Zhang, L.L. Zhang, MnO_2-based nanostructures for high-performance supercapacitors. *Journal of Materials Chemistry A* 3, 21380-21423 (2015)

[195] J. Kang, S. Zhang, Z. Zhang, Three-Dimensional Binder-Free Nanoarchitectures for Advanced Pseudocapacitors. *Advanced Materials* 29, 1700515 (2017)

[196] K. Zhang, X. Han, Z. Hu, X. Zhang, Z. Tao, J. Chen, Nanostructured Mn-based oxides for electrochemical energy storage and conversion. *Chemical Society Reviews* 44, 699-728 (2015)

[197] J.-G. Wang, F. Kang, B. Wei, Engineering of MnO_2-based nanocomposites for high-performance supercapacitors. *Progress in Materials Science* 74, 51-124 (2015)

[198] Y. Zhu, K. Rajouâ, S. Le Vot, O. Fontaine, P. Simon, F. Favier, Modifications of MXene layers for supercapacitors. *Nano Energy* 73, 104734 (2020)

[199] W. Zheng, J. Halim, P.O.Å. Persson, J. Rosen, M.W. Barsoum, MXene-based symmetric supercapacitors with high voltage and high energy density. *Materials Reports: Energy* 2, 100078 (2022)

[200] A. Patra, P. Mane, S.R. Polaki, B. Chakraborty, C.S. Rout, Enhanced charge storage performance of MXene based all-solid-state supercapacitor with vertical graphene arrays as the current collector. *Journal of Energy Storage* 54, 105355 (2022)

[201] S. Bai, M. Yang, J. Jiang, X. He, J. Zou, Z. Xiong, G. Liao, S. Liu, Recent advances of MXenes as electrocatalysts for hydrogen evolution reaction. *npj 2D Materials and Applications* 5, 78 (2021)

[202] J. Zhang, D. Jiang, L. Liao, L. Cui, R. Zheng, J. Liu, $Ti_3C_2T_x$ MXene based hybrid electrodes for wearable supercapacitors with varied deformation capabilities. *Chemical Engineering Journal* 429, 132232 (2022)

[203] A. Mateen, M.Z. Ansari, I. Hussain, S.M. Eldin, M.D. Albaqami, A.A.A. Bahajjaj, M.S. Javed, K.-Q. Peng, Ti_2CT_x–MXene aerogel based ultra–stable Zn–ion supercapacitor. *Composites Communications* 38, 101493 (2023)

[204] Y. Tan, Z. Zhu, X. Zhang, J. Zhang, Y. Zhou, H. Li, H. Qin, Y. Bo, Z. Pan, $Nb_4C_3T_x$ (MXene) as a new stable catalyst for the hydrogen evolution reaction. *International Journal of Hydrogen Energy* 46, 1955-1966 (2021)

[205] P.A. Rasheed, R.P. Pandey, F. Banat, S.W. Hasan, Recent advances in niobium MXenes: Synthesis, properties, and emerging applications. *Matter* 5, 546-572 (2022)

[206] H. He, Q. Xia, B. Wang, L. Wang, Q. Hu, A. Zhou, Two-dimensional vanadium carbide (V_2CT_x) MXene as supercapacitor electrode in seawater electrolyte. *Chinese Chemical Letters* 31, 984-987 (2020)

[207] H. Kim, B. Anasori, Y. Gogotsi, H.N. Alshareef, Thermoelectric Properties of Two-Dimensional Molybdenum-Based MXenes. *Chemistry of Materials* 29, 6472-6479 (2017)

[208] I. Persson, A. el Ghazaly, Q. Tao, J. Halim, S. Kota, V. Darakchieva, J. Palisaitis, M.W. Barsoum, J. Rosen, P.O.Å. Persson, Tailoring Structure, Composition, and Energy Storage Properties of MXenes from Selective Etching of In-Plane, Chemically Ordered MAX Phases. *Small* 14, 1703676 (2018)

[209] L. Dong, H. Chu, Y. Li, X. Ma, H. Pan, S. Zhao, D. Li, Surface functionalization of Ta_4C_3 MXene for broadband ultrafast photonics in the near-infrared region. *Applied Materials Today* 26, 101341 (2022)

[210] A. Anisha, D. Sriram Kumar, Performance analysis of Ta_4C_3 MXene based optically transparent patch antenna for terahertz communications. *Optik* 260, 168959 (2022)

[211] M.R. Lukatskaya, O. Mashtalir, C.E. Ren, Y. Dall'Agnese, P. Rozier, P.L. Taberna, M. Naguib, P. Simon, M.W. Barsoum, Y. Gogotsi, Cation Intercalation and High Volumetric Capacitance of Two-Dimensional Titanium Carbide. *Science* 341, 1502-1505 (2013)

[212] L. Liao, B. Wu, E. Kovalska, V. Mazánek, M. Veselý, I. Marek, L. Spejchalová, Z. Sofer, The Role of Alkali Cation Intercalates on the Electrochemical Characteristics of Nb_2CT_X MXene for Energy Storage. *Chemistry – A European Journal* 27, 13235-13241 (2021)

[213] S. Venkateshalu, J. Cherusseri, M. Karnan, K.S. Kumar, P. Kollu, M. Sathish, J. Thomas, S.K. Jeong, A.N. Grace, New Method for the Synthesis of 2D Vanadium Nitride (MXene) and Its Application as a Supercapacitor Electrode. *ACS Omega* 5, 17983-17992 (2020)

[214] H. He, J. Wang, Q. Xia, L. Wang, Q. Hu, A. Zhou, Effect of electrolyte on supercapacitor performance of two-dimensional molybdenum carbide (Mo_2CT_x) MXene prepared by hydrothermal etching. *Applied Surface Science* 568, 150971 (2021)

[215] R. Ma, Z. Chen, D. Zhao, X. Zhang, J. Zhuo, Y. Yin, X. Wang, G. Yang, F. Yi, $Ti_3C_2T_x$ MXene for electrode materials of supercapacitors. *Journal of Materials Chemistry A* 9, 11501-11529 (2021)

[216] F. Ming, H. Liang, G. Huang, Z. Bayhan, H.N. Alshareef, MXenes for Rechargeable Batteries Beyond the Lithium-Ion. *Advanced Materials* 33, 2004039 (2021)

[217] N. Chen, Y. Zhou, S. Zhang, H. Huang, C. Zhang, X. Zheng, X. Chu, H. Zhang, W. Yang, J. Chen, Tailoring Ti_3CNT_x MXene via an acid molecular scissor. *Nano Energy* 85, 106007 (2021)

[218] Q. Fu, J. Wen, N. Zhang, L. Wu, M. Zhang, S. Lin, H. Gao, X. Zhang, Free-standing $Ti_3C_2T_x$ electrode with ultrahigh volumetric capacitance. *RSC Advances* 7, 11998-12005 (2017)

[219] J. Li, X. Yuan, C. Lin, Y. Yang, L. Xu, X. Du, J. Xie, J. Lin, J. Sun, Achieving High Pseudocapacitance of 2D Titanium Carbide (MXene) by Cation Intercalation and Surface Modification. *Advanced Energy Materials* 7, 1602725 (2017)

[220] X. Mu, D. Wang, F. Du, G. Chen, C. Wang, Y. Wei, Y. Gogotsi, Y. Gao, Y. Dall'Agnese, Revealing the Pseudo-Intercalation Charge Storage Mechanism of MXenes in Acidic Electrolyte. *Advanced Functional Materials* 29, 1902953 (2019)

[221] G.R. Berdiyorov, M.E. Madjet, K.A. Mahmoud, Ionic sieving through $Ti_3C_2(OH)_2$ MXene: First-principles calculations. *Applied Physics Letters* 108, 113110 (2016)

[222] M. Ashton, R.G. Hennig, S.B. Sinnott, Computational characterization of lightweight multilayer MXene Li-ion battery anodes. *Applied Physics Letters* 108, 023901 (2016)

[223] R.B. Rakhi, B. Ahmed, M.N. Hedhili, D.H. Anjum, H.N. Alshareef, Effect of Postetch Annealing Gas Composition on the Structural and Electrochemical Properties of Ti_2CT_x MXene Electrodes for Supercapacitor Applications. *Chemistry of Materials* 27, 5314-5323 (2015)

[224] M. Hu, T. Hu, Z. Li, Y. Yang, R. Cheng, J. Yang, C. Cui, X. Wang, Surface Functional Groups and Interlayer Water Determine the Electrochemical Capacitance of $Ti_3C_2T_x$ MXene. *ACS Nano* 12, 3578-3586 (2018)

[225] Z. Pan, F. Cao, X. Hu, X. Ji, A facile method for synthesizing CuS decorated Ti_3C_2 MXene with enhanced performance for asymmetric supercapacitors. *Journal of Materials Chemistry A* 7, 8984-8992 (2019)

[226] C. Chen, M. Boota, P. Urbankowski, B. Anasori, L. Miao, J. Jiang, Y. Gogotsi, Effect of glycine functionalization of 2D titanium carbide (MXene) on charge storage. *Journal of Materials Chemistry A* 6, 4617-4622 (2018)

[227] X. Chen, Y. Zhu, M. Zhang, J. Sui, W. Peng, Y. Li, G. Zhang, F. Zhang, X. Fan, N-Butyllithium-Treated $Ti_3C_2T_x$ MXene with Excellent Pseudocapacitor Performance. *ACS Nano* 13, 9449-9456 (2019)

[228] H. Huang, X. Chu, Y. Xie, B. Zhang, Z. Wang, Z. Duan, N. Chen, Z. Xu, H. Zhang, W. Yang, $Ti_3C_2T_x$ MXene-Based Micro-Supercapacitors with Ultrahigh Volumetric Energy Density for All-in-One Si-Electronics. *ACS Nano* 16, 3776-3784 (2022)

[229] M. Hu, Z. Li, G. Li, T. Hu, C. Zhang, X. Wang, All-Solid-State Flexible Fiber-Based MXene Supercapacitors. *Advanced Materials Technologies* 2, 1700143 (2017)

[230] M. Naguib, J. Halim, J. Lu, K.M. Cook, L. Hultman, Y. Gogotsi, M.W. Barsoum, New Two-Dimensional Niobium and Vanadium Carbides as Promising Materials for Li-Ion Batteries. *Journal of the American Chemical Society* 135, 15966-15969 (2013)

[231] O. Mashtalir, M.R. Lukatskaya, M.-Q. Zhao, M.W. Barsoum, Y. Gogotsi, Amine-Assisted Delamination of Nb_2C MXene for Li-Ion Energy Storage Devices. *Advanced Materials* 27, 3501-3506 (2015)

[232] M. Ghidiu, M. Naguib, C. Shi, O. Mashtalir, L.M. Pan, B. Zhang, J. Yang, Y. Gogotsi, S.J.L. Billinge, M.W. Barsoum, Synthesis and characterization of two-dimensional Nb_4C_3 (MXene). *Chemical Communications* 50, 9517-9520 (2014)

[233] P.A. Rasheed, R.P. Pandey, T. Gomez, M. Naguib, K.A. Mahmoud, Large interlayer spacing $Nb_4C_3T_x$ (MXene) promotes the ultrasensitive electrochemical detection of Pb2+ on glassy carbon electrodes. *RSC Advances* 10, 24697-24704 (2020)

[234] S.-Y. Pang, W.-F. Io, L.-W. Wong, J. Zhao, J. Hao, Efficient Energy Conversion and Storage Based on Robust Fluoride-Free Self-Assembled 1D Niobium Carbide in 3D Nanowire Network. *Advanced Science* 7, 1903680 (2020)

[235] J. Xiao, J. Wen, J. Zhao, X. Ma, H. Gao, X. Zhang, A safe etching route to synthesize highly crystalline Nb_2CT_x MXene for high performance asymmetric supercapacitor applications. *Electrochimica Acta* 337, 135803 (2020)

[236] S. Zhao, C. Chen, X. Zhao, X. Chu, F. Du, G. Chen, Y. Gogotsi, Y. Gao, Y. Dall'Agnese, Flexible $Nb_4C_3T_x$ Film with Large Interlayer Spacing for High-Performance Supercapacitors. *Advanced Functional Materials* 30, 2000815 (2020)

[237] S. Zhao, X. Wang, N. Kurra, Y. Gogotsi, Y. Gao, Effect of pinholes in Nb_4C_3 MXene sheets on its electrochemical behavior in aqueous electrolytes. *Electrochemistry Communications* 142, 107380 (2022)

[238] Q. Shan, X. Mu, M. Alhabeb, C.E. Shuck, D. Pang, X. Zhao, X.-F. Chu, Y. Wei, F. Du, G. Chen, Y. Gogotsi, Y. Gao, Y. Dall'Agnese, Two-dimensional vanadium carbide (V_2C) MXene as electrode for supercapacitors with aqueous electrolytes. *Electrochemistry Communications* 96, 103-107 (2018)

[239] A. VahidMohammadi, M. Mojtabavi, N.M. Caffrey, M. Wanunu, M. Beidaghi, Assembling 2D MXenes into Highly Stable Pseudocapacitive Electrodes with High Power and Energy Densities. *Advanced Materials* 31, 1806931 (2019)

[240] X. Wang, S. Lin, H. Tong, Y. Huang, P. Tong, B. Zhao, J. Dai, C. Liang, H. Wang, X. Zhu, Y. Sun, S. Dou, Two-dimensional V_4C_3 MXene as high performance electrode materials for supercapacitors. *Electrochimica Acta* 307, 414-421 (2019)

[241] B. Anasori, M.R. Lukatskaya, Y. Gogotsi, 2D metal carbides and nitrides (MXenes) for energy storage. *Nature Reviews Materials* 2, 16098 (2017)

[242] F. Ming, H. Liang, W. Zhang, J. Ming, Y. Lei, A.-H. Emwas, H.N. Alshareef, Porous MXenes enable high performance potassium ion capacitors. *Nano Energy* 62, 853-860 (2019)

[243] Y. Guan, S. Jiang, Y. Cong, J. Wang, Z. Dong, Q. Zhang, G. Yuan, Y. Li, X. Li, A hydrofluoric acid-free synthesis of 2D vanadium carbide (V_2C) MXene for supercapacitor electrodes. *2D Materials* 7, 025010 (2020)

[244] W. Chen, L. Zhang, H. Ren, T. Miao, Z. Wang, K. Zhan, J. Yang, B. Zhao, V_2CT_x MXene as novel anode for aqueous asymmetric supercapacitor with superb durability in $ZnSO_4$ electrolyte. *Journal of Colloid and Interface Science* 626, 59-67 (2022)

[245] Z.W. Seh, K.D. Fredrickson, B. Anasori, J. Kibsgaard, A.L. Strickler, M.R. Lukatskaya, Y. Gogotsi, T.F. Jaramillo, A. Vojvodic, Two-Dimensional Molybdenum Carbide (MXene) as an Efficient Electrocatalyst for Hydrogen Evolution. *ACS Energy Letters* 1, 589-594 (2016)

[246] A. Byeon, C.B. Hatter, J.H. Park, C.W. Ahn, Y. Gogotsi, J.W. Lee, Molybdenum oxide/carbon composites derived from the CO_2 oxidation of Mo_2CT_x (MXene) for lithium ion battery anodes. *Electrochimica Acta* 258, 979-987 (2017)

[247] Y. Guo, S. Jin, L. Wang, P. He, Q. Hu, L.-Z. Fan, A. Zhou, Synthesis of two-dimensional carbide Mo_2CT_x MXene by hydrothermal etching with fluorides and its thermal stability. *Ceramics International* 46, 19550-19556 (2020)

[248] B. Ahmed, A.E. Ghazaly, J. Rosen, i-MXenes for Energy Storage and Catalysis. *Advanced Functional Materials* 30, 2000894 (2020)

[249] Q. Tao, M. Dahlqvist, J. Lu, S. Kota, R. Meshkian, J. Halim, J. Palisaitis, L. Hultman, M.W. Barsoum, P.O.Å. Persson, J. Rosen, Two-dimensional $Mo_{1.33}C$ MXene with divacancy ordering prepared from parent 3D laminate with in-plane chemical ordering. *Nature Communications* 8, 14949 (2017)

[250] H. Lind, J. Halim, S.I. Simak, J. Rosen, Investigation of vacancy-ordered $Mo_{1.33}$ MXene from first principles and x-ray photoelectron spectroscopy. *Physical Review Materials* 1, 044002 (2017)

[251] A.S. Etman, J. Halim, J. Rosen, Fabrication of $Mo_{1.33}CT_z$ (MXene)–cellulose freestanding electrodes for supercapacitor applications. *Materials Advances* 2, 743-753 (2021)

[252] X. Xiao, Z. Peng, C. Chen, C. Zhang, M. Beidaghi, Z. Yang, N. Wu, Y. Huang, L. Miao, Y. Gogotsi, J. Zhou, Freestanding MoO_{3-x} nanobelt/carbon nanotube films for Li-ion intercalation pseudocapacitors. *Nano Energy* 9, 355-363 (2014)

[253] A. El-Ghazaly, J. Halim, B. Ahmed, A.S. Etman, J. Rosen, Exploring the electrochemical behavior of $Mo_{1.33}CT_z$ MXene in aqueous sulfates electrolytes: Effect of intercalating cations on the stored charge. *Journal of Power Sources* 531, 231302 (2022)

[254] R. Syamsai, A.N. Grace, Ta_4C_3 MXene as supercapacitor electrodes. *Journal of Alloys and Compounds* 792, 1230-1238 (2019)

[255] A. Rafieerad, A. Amiri, G.L. Sequiera, W. Yan, Y. Chen, A.A. Polycarpou, S. Dhingra, Development of Fluorine-Free Tantalum Carbide MXene Hybrid Structure as a Biocompatible Material for Supercapacitor Electrodes. *Advanced Functional Materials* 31, 2100015 (2021)

[256] S. Kumar, N. Kumari, Y. Seo, MXenes: Versatile 2D materials with tailored surface chemistry and diverse applications. *Journal of Energy Chemistry* 90, 253-293 (2024)

[257] O. Mashtalir, M. Naguib, V.N. Mochalin, Y. Dall'Agnese, M. Heon, M.W. Barsoum, Y. Gogotsi, Intercalation and delamination of layered carbides and carbonitrides. *Nature Communications* 4, 1716 (2013)

[258] X. Wang, H. Li, H. Li, S. Lin, W. Ding, X. Zhu, Z. Sheng, H. Wang, X. Zhu, Y. Sun, 2D/2D 1T-MoS_2/Ti_3C_2 MXene Heterostructure with Excellent Supercapacitor Performance. *Advanced Functional Materials* 30, 0190302 (2020)

[259] Y.-T. Du, X. Kan, F. Yang, L.-Y. Gan, U. Schwingenschlögl, MXene/Graphene Heterostructures as High-Performance Electrodes for Li-Ion Batteries. *ACS Applied Materials & Interfaces* 10, 32867-32873 (2018)

[260] M.S. Javed, A. Mateen, I. Hussain, A. Ahmad, M. Mubashir, S. Khan, M.A. Assiri, S.M. Eldin, S.S.A. Shah, W. Han, Recent progress in the design of advanced MXene/metal oxides-hybrid materials for energy storage devices. *Energy Storage Materials* 53, 827-872 (2022)

[261] I. Hussain, C. Lamiel, M.S. Javed, M. Ahmad, S. Sahoo, X. Chen, N. Qin, S. Iqbal, S. Gu, Y. Li, C. Chatzichristodoulou, K. Zhang, MXene-based heterostructures: Current trend and development in electrochemical energy storage devices. *Progress in Energy and Combustion Science* 97, 101097 (2023)

[262] H. Li, F. Musharavati, E. Zalenezhad, X. Chen, K.N. Hui, K.S. Hui, Electrodeposited NiCo layered double hydroxides on titanium carbide as a binder-free electrode for supercapacitors. *Electrochimica Acta* 261, 178-187 (2018)

[263] Y. Wang, S. Shen, M. Yang, B. Yong, Y. Liang, D. Ma, S. Wang, P. Zhang, Sandwich-like MXene bridged heterostructure electrode enables anti-aggregation and superior storage for aqueous zinc-ion batteries. *Applied Surface Science* 635, 157727 (2023)

[264] W. Zhao, Y. Lei, Y. Zhu, Q. Wang, F. Zhang, X. Dong, H.N. Alshareef, Hierarchically structured $Ti_3C_2T_x$ MXene paper for Li-S batteries with high volumetric capacity. *Nano Energy* 86, 106120 (2021)

[265] S.R. K. A, N. Barman, S. Radhakrishnan, R. Thapa, C.S. Rout, Hierarchical architecture of the metallic $VTe_2/Ti_3C_2T_x$ MXene heterostructure for supercapacitor applications. *Journal of Materials Chemistry A* 10, 23590-23602 (2022)

[266] Z. Liu, H. Xiong, Y. Luo, L. Zhang, K. Hu, L. Zhang, Y. Gao, Z.-A. Qiao, Interface-Induced Self-Assembly Strategy Toward 2D Ordered Mesoporous Carbon/MXene Heterostructures for High-Performance Supercapacitors. *ChemSusChem* 14, 4422-4430 (2021)

[267] X. Feng, M. Xia, J. Ning, D. Wang, Interface-Modified $Ti_3C_2T_x$ MXene/1T-WSe_2 Heterostructure for High-Capacitance Micro-Supercapacitors. *ACS Applied Energy Materials* (2023)

[268] K. Nasrin, V. Sudharshan, M. Arunkumar, M. Sathish, 2D/2D Nanoarchitectured Nb_2C/Ti_3C_2 MXene Heterointerface for High-Energy Supercapacitors with Sustainable Life Cycle. *ACS Applied Materials & Interfaces* 14, 21038-21049 (2022)

[269] K. Nasrin, V. Sudharshan, K. Subramani, M. Karnan, M. Sathish, In-Situ Synergistic 2D/2D MXene/BCN Heterostructure for Superlative Energy Density Supercapacitor with Super-Long Life. *Small* 18, 2106051 (2022)

[270] J. Yan, C.E. Ren, K. Maleski, C.B. Hatter, B. Anasori, P. Urbankowski, A. Sarycheva, Y. Gogotsi, Flexible MXene/Graphene Films for Ultrafast Supercapacitors with Outstanding Volumetric Capacitance. *Advanced Functional Materials* 27, 1701264 (2017)

[271] H. Zhou, F. Wu, L. Fang, J. Hu, H. Luo, T. Guan, B. Hu, M. Zhou, Layered NiFe-LDH/MXene nanocomposite electrode for high-performance supercapacitor. *International Journal of Hydrogen Energy* 45, 13080-13089 (2020)

[272] Y. Wang, H. Dou, J. Wang, B. Ding, Y. Xu, Z. Chang, X. Hao, Three-dimensional porous MXene/layered double hydroxide composite for high performance supercapacitors. *Journal of Power Sources* 327, 221-228 (2016)

[273] H. Niu, X. Yang, Q. Wang, X. Jing, K. Cheng, K. Zhu, K. Ye, G. Wang, D. Cao, J. Yan, Electrostatic self-assembly of MXene and edge-rich CoAl layered double hydroxide on molecular-scale with superhigh volumetric performances. *Journal of Energy Chemistry* 46, 105-113 (2020)

[274] C. Sun, P. Zuo, W. Sun, R. Xia, Z. Dong, L. Zhu, J. Lv, G. Deng, L. Tan, Y. Dai, Self-assembly of Alternating Stacked 2D/2D $Ti_3C_2T_x$ MXene/ZnMnNi LDH van der Waals Heterostructures with Ultrahigh Supercapacitive Performance. *ACS Applied Energy Materials* 3, 10242-10254 (2020)

[275] X. Wang, H. Li, H. Li, S. Lin, J. Bai, J. Dai, C. Liang, X. Zhu, Y. Sun, S. Dou, Heterostructures of Ni–Co–Al layered double hydroxide assembled on V_4C= MXene for high-energy hybrid supercapacitors. *Journal of Materials Chemistry A* 7, 2291-2300 (2019)

[276] B. Shen, X. Hu, H.-T. Ren, H.-K. Peng, B.-C. Shiu, J.-H. Lin, C.-W. Lou, T.-T. Li, Rosette-like (Ni,Co)Se_2@Nb_2CT_x MXene heterostructure with abundant Se vacancies for high-performance flexible supercapacitor electrodes. *Chemical Engineering Journal* 484, 149440 (2024)

[277] X. Yang, Y. Tian, S. Li, Y.-P. Wu, Q. Zhang, D.-S. Li, S. Zhang, Heterogeneous Ni-MOF/V_2CT_x–MXene hierarchically-porous nanorods for robust and high energy density hybrid supercapacitors. *Journal of Materials Chemistry A* 10, 12225-12234 (2022)

[278] B. Shen, X. Liao, X. Hu, H.-T. Ren, J.-H. Lin, C.-W. Lou, T.-T. Li, A hollow nano-flower $NiCo_2O_4$@Nb_2CT_x MXene heterostructure via interfacial engineering for high-performance flexible supercapacitor electrodes. *Journal of Materials Chemistry A* 11, 16823-16837 (2023)

[279] Y. Wen, T.E. Rufford, X. Chen, N. Li, M. Lyu, L. Dai, L. Wang, Nitrogen-doped $Ti_3C_2T_x$ MXene electrodes for high-performance supercapacitors. *Nano Energy* 38, 368-376 (2017)

[280] Z. Liu, Y. Tian, S. Li, L. Wang, B. Han, X. Cui, Q. Xu, Revealing High-Rate and High Volumetric Pseudo-Intercalation Charge Storage from Boron-Vacancy Doped MXenes. *Advanced Functional Materials* 33, 2301994 (2023)

[281] M. Cai, X. Wei, H. Huang, F. Yuan, C. Li, S. Xu, X. Liang, W. Zhou, J. Guo, Nitrogen-doped $Ti_3C_2T_x$ MXene prepared by thermal decomposition of ammonium salts and its application in flexible quasi-solid-state supercapacitor. *Chemical Engineering Journal* 458, 141338 (2023)

[282] Y. Wen, R. Li, J. Liu, Z. Wei, S. Li, L. Du, K. Zu, Z. Li, Y. Pan, H. Hu, A temperature-dependent phosphorus doping on $Ti_3C_2T_x$ MXene for enhanced supercapacitance. *Journal of Colloid and Interface Science* 604, 239-247 (2021)

[283] N. Zhang, M.-y. Wang, J.-Y. Liu, Prediction of single-boron anchored on MXene catalysts for high-efficient electrocatalytic nitrogen reduction reaction. *Molecular Catalysis* 531, 112658 (2022)

[284] C. Lu, L. Yang, B. Yan, L. Sun, P. Zhang, W. Zhang, Z. Sun, Nitrogen-Doped Ti_3C_2 MXene: Mechanism Investigation and Electrochemical Analysis. *Advanced Functional Materials* 30, 2000852 (2020)

[285] L. Chen, Y. Bi, Y. Jing, J. Dai, Z. Li, C. Sun, A. Meng, H. Xie, M. Hu, Phosphorus Doping Strategy-Induced Synergistic Modification of Interlayer Structure and Chemical State in $Ti_3C_2T_x$ toward Enhancing Capacitance, Molecules, 2023.

[286] F. Yang, D. Hegh, D. Song, J. Zhang, K.A.S. Usman, C. Liu, Z. Wang, W. Ma, W. Yang, S. Qin, J.M. Razal, Synthesis of nitrogen-sulfur co-doped $Ti_3C_2T_x$ MXene with enhanced electrochemical properties. *Materials Reports: Energy* 2, 100079 (2022)

[287] Y. Tang, J. Zhu, W. Wu, C. Yang, W. Lv, F. Wang, Synthesis of Nitrogen-Doped Two-Dimensional Ti_3C_2 with Enhanced Electrochemical Performance. *Journal of The Electrochemical Society* 164, A923 (2017)

[288] C. Yang, W. Que, X. Yin, Y. Tian, Y. Yang, M. Que, Improved capacitance of nitrogen-doped delaminated two-dimensional titanium carbide by urea-assisted synthesis. *Electrochimica Acta* 225, 416-424 (2017)

[289] C. Yang, W. Que, Y. Tang, Y. Tian, X. Yin, Nitrogen and Sulfur Co-Doped 2D Titanium Carbides for Enhanced Electrochemical Performance. *Journal of The Electrochemical Society* 164, A1939 (2017)

[290] P. Kaewpijit, J. Qin, P. Pattananuwat, Preparation of MXene/N, S doped graphene electrode for supercapacitor application. *IOP Conference Series: Materials Science and Engineering* 600, 012008 (2019)

[291] C. Yang, Y. Tang, Y. Tian, Y. Luo, X. Yin, W. Que, Methanol and Diethanolamine Assisted Synthesis of Flexible Nitrogen-Doped Ti_3C_2 (MXene) Film for Ultrahigh Volumetric Performance Supercapacitor Electrodes. *ACS Applied Energy Materials* 3, 586-596 (2020)

[292] Z. Pan, X. Ji, Facile synthesis of nitrogen and oxygen co-doped C@Ti_3C_2 MXene for high performance symmetric supercapacitors. *Journal of Power Sources* 439, 227068 (2019)

[293] D. Su, J. Zhang, S. Dou, G. Wang, Polypyrrole hollow nanospheres: stable cathode materials for sodium-ion batteries. *Chemical Communications* 51, 16092-16095 (2015)

[294] P.W.M. Blom, Polymer Electronics: To Be or Not to Be? *Advanced Materials Technologies* 5, 2000144 (2020)

[295] M. Fei, R. Lin, Y. Deng, H. Xian, R. Bian, X. Zhang, J. Cheng, C. Xu, D. Cai, Polybenzimidazole/Mxene composite membranes for intermediate temperature polymer electrolyte membrane fuel cells. *Nanotechnology* 29, 035403 (2018)

[296] M. Naguib, T. Saito, S. Lai, M.S. Rager, T. Aytug, M. Parans Paranthaman, M.-Q. Zhao, Y. Gogotsi, $Ti_3C_2T_x$ (MXene)–polyacrylamide nanocomposite films. *RSC Advances* 6, 72069-72073 (2016)

[297] Z. Ling, C.E. Ren, M.-Q. Zhao, J. Yang, J.M. Giammarco, J. Qiu, M.W. Barsoum, Y. Gogotsi, Flexible and conductive MXene films and nanocomposites with high capacitance. *Proceedings of the National Academy of Sciences* 111, 16676-16681 (2014)

[298] X. Cheng, J. Zhang, J. Ren, N. Liu, P. Chen, Y. Zhang, J. Deng, Y. Wang, H. Peng, Design of a Hierarchical Ternary Hybrid for a Fiber-Shaped Asymmetric Supercapacitor with High Volumetric Energy Density. *The Journal of Physical Chemistry C* 120, 9685-9691 (2016)

[299] G.A. Snook, P. Kao, A.S. Best, Conducting-polymer-based supercapacitor devices and electrodes. *Journal of Power Sources* 196, 1-12 (2011)

[300] Y. Wang, Y. Ding, X. Guo, G. Yu, Conductive polymers for stretchable supercapacitors. *Nano Research* 12, 1978-1987 (2019)

[301] X. Wu, B. Huang, R. Lv, Q. Wang, Y. Wang, Highly flexible and low capacitance loss supercapacitor electrode based on hybridizing decentralized conjugated polymer chains with MXene. *Chemical Engineering Journal* 378, 122246 (2019)

[302] C. Zhang, S. Xu, D. Cai, J. Cao, L. Wang, W. Han, Planar supercapacitor with high areal capacitance based on Ti_3C_2/Polypyrrole composite film. *Electrochimica Acta* 330, 135277 (2020)

[303] W. Wu, D. Wei, J. Zhu, D. Niu, F. Wang, L. Wang, L. Yang, P. Yang, C. Wang, Enhanced electrochemical performances of organ-like Ti_3C_2 MXenes/polypyrrole composites as supercapacitors electrode materials. *Ceramics International* 45, 7328-7337 (2019)

[304] W. Liang, I. Zhitomirsky, MXene-polypyrrole electrodes for asymmetric supercapacitors. *Electrochimica Acta* 406, 139843 (2022)

[305] M. Zhu, Y. Huang, Q. Deng, J. Zhou, Z. Pei, Q. Xue, Y. Huang, Z. Wang, H. Li, Q. Huang, C. Zhi, Highly Flexible, Freestanding Supercapacitor Electrode with Enhanced Performance Obtained by Hybridizing Polypyrrole Chains with MXene. *Advanced Energy Materials* 6, 1600969 (2016)

[306] M. Boota, B. Anasori, C. Voigt, M.-Q. Zhao, M.W. Barsoum, Y. Gogotsi, Pseudocapacitive Electrodes Produced by Oxidant-Free Polymerization of Pyrrole between the Layers of 2D Titanium Carbide (MXene). *Advanced Materials* 28, 1517-1522 (2016)

[307] J. Yan, Y. Ma, C. Zhang, X. Li, W. Liu, X. Yao, S. Yao, S. Luo, Polypyrrole–MXene coated textile-based flexible energy storage device. *RSC Advances* 8, 39742-39748 (2018)

[308] J.V. Vaghasiya, C.C. Mayorga-Martinez, J. Vyskočil, M. Pumera, Flexible wearable MXene Ti_3C_2-Based power patch running on sweat. *Biosensors and Bioelectronics* 205, 114092 (2022)

[309] J. Fu, J. Yun, S. Wu, L. Li, L. Yu, K.H. Kim, Architecturally Robust Graphene-Encapsulated MXene Ti_2CT_x@Polyaniline Composite for High-Performance Pouch-Type Asymmetric Supercapacitor. *ACS Applied Materials & Interfaces* 10, 34212-34221 (2018)

[310] A. VahidMohammadi, J. Moncada, H. Chen, E. Kayali, J. Orangi, C.A. Carrero, M. Beidaghi, Thick and freestanding MXene/PANI pseudocapacitive electrodes with ultrahigh specific capacitance. *Journal of Materials Chemistry A* 6, 22123-22133 (2018)

[311] H. Xu, D. Zheng, F. Liu, W. Li, J. Lin, Synthesis of an MXene/polyaniline composite with excellent electrochemical properties. *Journal of Materials Chemistry A* 8, 5853-5858 (2020)

[312] Y. Ren, J. Zhu, L. Wang, H. Liu, Y. Liu, W. Wu, F. Wang, Synthesis of polyaniline nanoparticles deposited on two-dimensional titanium carbide for high-performance supercapacitors. *Materials Letters* 214, 84-87 (2018)

[313] X. Wang, D. Zhang, H. Zhang, L. Gong, Y. Yang, W. Zhao, S. Yu, Y. Yin, D. Sun, In situ polymerized polyaniline/MXene (V_2C) as building blocks of supercapacitor and ammonia sensor self-powered by electromagnetic-triboelectric hybrid generator. *Nano Energy* 88, 106242 (2021)

[314] J. Wang, D. Jiang, M. Zhang, Y. Sun, M. Jiang, Y. Du, J. Liu, Ice crystal-assisted intercalation of PANI within $Ti_3C_2T_x$ MXene thin films for flexible supercapacitor electrodes with simultaneously high mechanical strength and rate performance. *Journal of Materials Chemistry A* 11, 1419-1429 (2023)

[315] L. Qin, Q. Tao, A. El Ghazaly, J. Fernandez-Rodriguez, P.O.Å. Persson, J. Rosen, F. Zhang, High-Performance Ultrathin Flexible Solid-State Supercapacitors Based on Solution Processable $Mo_{1.33}C$ MXene and PEDOT:PSS. *Advanced Functional Materials* 28, 1703808 (2018)

[316] L. Li, N. Zhang, M. Zhang, X. Zhang, Z. Zhang, Flexible $Ti_3C_2T_x$/PEDOT:PSS films with outstanding volumetric capacitance for asymmetric supercapacitors. *Dalton Transactions* 48, 1747-1756 (2019)

[317] J. Zhang, S. Seyedin, S. Qin, Z. Wang, S. Moradi, F. Yang, P.A. Lynch, W. Yang, J. Liu, X. Wang, J.M. Razal, Highly Conductive $Ti_3C_2T_x$ MXene Hybrid Fibers for Flexible and Elastic Fiber-Shaped Supercapacitors. *Small* 15, 1804732 (2019)

[318] I. Amin, H.v.d. Brekel, K. Nemani, E. Batyrev, A. de Vooys, H. van der Weijde, B. Anasori, N.R. Shiju, $Ti_3C_2T_x$ MXene Polymer Composites for Anticorrosion: An Overview and Perspective. *ACS Applied Materials & Interfaces* 14, 43749-43758 (2022)

[319] H. Riazi, S.K. Nemani, M.C. Grady, B. Anasori, M. Soroush, Ti_3C_2 MXene–polymer nanocomposites and their applications. *Journal of Materials Chemistry A* 9, 8051-8098 (2021)

[320] T. Habib, X. Zhao, S.A. Shah, Y. Chen, W. Sun, H. An, J.L. Lutkenhaus, M. Radovic, M.J. Green, Oxidation stability of $Ti_3C_2T_x$ MXene nanosheets in solvents and composite films. *npj 2D Materials and Applications* 3, 8 (2019)

[321] W. Luo, Y. Ma, T. Li, H.K. Thabet, C. Hou, M.M. Ibrahim, S.M. El-Bahy, B.B. Xu, Z. Guo, Overview of MXene/conducting polymer composites for supercapacitors. *Journal of Energy Storage* 52, 105008 (2022)

[322] W.L. Liu, Y.Q. Guo, T. Lin, H.C. Peng, Y.P. Yu, F. Yang, S. Chen, High-performance supercapacitor electrodes of MXene/PANI/carbon fiber hybrid composites with 2D/0D/1D hierarchical nanostructures. *Journal of Alloys and Compounds* 926, 166855 (2022)

[323] K. Gong, K. Zhou, X. Qian, C. Shi, B. Yu, MXene as emerging nanofillers for high-performance polymer composites: A review. *Composites Part B: Engineering* 217, 108867 (2021)

[324] G.J. Adekoya, O.C. Adekoya, R.E. Sadiku, Y. Hamam, S.S. Ray, Applications of MXene-Containing Polypyrrole Nanocomposites in Electrochemical Energy Storage and Conversion. *ACS Omega* 7, 39498-39519 (2022)

[325] J. Yang, W. Bao, P. Jaumaux, S. Zhang, C. Wang, G. Wang, MXene-Based Composites: Synthesis and Applications in Rechargeable Batteries and Supercapacitors. *Advanced Materials Interfaces* 6, 1802004 (2019)

[326] S.A. Zahra, E. Ceesay, S. Rizwan, Zirconia-decorated V_2CT_x MXene electrodes for supercapacitors. *Journal of Energy Storage* 55, 105721 (2022)

[327] S.A. Zahra, B. Anasori, M.Z. Iqbal, F. Ravaux, M. Al Tarawneh, S. Rizwan, Enhanced electrochemical performance of vanadium carbide MXene composites for supercapacitors. *APL Materials* 10, (2022)

[328] Y. Zhou, K. Maleski, B. Anasori, J.O. Thostenson, Y. Pang, Y. Feng, K. Zeng, C.B. Parker, S. Zauscher, Y. Gogotsi, J.T. Glass, C. Cao, $Ti_3C_2T_x$ MXene-Reduced Graphene Oxide Composite Electrodes for Stretchable Supercapacitors. *ACS Nano* 14, 3576-3586 (2020)

[329] Y. Yu, Q. Fan, Z. Li, P. Fu, MXene-based electrode materials for supercapacitors: Synthesis, properties, and optimization strategies. *Materials Today Sustainability* 24, 100551 (2023)

[330] Z. Liu, X. Yuan, S. Zhang, J. Wang, Q. Huang, N. Yu, Y. Zhu, L. Fu, F. Wang, Y. Chen, Y. Wu, Three-dimensional ordered porous electrode materials for electrochemical energy storage. *NPG Asia Materials* 11, 12 (2019)

[331] A.S. Etman, J. Halim, J. Rosen, Mixed MXenes: $Mo_{1.33}CT_z$ and $Ti_3C_2T_z$ freestanding composite films for energy storage. *Nano Energy* 88, 106271 (2021)

[332] J. Azadmanjiri, L. Dĕkanovský, Z. Sofer, Boosting energy storage performance of $Ti_3C_2T_x$ composite supercapacitors via decorated chalcogen (S, Se, Te) and new phase-formed binding sites. *Materials Today Sustainability* 21, 100322 (2023)

[333] D.N. Ampong, E. Agyekum, F.O. Agyemang, K. Mensah-Darkwa, A. Andrews, A. Kumar, R.K. Gupta, MXene: fundamentals to applications in electrochemical energy storage. *Discover Nano* 18, 3 (2023)

[334] N. Anjum, O.A. Ekuase, V.O. Eze, O.I. Okoli, Ti-based MXenes for Energy Storage Applications: Structure, Properties, Processing Parameters and Stability. *ECS Journal of Solid State Science and Technology* 11, 093008 (2022)

[335] I. Pathak, D. Acharya, K. Chhetri, P. Chandra Lohani, S. Subedi, A. Muthurasu, T. Kim, T.H. Ko, B. Dahal, H.Y. Kim, $Ti_3C_2T_x$ MXene embedded metal–organic framework-based porous electrospun carbon nanofibers as a freestanding electrode for supercapacitors. *Journal of Materials Chemistry A* 11, 5001-5014 (2023)

[336] H. Shao, K. Xu, Y.-C. Wu, A. Iadecola, L. Liu, H. Ma, L. Qu, E. Raymundo-Piñero, J. Zhu, Z. Lin, P.-L. Taberna, P. Simon, Unraveling the charge storage mechanism of $Ti_3C_2T_x$ MXene electrode in acidic electrolyte. *ACS Energy Letters* XXXX, (2020)

[337] L. Li, N. Zhang, M. Zhang, L. Wu, X. Zhang, Z. Zhang, Ag-Nanoparticle-Decorated 2D Titanium Carbide (MXene) with Superior Electrochemical Performance for Supercapacitors. *ACS Sustainable Chemistry & Engineering* 6, 7442-7450 (2018)

[338] C.-W. Kan, Y.-L. Lam, Future Trend in Wearable Electronics in the Textile Industry, Applied Sciences, 2021.

[339] A. Inman, T. Hryhorchuk, L. Bi, R. Wang, B. Greenspan, T. Tabb, E.M. Gallo, A. VahidMohammadi, G. Dion, A. Danielescu, Y. Gogotsi, Wearable energy storage with MXene textile supercapacitors for real world use. *Journal of Materials Chemistry A* 11, 3514-3523 (2023)

[340] S. Iravani, R.S. Varma, MXene-based wearable supercapacitors and their transformative impact on healthcare. *Materials Advances* 4, 4317-4332 (2023)

[341] S.P. Sreenilayam, I. Ul Ahad, V. Nicolosi, D. Brabazon, MXene materials based printed flexible devices for healthcare, biomedical and energy storage applications. *Materials Today* 43, 99-131 (2021)

[342] W. Song, X. Yin, D. Liu, W. Ma, M. Zhang, X. Li, P. Cheng, C. Zhang, J. Wang, Z.L. Wang, A highly elastic self-charging power system for simultaneously harvesting solar and mechanical energy. *Nano Energy* 65, 103997 (2019)

[343] J. Lv, J. Chen, P.S. Lee, Sustainable wearable energy storage devices self-charged by human-body bioenergy. *SusMat* 1, 285-302 (2021)

[344] M.R. Repon, D. Mikučionienė, R. Milašius, T.K. Paul, C.M. Ahmed, S.Z. Hussain, A. Haji, Progress in MXene integrated wearable textile devices for thermotherapy. *Materials Today Communications* 37, 107251 (2023)

[345] S. Verma, U. Dwivedi, K. Chaturvedi, N. Kumari, M. Dhangar, S.A.R. Hashmi, R. Singhal, A.K. Srivastava, Progress of 2D MXenes based composites for efficient electromagnetic interference shielding applications: A review. *Synthetic Metals* 287, 117095 (2022)

[346] Y. Zhou, L. Yin, S. Xiang, S. Yu, H.M. Johnson, S. Wang, J. Yin, J. Zhao, Y. Luo, P.K. Chu, Unleashing the Potential of MXene-Based Flexible Materials for High-Performance Energy Storage Devices. *Advanced Science* n/a, 2304874 (2023)

[347] M. Weng, J. Zhou, Y. Ye, H. Qiu, P. Zhou, Z. Luo, Q. Guo, Self-chargeable supercapacitor made with MXene-bacterial cellulose nanofiber composite for wearable devices. *Journal of Colloid and Interface Science* 647, 277-286 (2023)

[348] S. Xu, Y. Dall'Agnese, G. Wei, C. Zhang, Y. Gogotsi, W. Han, Screen-printable microscale hybrid device based on MXene and layered double hydroxide electrodes for powering force sensors. *Nano Energy* 50, 479-488 (2018)

[349] M. Hu, Z. Li, H. Zhang, T. Hu, C. Zhang, Z. Wu, X. Wang, Self-assembled $Ti_3C_2T_x$ MXene film with high gravimetric capacitance. *Chemical Communications* 51, 13531-13533 (2015)

[350] C. Zhao, Q. Wang, H. Zhang, S. Passerini, X. Qian, Two-Dimensional Titanium Carbide/RGO Composite for High-Performance Supercapacitors. *ACS Applied Materials & Interfaces* 8, 15661-15667 (2016)

[351] M.-Q. Zhao, C.E. Ren, Z. Ling, M.R. Lukatskaya, C. Zhang, K.L. Van Aken, M.W. Barsoum, Y. Gogotsi, Flexible MXene/Carbon Nanotube Composite Paper with High Volumetric Capacitance. *Advanced Materials* 27, 339-345 (2015)

[352] X. Zhang, Y. Liu, S. Dong, J. Yang, X. Liu, Self-assembled three-dimensional $Ti_3C_2T_x$ nanosheets network on carbon cloth as flexible electrode for supercapacitors. *Applied Surface Science* 485, 1-7 (2019)

[353] X. Wang, Q. Fu, J. Wen, X. Ma, C. Zhu, X. Zhang, D. Qi, 3D $Ti_3C_2T_x$ aerogels with enhanced surface area for high performance supercapacitors. *Nanoscale* 10, 20828-20835 (2018)

[354] A. Amiri, Y. Chen, C. Bee Teng, M. Naraghi, Porous nitrogen-doped MXene-based electrodes for capacitive deionization. *Energy Storage Materials* 25, 731-739 (2020)

[355] L. Shao, J. Xu, J. Ma, B. Zhai, Y. Li, R. Xu, Z. Ma, G. Zhang, C. Wang, J. Qiu, MXene/RGO composite aerogels with light and high-strength for supercapacitor electrode materials. *Composites Communications* 19, 108-113 (2020)

[356] J. Zhu, X. Lu, L. Wang, Synthesis of a MoO3/Ti3C2Tx composite with enhanced capacitive performance for supercapacitors. *RSC Advances* 6, 98506-98513 (2016)

[357] A. Zaheer, S.A. Zahra, M.Z. Iqbal, A. Mahmood, S.A. Khan, S. Rizwan, Nickel-adsorbed two-dimensional Nb_2C MXene for enhanced energy storage applications. *RSC Advances* 12, 4624-4634 (2022)

[358] S. Xu, G. Wei, J. Li, W. Han, Y. Gogotsi, Flexible MXene–graphene electrodes with high volumetric capacitance for integrated co-cathode energy conversion/storage devices. *Journal of Materials Chemistry A* 5, 17442-17451 (2017)

[359] M. Zhang, J. Zhou, J. Yu, L. Shi, M. Ji, H. Liu, D. Li, C. Zhu, J. Xu, Mixed analogous heterostructure based on MXene and prussian blue analog derivative for high-performance flexible energy storage. *Chemical Engineering Journal* 387, 123170 (2020)

[360] K. Nasrin, V. Sudharshan, K. Subramani, M. Sathish, Insights into 2D/2D MXene Heterostructures for Improved Synergy in Structure toward Next-Generation Supercapacitors: A Review. *Advanced Functional Materials* 32, 2110267 (2022)

[361] X. Zhou, Y. Qin, X. He, Q. Li, J. Sun, Z. Lei, Z.-H. Liu, $Ti_3C_2T_x$ Nanosheets/$Ti_3C_2T_x$ Quantum Dots/RGO (Reduced Graphene Oxide) Fibers for an All-Solid-State Asymmetric Supercapacitor with High Volume Energy Density and Good Flexibility. *ACS Applied Materials & Interfaces* 12, 11833-11842 (2020)

[362] T. Zhou, C. Wu, Y. Wang, A.P. Tomsia, M. Li, E. Saiz, S. Fang, R.H. Baughman, L. Jiang, Q. Cheng, Super-tough MXene-functionalized graphene sheets. *Nature Communications* 11, 2077 (2020)

[363] L. Yang, W. Zheng, P. Zhang, J. Chen, W. Zhang, W.B. Tian, Z.M. Sun, Freestanding nitrogen-doped d-Ti_3C_2/reduced graphene oxide hybrid films for high performance supercapacitors. *Electrochimica Acta* 300, 349-356 (2019)

[364] Z. Li, Y. Dall'Agnese, J. Guo, H. Huang, X. Liang, S. Xu, Flexible freestanding all-MXene hybrid films with enhanced capacitive performance for powering a flex sensor. *Journal of Materials Chemistry A* 8, 16649-16660 (2020)

[365] B. Shen, X. Liao, X. Zhang, H.-T. Ren, J.-H. Lin, C.-W. Lou, T.-T. Li, Synthesis of Nb_2C MXene-based 2D layered structure electrode material for high-performance battery-type supercapacitors. *Electrochimica Acta* 413, 140144 (2022)

[366] L. Qin, Y. Liu, S. Zhu, D. Wu, G. Wang, J. Zhang, Y. Wang, L. Hou, C. Yuan, Formation and operating mechanisms of single-crystalline perovskite $NaNbO_3$ nanocubes/few-layered Nb_2CT_x MXene hybrids towards Li-ion capacitors. *Journal of Materials Chemistry A* 9, 20405-20416 (2021)

[367] Shaobo Tu, Qiu Jiang, Xixiang Zhang, and Husam N. Alshareef, Large Dielectric Constant Enhancement in MXene Percolative Polymer Composites, *ACS Nano 12* (4), 3369-3377 (2018)